Title

Extreme Ductility in Freestanding Glassy Polymer Thin Films

Author

Velez, Nathan Robert

Publication Date

2021

Peer reviewed|Thesis/dissertation

Extreme Ductility in Freestanding Glassy Polymer Thin Films

by

Nathan Velez

A dissertation submitted in partial satisfaction of the

requirements for the degree of

Doctor of Philosophy

in

Engineering – Materials Science and Engineering

in the

Graduate Division

of the

University of California, Berkeley

Committee in charge:

Professor Andrew Minor, Chair
Professor Mary Cooper Scott
Professor Peter Hosemann

Spring 2021

Extreme Ductility in Glassy Polymer Thin Films

Abstract

Extreme Ductility in Glassy Polymer Thin Films

by

Nathan Velez

Doctor of Philosophy in Materials Science and Engineering

University of California, Berkeley

Professor Andrew M. Minor, Chair

In this dissertation the mechanical and thermodynamic properties of microtomed thin films of glassy polymers is investigated using unique techniques and methods developed for this purpose. The novel methodology developed led to the discovery of unexpected mechanical properties in glassy polymer thin films prepared *via* microtomy, primarily the extreme ductility in nominally brittle materials: polystyrene (PS) and poly(methyl methacrylate) (PMMA). To investigate the origins of this phenomenon, the technique was developed further to provide a means to probe temperature dependent properties of the films, with the specific interest in measuring the glass transition temperature (T_g). Temperature-controlled dynamic mechanical analysis (DMA) experiments were carried out, revealing T_g depression never before measured in glassy polymer thin films with thickness above 100 nm.

The experimental methods are detailed in Chapter 1, beginning with the introduction of the micro-electromechanical system (MEMS) device, known as a push-to-pull (PTP) device. The PTP device was pivotal in the research herein but first required adaptations before it could be used to characterize polymeric materials, as its original design was intended for hard materials. The development of novel sample preparation techniques was also required to successfully utilize the PTP device for characterization of polymer thin films. These developments, as well as the challenges and limitations of the technique, are also outlined. This includes the topic of ion and electron beam irradiation effects, which are considerably more problematic and require additional precautions when compared to most hard materials, such as metals.

Results from PTP device testing of microtomed thin films of two polymer glasses, PS and PMMA, are presented and discussed in the proceeding chapters with a primary focus on the extreme ductility observed in both materials. These results include quantitative tensile testing, *in situ* and *postmortem* optical microscopy, *postmortem* transmission electron microscopy (TEM), and temperature-controlled DMA testing. Aside from the extreme ductility, analysis of the stress-strain relationship revealed a significant reduction of the elastic modulus and a thickness-dependent trend with respect to the strain softening amplitude. The quality of these results was verified by *in situ* optical microscopy, which also allowed for larger strains to be reached. *Postmortem* TEM investigations provided detailed imaging of the deformation microstructure, which showed a dependence on the thermal history of the film.

Analysis of these results, in concert with current theory in polymer physics, are discussed and a hypothesis to describe the underlying mechanisms at work is proposed. In short, microtomy produces films with fractured surfaces containing a high concentration of chain ends and a distribution of reduced molecular weight (M_w). These attributes are believed to enhance segmental mobility of chains not only at the surface, but also those deeper within the film. Direct evidence and theoretical support for these claims are presented and discussed in this dissertation.

Finally, the potential applications of these findings as well as future research opportunities enabled by the development of the novel PTP device technique described herein are examined.

This dissertation is dedicated to Katy,

love of my life and best friend.

Contents

List of Figures

Acknowledgements

Inspired by amazing people, encouraged by wise mentors, and supported by new friendships, the people I encountered in graduate school shaped an unforgettable experience that will resonate throughout the rest of my life. When I reflect upon the growth and accomplishments I have made during these past years, I am humbled by the fact that I could not have made the journey alone. In the forefront of those crucial to my endeavors is my research advisor, Professor Andrew Minor. Always encouraging, respectful, and easy to talk to, I feel lucky to have had such a great advisor. Our meetings always left me feeling more motivated and less panicked about my research. His commitment to the wellbeing his group and genuine interest in his students' progression is not only a reflection of his great leadership, but also that of a good person. I truly admire his ability to live a balanced life, wearing more hats than I could keep track of, including those for his family. For this I consider Prof. Minor a mentor, a role model, and a friend.

I am also grateful for Professor Mary Cooper Scott and Professor Peter Hosemann, not only for serving on my dissertation committee, but also for the though-provoking and hilarious conversations at La Val's. I admire both Prof. Scott and Prof. Hosemann and I am honored to have them on my dissertation committee.

I cannot thank Dr. Frances Allen enough for the guidance and support over the years. Especially in my first couple years, Dr. Allen extended her experience and knowledge while offering words of encouragement in her calm, reassuring voice. I was constantly amazed by the depth of her scientific knowledge, microscopy skills, and exquisite grammar (making for a wonderful editor). I also owe much of my success to the outstanding staff at NCEM, specifically Marissa Lisbee, Dr. Rohan Dhall, John Turner, and Dr. Karen Bustillo. Their knowledge and insight were invaluable, exceeded only by their patience and kindness.

I also want to thank our collaborators Dr. Greg Meyers and Mary Ann Jones and the rest of the Dow folks that intermittently joined our conference calls. I am especially thankful to Dr. Meyers for his patience and positivity. Special thanks to Professor Sanjay Govindjee for productive conversations and FEA simulations, as well as Professor Wei Li for fabricating the custom PTP devices during his post-doc in Professor Pister's group.

Professor Oscar Dubon was a constant voice of encouragement and was an invaluable source advice during my first year when I was searching for a research advisor. With a genuine interest in my success, he would always stop to chat and see how I was doing anytime we would cross paths.

Last, but not least, I would not have decided to apply to graduate school if it wasn't for the persistent encouragement from Dr. Valita Jones. Valita was my first true mentor in every sense of the word. I will always cherish our conversations, whether it was convincing me to apply to graduate school, challenging my worldview, or giving me relationship advice.

This research would not have been possible without support by the Dow University Partnership Initiative Program and access to the Molecular Foundry at Lawrence Berkeley National Laboratory, supported by the U.S. Department of Energy under Contract # DE-AC02-05CH11231.

Chapter 1 – Introduction

1.1 Glassy Polymers

Polymeric materials can be categorized based upon their ability to crystallize or not. The latter are known as glassy polymers: completely amorphous as they are unable to form crystallites no matter how slowly they are cooled from the melt. This is typically due to large side groups that pose steric hindrances to ordering. Atactic polystyrene is a classic example of a glassy polymer, where the large phenyl side group restricts molecular chains from rearranging. This frustrated vitrification leaves glassy polymers in a non-equilibrium state, forming a network of entangled molecular chains. This non-equilibrium solid state and lack of ordering leads to several interesting material properties. For example, the amorphous structure gives glassy polymers their high transparency, an attribute realized in many applications.

Similar to other glass formers, glassy polymers experience a glass transition at a temperature denoted as T_g. Below this temperature, the time scale for molecular motion is much longer than the experimental time scale, affecting every material property from the specific volume to the elastic modulus. Whether or not this transition is a true second-order thermodynamic transition or a kinetic phenomenon is still unanswered and remains a topic of debate within the polymer community. Nonetheless, T_g is an important intrinsic property of all polymers, since semicrystalline polymers have a T_g associated with the glassy domains between crystallites. There is much to be said regarding the topic of T_g, far more than can be covered here, but there is one experimental point worth mentioning that is relevant to this dissertation. The measured value for T_g depends somewhat on the experimental method and parameters used. This is, in part, because there are several molecular relaxation modes present within the polymer glass that can be probed, often simultaneously. Another reason for variation between techniques is that whichever property is being monitored as a function of temperature will experience a second-order transition that spans a temperature range, so the value reported depends slightly on the convention used. For example, the change in heat capacity in differential scanning calorimetry is roughly sigmoidal, where T_g can be taken at either the onset or midpoint of the transition.[1] Another distinction between measurement methods is whether probing is done in the time domain or frequency domain, such as dynamic mechanical analysis (DMA). In DMA experiments, the measured T_g will often depend on the frequency used, relating to the specific relaxation modes of the polymer being probed. This is not to say that T_g is undefined by any means, since various methods often agree within a few degrees, but rather that care must be taken when comparing various characterization techniques.

With that being said, the T_g of a glassy polymer represents the thermal energy required to overcome local energy barriers, allowing chain segments to slide past one another other (given constant pressure).[1] The energy barriers consist of interchain interactions (Van der Waals force) and steric hindrances ("caging"). Overcoming these barriers can be accomplished by stretching, bending, or rotating covalent bonds in the backbone or side groups of the polymer chain. This process is a dynamic one, where a "caged" segment will have to wait for collective motion in

neighboring chain segments before space becomes available for it to move into (cooperative motion). This type of motion is the slowest and first to be frozen out upon cooling, labeled α-relaxations. Faster, highly localized motions without the ability for cooperative motion are also present at even lower temperatures, for example the vibrations of side groups. Therefore, when mechanical stress is applied to a glassy polymer the response will greatly depend on the relative time scale of deformation (strain rate) *versus* the relaxation dynamics of the polymer chains. This typically leads to brittle behavior below T_g and ductile behavior above T_g for a given polymer. It is worth noting that the ductile-to-brittle transition temperature is not exactly the same as T_g, rather it is nearby but typically lower than T_g.

In tension, a polymer glass will deform in one of two primary modes: shear yielding or crazing. Crazing is a yielding phenomenon unique to polymers and is typically associated with brittle behavior, although it is not always seen in brittle fracture and may even be present in ductile polymers such as polycarbonate (PC). A craze is crack-like feature in which the opening is bridged by uncoiled molecular fibrils (Figure 1.1). The initiation of crazes remains unclear but is generally accepted to be a surface phenomenon.[2] Whether or not crazing will be the dominant deformation mode for a polymer glass under tension highly depends on several intrinsic and extrinsic factors. For example, with increasing temperature and pressure, crazing is suppressed and shear yielding dominates; whereas polymers with high chain stiffness tend to craze when below their respective T_g.[2] Since the ductility and yield behavior of glassy polymers are often limited by their crazing behavior, understanding the mechanisms operating at a molecular level is an important material objective.

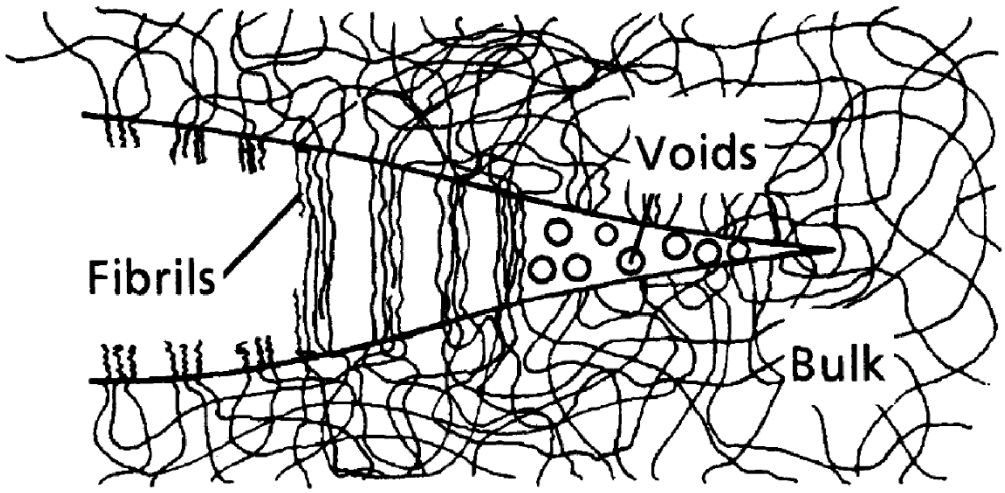

Figure 1.1. Schematic of crazing in various stages. At the tip of the crack, voids form and coalesce leading to fibrilization of molecular chains which bridge the crack opening. Further strain causes craze breakdown, through chain scission or pullout, typically followed by crack propagation and

global fracture. Schematic adapted from Hartwig, G. Fracture Behavior of Polymers. In *Polymer Properties at Room and Cryogenic Temperatures.*[3]

1.2 Prior thin film investigations

Early investigations to study crazing morphology in polystyrene used transmission electron microscopy (TEM) to reveal their detailed structure.[4,5] Solvent cast or microtomed thin films, with a nominal thickness less than a micron, were necessary to allow the crazes in deformed specimens to be transparent to the electron beam. These investigations pioneered the theoretical framework behind crazing mechanics through TEM microstructure analysis but lacked the capability to quantitatively measure the mechanical response of the films during deformation. Due to their use in emerging technologies such as microelectronics, dielectric stacks, optical reflectors, coatings, and membrane filters the mechanical stability of polymer thin and ultrathin films (thicknesses <1μm and <100 nm, respectively) have become increasingly relevant.[6] Conventional small-scale mechanical testing methods, such as nanoindentation, have achieved much success with metals and ceramics but suffer many challenges when attempting to characterize polymer thin films.[7] Freestanding thin films are fragile and difficult to manipulate, and supported thin films are strongly influenced by the underlying substrate.[8] For example, interactions between an indentation probe and the polymer surface introduce artifacts that not only complicate analysis, but alter the mechanical response of the polymer such that it does not properly represent the intrinsic properties.[9,10] These challenges have prompted the development of many novel mechanical testing techniques designed for polymer thin films.

Of the current nanomechanical testing techniques available for polymers, only a handful are capable of quantitatively measuring the deformation of freestanding thin films. Bay *et al*. proposed a technique in which a spin-cast film of polystyrene has been laser cut into a tensile specimen and suspended across a load frame.[11] Another freestanding technique is the microbubble bulge test developed by O'Connell *et al*. In this technique, polymer films are suspended across an array of micro-wells which can be pressurized with air at elevated temperatures to cause the film to bulge into a hemispherical bubble (Figure 1.2c). Mechanical properties are indirectly determined by measuring the size of the bulge using atomic force microscopy (AFM) with respect to known air pressure and temperature.[12] Stafford *et al.* developed a buckling-based technique in which a polymer thin film supported on a polydimethylsiloxane (PDMS) sheet is strained until the thin film buckles from lateral contraction of the substrate (Figure 1.2a).[6] The elastic modulus of the polymer thin film is then calculated by measuring the characteristic wavelength of the buckled film. While the buckling metrology method is quite elegant, the technique lacks the ability to measure the mechanical response at large deformations. Several researchers have used water to support polymer thin films for instrumented tensile testing (Figure 1.2b, d).[13–15] These "pseudo-

freestanding" methods have generated varied results in polystyrene and do not fully account for how the water-polymer interface might affect chain conformation and mobility.[11]

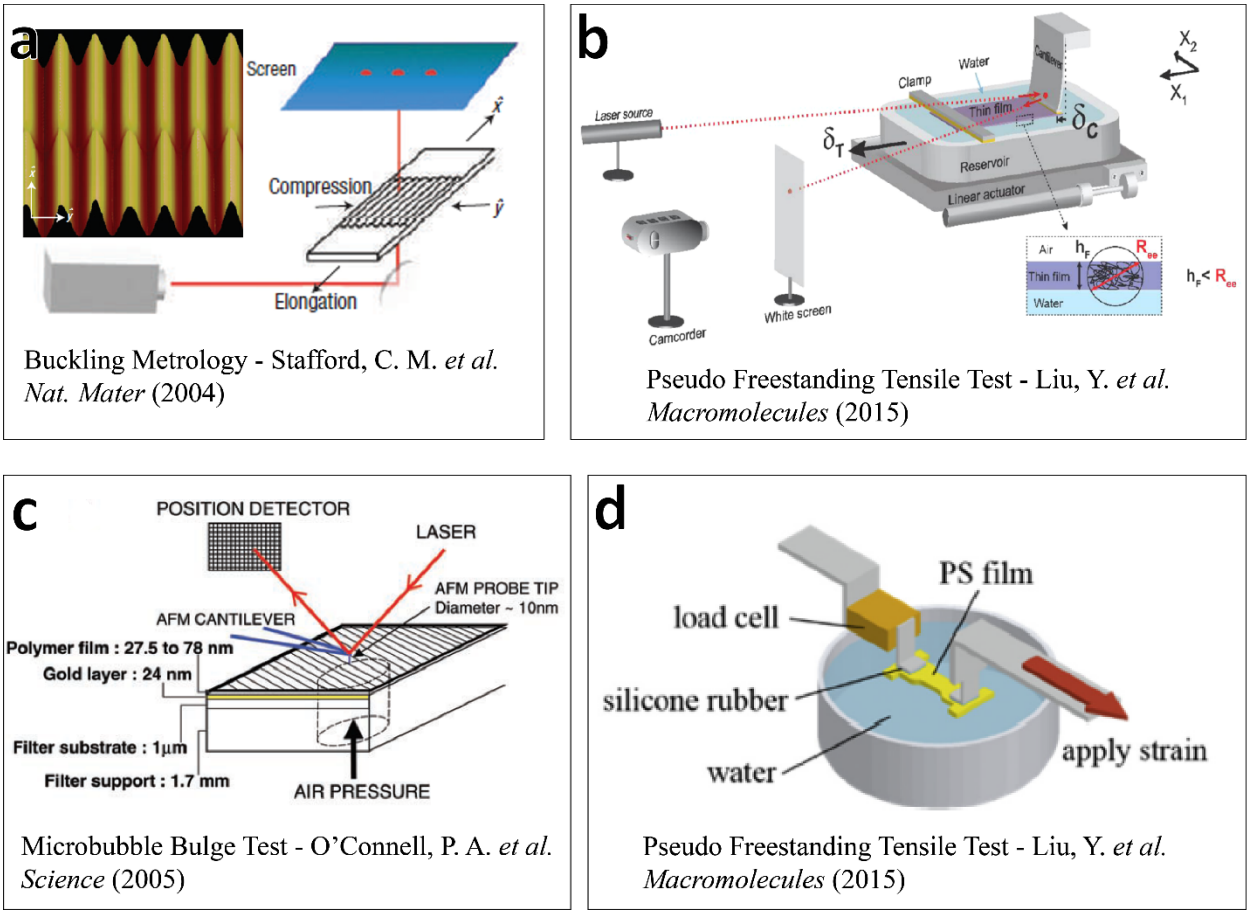

Figure 1.2. Examples of other polymer thin film mechanical testing methods in the literature.

An extensive review of all polymer thin film mechanical testing techniques is outside the scope of this dissertation, but several trends relevant to this work are worth noting. The body of experimental work focusing on the mechanical properties of polymer thin films is relatively small, especially when compared to similar research focused on the thickness dependence of the glass transition temperature (T_g). In both areas of research the material primarily studied is polystyrene, which is why it was also one of the materials selected for this work.[5,6,11–22] The thin-film effect regarding thermodynamic properties (i.e. T_g depression) has been thoroughly characterized and is accompanied by strong theoretical support (Figure 1.3).[18,19] While the mechanisms behind T_g depression are fundamentally related to mechanical properties, characterizing thin-film effects on mechanical properties has presented many challenges, and this is apparent in the lack of consensus in the literature. For example, consider the elastic modulus of polystyrene films as a function of

thickness. Buckling experiments report an exponential decrease in the elastic modulus as the thickness is reduced, with an order of magnitude drop reported for the thinnest films tested (5 nm).[21] This trend agrees with carefully performed nanoindentation experiments,[23] local stiffness measurements performed by fluorescence caging experiments,[24] and direct stress-strain measurements taken from flat punch squeeze flow testing[25] as well as pseudo-freestanding tensile tests.[26] Contrary to these findings, no measurable change in the elastic modulus was reported by capillary wrinkling,[27] two separate pseudo-freestanding tensile tests,[13,15] and freestanding tensile tests.[11] The pseudo-freestanding tensile tests performed by Hasegawa *et al*. also showed no change in the elastic modulus, however the authors did report a decrease in the crazing stress.[15] Similarly, the pseudo-freestanding and freestanding tensile testing reported by Bay *et al*. captured images that revealed a thickness-dependent transition from crazing to an array of shear deformation zones (SDZ) in ultrathin films with only a slight change in the elastic modulus.[11,13]

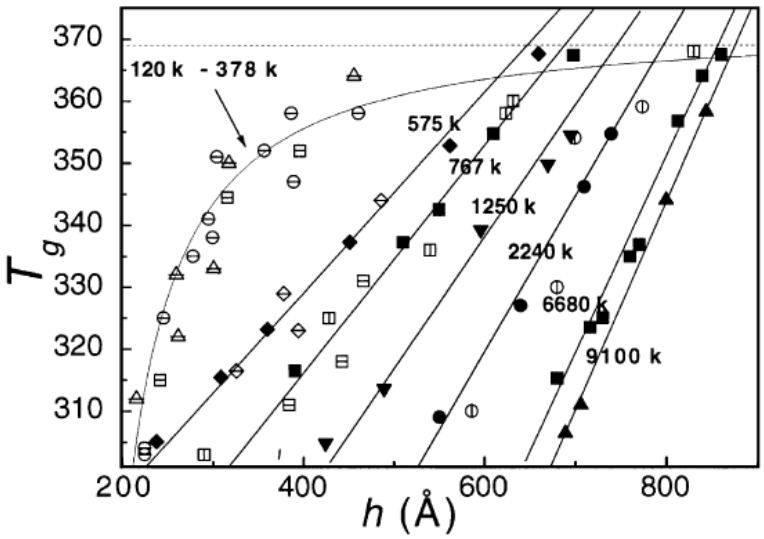

Figure 1.3. Plot of T_g as a function of thickness (h) for freestanding thin films (logarithmic curve) and supported thin films (linear curves) of polystyrene. Multiple datasets from several studies are plotted, represented by different symbol types. Note that T_g in freestanding films is independent of molecular weight (for the range shown). Figure adapted from Forrest, J. A.; Dalnoki-Veress, K. *Adv. Coll. Interf. Sci.* (2001).[28]

Even though there are conflicting reports on the nature of thickness-dependent mechanical properties, there is a commonality with regard to the onset thickness for which the mechanical behavior of polymer thin films begins to deviate from bulk. The thin-film effect with regard to the elastic modulus is often reported to begin to appear for film thicknesses less than 100 nm, followed by a more dramatic effect when the film is tens of nanometers thick.[11,13–15,21,23] Several studies

propose the dramatic change in the elastic modulus is a consequence of the film thickness approaching the characteristic coil size of a single polymer chain; some comparing to the root-mean-square end-to-end distance of the polymer chain, R_{ee},[11,13–15] while others use the radius of gyration, R_g.[21,29] In the work by Bay *et al.*, the transition to shear yielding occurred when the film thickness approached R_{ee}, which is dictated by the molecular weight. This is a significant distinction in comparison to our findings where the polystyrene films tested in this work were thicker than 200 nm, which is several times larger than R_{ee} (36 nm) for the molecular weight used in this study. While precedence suggests that glassy polymer films thicker than 200 nm should be regarded as bulk, our experiments reveal an exception to this trend.

One distinguishing feature of the testing method presented in this dissertation is that our thin films are produced *via* microtomy, whereas the aforementioned techniques employ spin-casting to fabricate polymer thin films for mechanical testing. Spin casting is known to induce elongated chain conformations[30] and leave residual solvent trapped[31] within the polymer thin film. Annealing under vacuum is typically applied to address these issues, but there is evidence suggesting that conventional temperatures and times are insufficient to equilibrate the chain conformations.[32–34] Furthermore, there are data from small-angle neutron scattering experiments on spin-cast polystyrene thin films that suggest the chain conformation diverges from the classic Gaussian coil to a flattened ellipsoid conformation to accommodate the confinement.[35,36] In light of these studies, it is generally accepted that care must be taken with preparing polymer thin films and that the processing route can greatly affect the mechanical and thermodynamic properties. Herein lies the basis for the dramatic change in physical properties measured in microtomed thin films of glassy polymers presented in this dissertation.

Chapter 2 – Experimental Technique and Development

2.1 Overview

A method for small-scale testing and imaging of free-standing, microtomed polymer films using a push-to-pull device is presented in this chapter. Central to this method was the development of a sample preparation technique which utilized solvents at cryogenic temperatures to transfer and deposit delicate thin films onto the microfabricated push-to-pull devices. The preparation of focused ion beam (FIB) milled tensile specimens enabled quantitative *in situ* TEM tensile testing, but artifacts associated with ion and electron beam irradiation motivated the development of a FIB-free specimen preparation method. The FIB-free method was enabled by the design and fabrication of oversized strain-locking push-to-pull devices. An adaptation for push-to-pull devices to be compatible with an instrumented nanoindenter expanded the testing capabilities to include *in situ* heating. These innovations provided quantitative mechanical testing, *postmortem* TEM imaging, and the ability to measure the glass transition temperature, *via* dynamic mechanical analysis, of freestanding polymer films.

2.2 Background: The push-to-pull device

Small-scale mechanical testing methods offer many advantages over their macroscopic counterparts. The mechanical properties of materials often depend on mechanisms operating at length scales spanning several orders of magnitude. By reducing the size of the test specimen, features of interest can be isolated and measured independently. For example, single crystal plasticity can be studied for complex alloys,[37–39] or near specific grain boundary structures.[40] Small-scale testing also provides a means to study size effects in materials in which one or more dimensions have been reduced to the micro- or nano-scale, for example as in nanopillar compression testing.[41] Another motivation for small-scale testing methods is to investigate materials that are inherently small such as: nanowires,[42] thin films,[43] and biological specimens[44]. Finally, the powerful imaging and analytical capabilities of transmission electron microscopy (TEM) can be used to characterize materials if they are thin enough to be electron transparent. As will be elaborated upon, TEM can also be combined with mechanical testing platforms to enable *in situ* and *postmortem* experiments, specifically through the use of push-to-pull (PTP) devices (Figure 2.1).[45,46]

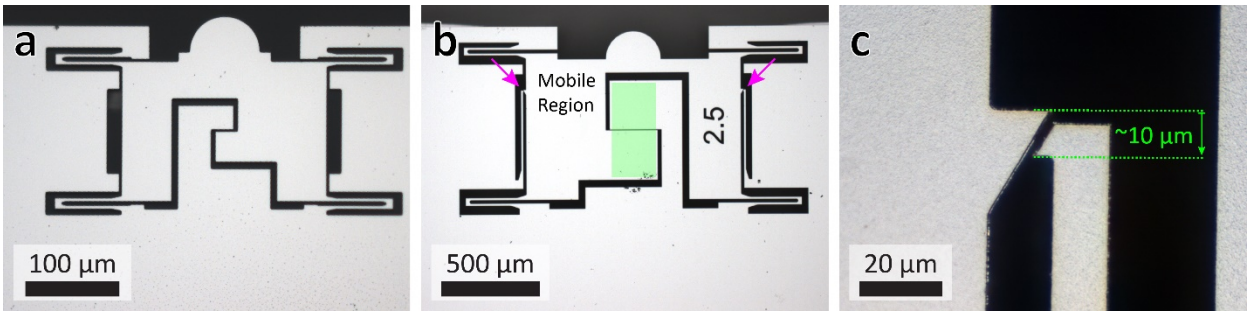

Figure 2.1. a) Optical image of a commercially available (non-locking) PTP device. b) Optical image of an oversized PTP device with custom designed strain-locking mechanisms incorporated into the device (indicated by arrows). The locking PTP device is shown here with a 2.5 µm tensile gap and the green shaded area represents the region in which a specimen can be deposited without requiring FIB milling. a-b) Both PTP devices are actuated by an in-plane force applied to the rounded top portion of the mobile region, which is suspended by four springs. Upon actuation, the horizonal gap in the center is widened to impart a tensile force on a specimen spanning the gap. c) Close-up image of one of the two strain-locking mechanisms from (b). The minimum displacement (~10 µm) required to engage the strain-locking mechanism is annotated.

In polymeric materials, the prevailing method for thin film preparation is spin-casting. This requires the polymer to be dissolved in a solvent, which is incompatible with many polymer systems of interest such as: polymer blends, polymer composites, and highly immiscible polymers. A key advantage of our technique is the variety of samples that can be tested in tension, including films that are microtomed from bulk that contain composite particles or phase interfaces to be preserved.

This chapter details the advantages and disadvantages of PTP-based methods for small-scale mechanical testing of free-standing, microtomed polymer thin films. The development of these methods has led to the discovery of a previously unknown phenomenon in thin films of polystyrene (PS) and poly(methyl methacrylate) (PMMA), where it was found that the fractured surfaces imparted by microtomy can lead to extreme ductility in polymers which are otherwise known to be brittle in their bulk form.[47–50] As a result, even though microtomy is established as a standard sample preparation method for microscopy of polymers, it is clear that the mechanical properties of freestanding thin films prepared in this way can deviate significantly from their bulk counterparts.

2.3 Preliminary results & discussion

2.3.1 FIB-milled tensile specimens

Employing the cyro-solvent manipulation technique (see 2.4.3), microtomed films of PS were deposited onto non-locking, commercially available PTP devices (Figure 2.2a). It was not possible to prepare films with in-plane dimensions small enough such that material did not extend

beyond the tensile region, hindering proper actuation of the PTP device. Thus, FIB milling was used to remove excess material and shape the tensile specimen.

Despite the precautions taken to avoid electron and ion beam exposure of the tensile specimen, unavoidable ion beam damage was present at the milled edges of the dogbone. Ion irradiation of polymers in known to cause chain scission of the carbon backbone and may subsequently produce radicals.[51] This can induce crosslinking through new bond formations between neighboring polymer chains. Additionally, scattered ions may embed into the polymer and, due to the low thermal conductivity of polymers, may cause local heating to occur.[52] Attempts to minimize these effects included using the FIB to widen the tensile gap of the PTP device, so that larger tensile specimens could be prepared. This was to reduce the volume fraction of material exposed to ion irradiation. Additionally, FIB milling using a helium ion microscope, rather than the typical gallium FIB, was employed to reduce ion implantation at the edges due to the much larger stopping distance of the light ions.[53] However, despite our best efforts during the FIB preparation, the mechanical response of the polymer films tested in this manner were dominated by the ion irradiated edges. As shown in Figure 2.2, FIB-milled PS films led to stiffening that resulted in an elastic modulus up to three times larger than that of bulk tensile specimens, likely due to FIB-induced crosslinking at the edges. This was the case even when the width of the dogbone was increased to 13.5 µm (nearly spanning the entire width of the tensile gap), to reduce the volume fraction of the irradiated edges. Thus, in order to obtain meaningful quantitative measurements a FIB-free sample preparation technique was employed.

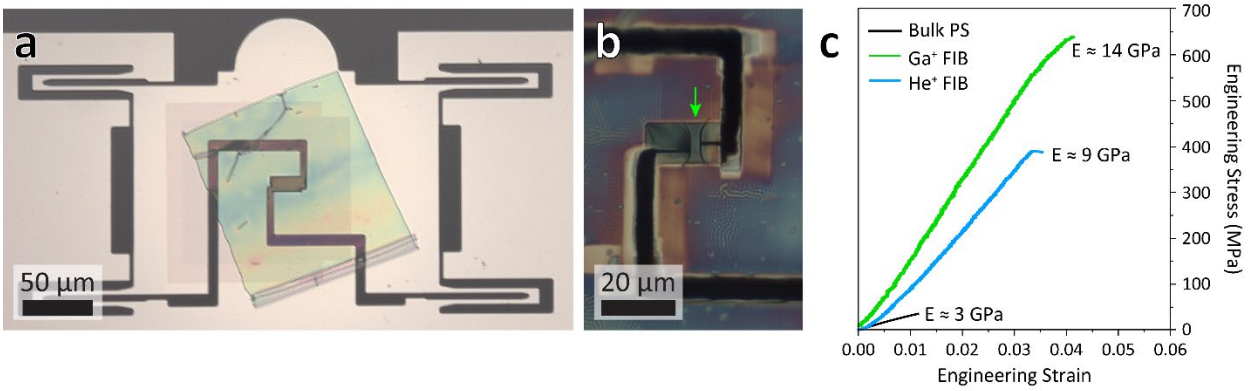

Figure 2.2. a) Microtomed film (270 nm thick) of an elastomer deposited onto a commercial PTP device with a tensile gap that has been FIB milled to be ~11 µm instead of the standard 2.5 µm. b) FIB milled tensile specimen with a dogbone geometry (indicated by arrow). The surrounding wrinkling pattern was induced through ion beam exposure, which was not present at the tensile specimen to indicate that proper precautions were taken to avoid exposure during the FIB milling process. The dogbone shown was 280 nm thick and 2.3 µm wide. c) Comparison of the mechanical responses for PS tensile specimens: microtomed film with a gallium FIB milled dogbone (green curve), microtomed film with a helium FIB milled dogbone (blue curve), and an injection molded

bulk PS dogbone (black curve). While helium ion milling offers some improvement, the mechanical response is still significantly altered by the irradiation damage at the edges, likely enhanced due to sample drift during the longer milling times. The thicknesses for the gallium and helium FIB milled PS films were 330 and 140 nm, and the widths 13.5 and 0.8 µm, respectively. The strain rate used in the bulk tensile test was 0.01 s^{-1} and 0.0008 s^{-1} for the PTP tests.

2.3.2 FIB-free tensile specimens

As mentioned, a microtomed film could not be prepared small enough such that it would not extend beyond the tensile gap. This prompted the design and fabrication of larger PTP devices with a tensile region wide enough to deposit a microtomed film without the need for any FIB milling (Figure 2.1b). The new design also incorporated a strain-locking mechanism which allowed the tensile gap to be held open for *postmortem* imaging, by either TEM or optical microscopy (Figure 2.1c). Standard bulk silicon microfabrication was used to produce the oversized locking PTP devices. The smallest feature size was limited to about 2 µm using standard photolithography in contact mode. Because of this limitation, a minimum displacement of roughly 10 µm was required for the strain-locking mechanism to reach the locked position of the device (Figure 2.1c). Thus, various tensile gap sizes were fabricated to predetermine the amount of strain that would be held in the locked position. Using the cryo-solvent manipulation method described in Section 2.4 and the newly designed locking PTP devices, microtomed polymer films could be deposited across the tensile gap without extending beyond the width of the tensile region (Figure 2.3a, b). This avoided the need for FIB milling and the accompanying artifacts. As a result, it was discovered that microtomed PS becomes extremely ductile compared to bulk tensile tests due to the microtoming causing an effect analogous to mechanical rejuvenation, as will be discussed in the proceeding chapters.[47]

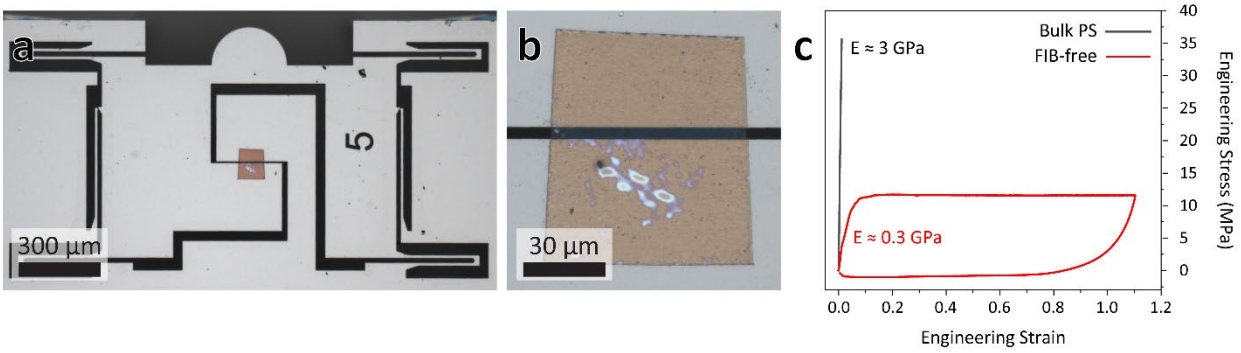

Figure 2.3. a) Microtomed film (230 nm thick) of PMMA deposited onto an oversized locking PTP device with a tensile gap of 5 µm using the cryo-solvent manipulation technique. b) Magnified image of the same film shown prior to mechanical testing (postmortem image shown in Figure 2.6e). c) Comparison of the mechanical responses for a bulk, injection molded tensile specimen (black curve) and a microtomed, FIB-free specimen (red curve) of PS. By avoiding the artifacts

induced by ion and electron beam irradiation, the discovery of extreme ductility in microtomed films of PS was made possible through FIB-free specimen preparation (note that fracture did not occur). The thickness of the FIB-free film of PS was 450 nm, with a strain rate of 0.03 s^{-1} used during the PTP test.

2.3.3 *In situ* TEM mechanical testing

The original design intent of the commercial PTP device was to enable *in situ* TEM mechanical testing.[45] This was performed by mounting the device into a specialized TEM holder equipped with an indenter capable of depth and force sensing (Bruker-Hysitron PI 95). This provided the means to acquire the mechanical response of the material with correlated TEM imaging. The cryo-manipulation method enabled *in situ* TEM mechanical testing of polymer films (Figure 2.4). Quantitative analysis, however, is limited by the damaging effects of the electron beam. Similar to ion beam irradiation, the electron beam inflicts localized heating and radiolysis in polymers that significantly alter their mechanical properties.[54] As shown in Figure 2.4c, the stress-strain curves for an elastomer are dramatically affected by the electron beam during *in situ* testing compared to PTP testing with the electron beam off. These effects were expected to affect PS and PMMA similarly and so alternative characterization methods were explored, as discussed below. Therefore, the beam sensitivity of the material must be considered when attempting to acquire quantitative, *in situ* TEM mechanical data.

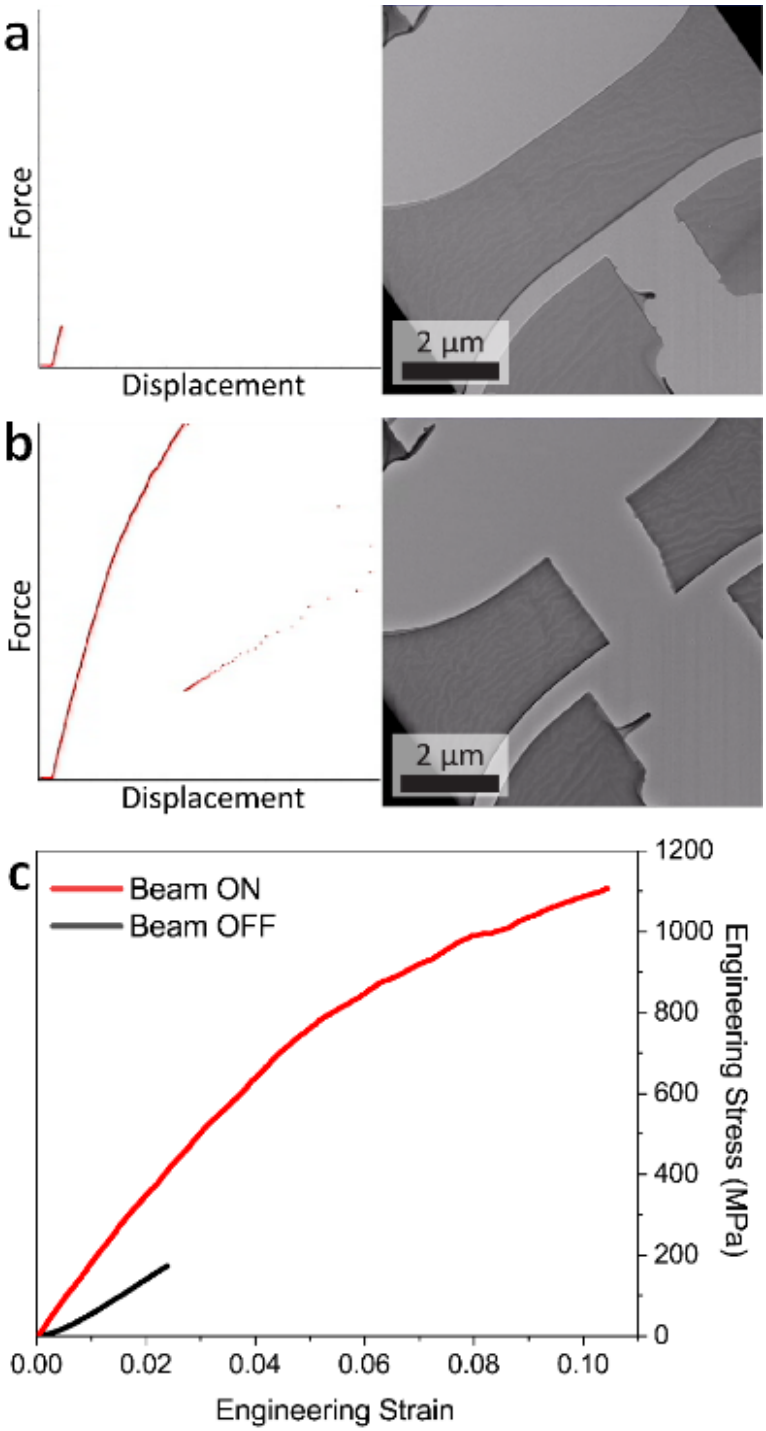

Figure 2.4. a-b) Video snapshots from an in situ TEM tensile test with correlated force-displacement curve of a microtomed elastomer film, FIB milled into a dogbone geometry. a) Snapshot from the beginning of the test. b) Snapshot just after the specimen fractured. c) Resultant stress-strain curve for the in situ test shown (red) in comparison to an identically prepared specimen in which the electron beam was blanked during the test (black). The stark difference between these two results highlights the sensitivity many polymeric materials have to the electron

beam of the TEM (300 kV JEOL 3010). The thicknesses for these two films were 300 and 270 nm for the in situ test and 'blind' test, respectively.

2.3.4 Adaptation for quantitative testing with a nanoindenter

Since our locking PTP devices allow for larger tensile specimens, larger loads are required to strain these specimens. Because of this, the load limit for the indenting TEM holder was often exceeded. To overcome this limitation, a mount was designed to fix the locking PTP vertically, enabling the use of an instrumented nanoindenter (Bruker-Hysitron TI 950 TriboIndenter) to perform quantitative testing (Figure 2.3c). Not only can this adaptation allow larger loads to be reached, but it extended all testing capabilities of the nanoindenter to both PTP and locking PTP devices that were not available with an indenting TEM holder. This includes the ability to perform temperature-controlled dynamic mechanical analysis (DMA) testing to measure the glass transition temperature of the free-standing polymer thin films (T_g). As shown in Figure 2.5, T_g could be determined by measuring the storage and loss stiffness, providing a tan-delta value as a function of temperature.[55] As determined by the peak in the tan-delta curve, the microtomed freestanding film of PS appears to have a reduction in T_g as compared to bulk measurements (T_g of bulk PS is 100 °C). This topic will be covered further in Chapters 4 and 5.

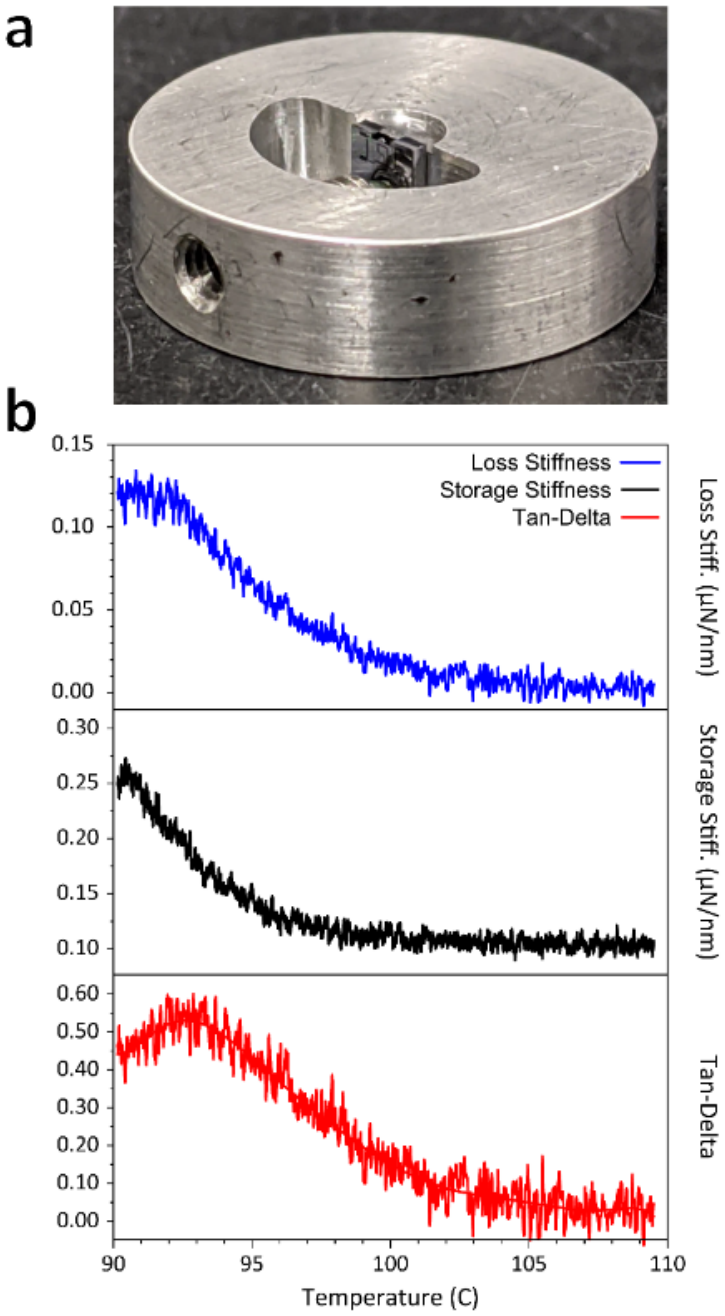

Figure 2.5. a) Custom fabricated mount designed to hold a locking PTP device upright for testing with an instrumented nanoindenter (different sized mount was also fabricated for the commercial PTP devices). A setscrew with a nylon tip holds the device firmly in the vertical position. The top surface of the mount is slightly higher than the device, which allows it to be sandwiched between two heating plates for temperature-controlled testing. b) Plot showing the results of a temperature-controlled DMA test on a microtomed, FIB-free film of PS. The thickness of the film was 140 nm,

and the dynamic mechanical test was performed at 4 Hz with a continuous temperature increase at a rate of 4 °C/min.

2.3.5 *In situ* optical microscopy & *postmortem* TEM imaging

To avoid electron beam induced artifacts, locking PTP experiments can be performed under an optical microscope to observe the deformation *in situ*. This can be done by fixing a pair of self-closing tweezers to the stage of an optical microscope to hold the locking PTP device under the objective lens (Figure 2.6a). By equipping a micromanipulator setup with a needle, the locking PTP device can be actuated while recording optical video or images (Figure 2.6b). After applying enough displacement to engage the strain-locking mechanism, the locking PTP can then be transferred into the TEM holder for *postmortem* TEM imaging (Figure 2.6c). The strain-locks provide more stability compared to holding strain with the indenting TEM holder, and even allow for the sample to be sputter coated in the deformed state to reduce electron beam sensitivity; both of these factors enhance the ability to obtain high quality TEM images *postmortem*.

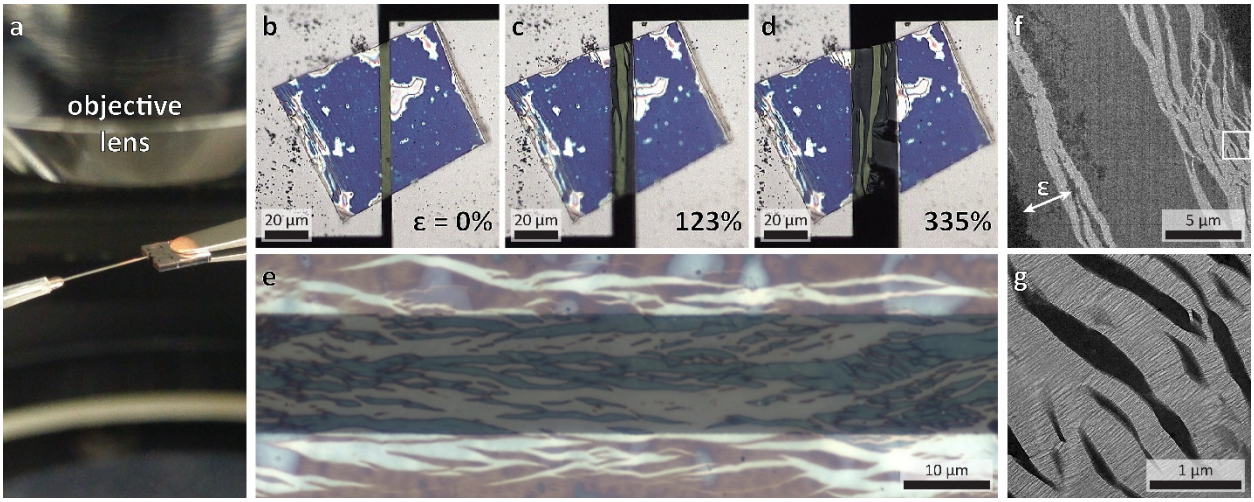

Figure 2.6. a) A locking PTP device held under the objective lens of an optical microscope, about to be actuated with a micromanipulator equipped with a metal needle. b-d) Video snapshots from an *in situ* locking PTP test of a microtomed, FIB-free film of PS (film thickness = 270 nm). The PS film reaches strains well beyond that of the bulk, as measured by the percent difference in the locking PTP gap (indicated in lower right corner of each snapshot). e) *Postmortem* optical image of a microtomed, FIB-free film of PMMA on a locking PTP device with the strain-locking mechanism engaged, which provided the mechanical stability required to obtain images at this magnification (film thickness = 260 nm). f) Low magnification TEM overview of a microtomed, FIB-free film of PS where the edges of the locking PTP tensile gap can be seen in the upper-right and lower-left corners (film thickness = 240 nm). g) Higher magnification of the region indicated in (f), revealing crazes not resolvable by the optical microscope. For PS, the crazing only occurred

in annealed films even though both annealed and unannealed films exhibited extreme ductility.[47] Enabled by the strain-locking feature of the locking PTP device, crucial TEM imaging of the films was permitted, revealing the dependence of the deformation mode on annealing at the microstructural level.

2.4 Sample preparation technique

2.4.1 Materials

The PS used for this study was anionically polymerized (M_w = 288,800 g/mol; M_n = 274,600 g/mol; M_w/M_n = 1.05) and was purchased from Pressure Chemical (Pittsburgh, PA) and provided by The Dow Chemical Company. The elastomer used was ethylene, 1-octene and was provided by The Dow Chemical Company. The PMMA was purchased from Sigma-Aldrich, manufactured by Goodfellow as a cast sheet (0.5 mm thick).

2.4.2 Microtomy

Glass and diamond blade microtomy was used to prepare PS and PMMA specimens with thicknesses on the order of 200 nm using an RMC PowerTome XL Ultramicrotome. As the glass transition temperature, T_g, of both of these polymer glasses is well above room temperature, sectioning was performed at room temperature. A glass knife trim tool was first used to reduce the size and shape the dimensions of the blockface of a bulk sample, after which sectioning was performed using a diamond knife equipped with a reservoir filled with deionized water. This allowed the films to float along the surface of the water as they were cut. The water not only serves as a convenient way to collect the floating specimens, but also reduces compression during sectioning to yield a more uniform thickness. Using a single-hair tool and a loop tool, the films can be retrieved and deposited onto an intermediate substrate. Filter paper was used to blot the water away from the loop tool when depositing the films onto this substrate. It is important that the films did not adhere to the intermediate substrate too strongly. To accomplish this, a silicon wafer substrate that was first roughened with high grit sandpaper and cleaned. This reduced the contact area between the polymer films and the substrate, lowering the adhesion and allowing them to be removed without damage. Success was also achieved using filter paper or “frosted” glass slides as intermediate substrates. Films less than 100 nm in thickness required a rougher substrate, as they tended to conform to the scratches on the surface and adhered more strongly than their thicker counterparts.

2.4.3 Cryo-solvent manipulation

Utilizing solvents at cryogenic temperatures provides a means to manipulate the fragile films and deposit them onto the PTP device (or any substrate). Three solvents were evaluated: ethanol, methanol, and isopropyl alcohol (IPA). These solvents were chosen because they were easily obtainable and incompatible with PS and PMMA. When the cryo-chamber was set to -165

°C, the methanol and IPA would quickly become solid and unusable. Ethanol, however, became a very viscous liquid, similar to the viscosity of honey at room temperature and is also very sticky. The viscous ethanol enabled the pickup and transfer of delicate specimens with accurate deposition onto the PTP device.

After preparing an intermediate substrate with several films deposited, it was placed into the microtome cryo-chamber and cooled to the desired temperature (depending on the solvent used). The intermediate substrate was fixed onto the knife holder by using double-sided tape which was compatible with cryogenic temperatures. The cryo-solvent manipulation was performed by first applying a small amount of solvent on the roughened intermediate substrate nearby the deposited films and a PTP device is placed on top in order to immobilize it during deposition (otherwise the PTP may cling to the single-hair tool). A smaller amount of solvent was then applied to the tensile region of a PTP device. For the oversized locking PTP devices, only enough solvent to cover the tensile region was used, where excess solvent may cause the film drift out of position during the final warm-up step. The tip single-hair tool was then dipped into a blob of solvent so that it was lightly coated. The sticky tip of the single-hair tool was then used to gently pick up a film from the roughened substrate, preferably at the corner of the film (Figure 2.7a). The film, attached to the end of the single-hair tool, was gently placed onto the small dab of solvent previously applied to the tensile region. The film was released from the single-hair tool as it was pulled away since the contact area between the film and the dab of solvent on the PTP device was much larger than at the tip of the hair (Figure 2.7b). The position of the deposited films can be adjusted by elevating the temperature until the solvent melts but does not evaporate. The single-hair tool can then be used to adjust the films into the desired position. This process can be performed by hand or by equipping a micromanipulator setup with a single-hair tool that extends into the cryo-chamber.

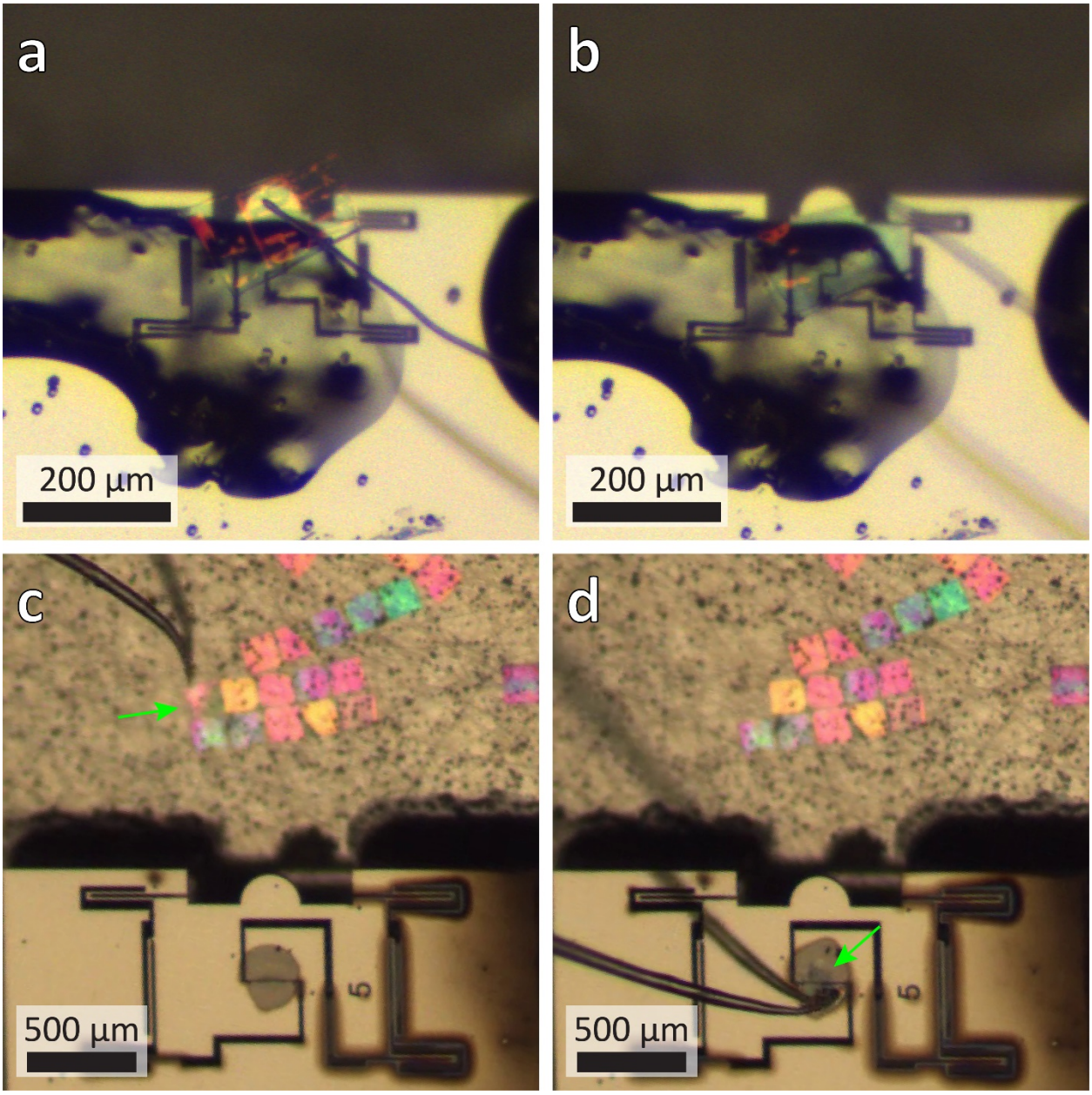

Figure 2.7. a) Microtomed film of PS clinging to the end of a single-hair tool extending into the cryogenic chamber of the microtome. Below the film, a dab of viscous ethanol covers a PTP device, ready for deposition. b) The PS film is shown deposited onto the PTP device by adhering to the viscous ethanol. Note that the film covers most of the mobile region of the device, which will require the use of a FIB to clear the trenches and shape the tensile specimen. c) Single-hair tool picking up a microtomed film of PMMA inside the cryogenic chamber. A small amount of IPA has been applied to the tensile region of a locking PTP device. The temperature is low enough such that the solvent remains liquid but does not readily evaporate. d) Image of the PMMA film from (c) just after deposition onto the locking PTP device by gently touching the film onto the liquid IPA previously applied to the tensile region (indicated by arrow). No FIB milling was required since the film does not extend beyond the tensile region of the locking PTP device.

It was found that the thin films could also be manipulated at slightly warmer temperatures (roughly -85 °C) at which the solvent remained in a liquid state, but low enough such that evaporation was suppressed. In this case, the same procedure as described for the viscous ethanol was used: a small amount of the solvent is painted onto a PTP device at the tensile gap and a small drop at the tip of the single-hair tool is used to pick up and deposit an individual film (Figure 2.7c, d – note here a locking PTP device was used). It was found that IPA worked best for cryo-solvent manipulation at the warmer setting. This is due to a common problem in cryo-microtomy, which is that water in the air freezes and "snows" into the cryo-chamber. The ice crystals land on the solvent in the cryo-chamber, melt and dissolve. It was observed that when ethanol was used, a critical concentration of water is reached such that the mixture freezes into a rigid solid. This creates limited window of time in which ethanol can be used for cryo-manipulation (this can be extended by the operator wearing a mask or face covering, which reduces moisture due to respiration entering the cryo-chamber). This problem, however, was not encountered with IPA. The warmer temperature not only reduced ice formation, but when ice mixed with the IPA it did not cause it to freeze. The advantage of using viscous ethanol is that the films are easier to pick up with the single-hair tool compared to using the liquid IPA method. Additionally, if cryo-microtomy is used to prepare specimens, as required for polymers with a T_g below room temperature, the viscous ethanol could be used to transfer films directly from the knife onto a PTP device mounted just below the knife edge, thus circumventing the need for an intermediate substrate. However, due to the problems with ice formation, using IPA at roughly -85 °C was the preferred method for preparing PTP specimens.

The final step in the sample transfer procedure is to elevate the temperature to ambient and let the solvent evaporate, leaving behind a film deposited firmly on the PTP device. Other solvents may also work, as long as the material is chemically resistant and can be wetted by the solvent.

2.4.4 FIB milling

The mobile region of a commercially available PTP device is about 0.7 mm^2, with a tensile gap of 2.5 μm and width of the tensile region of just under 19 μm (Figure 2.1a, 2.3a). This width is below the practical width of a polymer film that can be microtomed and deposited onto the device without extending beyond the tensile region, which would hinder proper actuation of the device and prevent quantitative analysis. Thus, focused ion beam (FIB) milling was used to clear the excess material and shape a tensile specimen. Using a Zeiss ORION NanoFab, milling (gallium and helium FIB) was performed blindly such that the gauge section was never imaged by the ions. This was achieved by using an optical image as a map, following the trenches of the device at a high enough magnification such that the material spanning the tensile gap was not exposed. The gallium FIB was used at higher currents (>1 nA at 30 kV) to clear the trenches up to the tensile region, then the helium FIB was used at a low current (10 pA at 25 kV) to shape the tensile specimen into a dogbone geometry (Figure 2.2a, b). Milling at low currents increases the milling time and so sample drift becomes more problematic. To minimize the effects of drift, only

the outline of the dogbone geometry was milled, one side at a time. After the outline was milled, the excess material on either side of the dogbone was cleared (Figure 2.2b). Note that the dogbone geometry was determined by scaling down the dimensions of a ATSM D638 type IV specimen.[56] The width of the narrow section was doubled to increase stability of the freestanding dogbone during handling and to reduce the volume of material irradiated by the FIB.

2.4.5 Quantitative PTP testing

A feedback controller was used to maintain a constant displacement rate during quantitative testing, for both the instrumented nanoindenter and the indenting TEM holder. The stiffness of the PTP devices ranged from 150 to 600 N/m, depending on the size and thickness of the device. No significant hysteresis was measured when the PTP device was cycled without a specimen. The stiffness of the PTP device was either determined ahead of time or was extracted from the unloading portion of the force-displacement curve after fracture or if there was slack present in the film.

Van der Waals attraction between the film and substrate was sufficient to fix the specimen across the PTP tensile gap. Slippage was only observed when bubbles of air trapped under the film prevented proper adhesion to the PTP device. Slippage events were easily identified in the force-displacement response as an abrupt drop in load much more dramatic than the load drop from strain softening. Additionally, concerns of slippage could be investigated after the fact by optical microscopy in two ways: 1) the interference color of the film changes when the film detaches from the PTP device surface after dramatic slippage in which half the film is no longer attached to the PTP device, 2) by comparing optical images taken before and after straining. With that being said, even when the film did not slip strain was observed to extend beyond the PTP gap edges when air pockets were present near the tensile gap.

Any slack in the film was removed from the force-displacement curve in accordance with ATSM D638 Annex A1 (toe compensation), which is done by fitting a line to initial linear response to extrapolate the actual zero value for displacement.[56] Additionally, once the spring force constant is subtracted from the data, the load is approximately zero until the end of the slack in the film is reached, indicating the value of displacement that correlates to zero strain (useful when the initial response of the material is non-linear). More often than not, this adjustment was not needed since the films would usually lay flat across the tensile gap.

2.5 Summary & outlook: Expanded utility of PTP devices

The PTP-based mechanical testing platform, which has had success in studying hard materials, has been adapted for small-scale testing of polymeric materials. Two key developments were described in this manuscript: (1) the cryo-solvent manipulation technique, which provided a means to transfer and deposit delicate polymer thin films, and (2) the design of an oversized locking push-to-pull device, which enabled FIB-free tensile specimen preparation and *postmortem* TEM analysis. A design of a vertical mount for use with instrumented nanoindenters expanded the types of experiments possible with PTP devices, including the ability to measure the glass transition temperature.

The cryo-solvent manipulation technique is not limited to PTP sample preparation. For example, using this technique it is possible to transfer microtomed films onto grids and silicon nitride windows for TEM and X-ray microscopy. While only results for monolithic polymers have been presented, the advantages of the locking PTP device testing platform may benefit more complicated polymer systems such as composites and blends. Finally, the increased tensile area of the locking PTP devices may accommodate other types of materials, such as biological materials for nanomechanical investigations that would not be possible with small commercial PTP devices.

Chapter 3 – Extreme ductility in freestanding polystyrene thin films

3.1 Overview

Freestanding polystyrene thin films were found to reach elongations two orders of magnitude larger than what is found in bulk tests. We performed planar tensile testing at multiple strain rates using a push-to-pull based technique to obtain a quantitative stress-strain response of microtomed thin films with thicknesses ranging from 200-500 nm. *In situ* optical microscopy combined with *postmortem* transmission electron microscopy experiments were able to reveal the progression and microstructure of the deformation. It was found that the films undergo shear yielding and that crazing only occurs if the films are thermally annealed prior to testing. Regardless of thermal pre-treatment, the microtomed thin films exhibited extreme ductility, which is at odds with previous reports on the mechanical properties of polystyrene thin films. The strain softening amplitude was also found to directly dependent upon the film thickness for unannealed thin films. Strain softening was not measured in thin films thermally annealed before quantitative testing. Comparisons to other relevant phenomena and current theoretical models are discussed in light of the extreme ductility that was found in what is a nominally brittle glassy polymer.

3.2 Motivation

The popularity of polystyrene as a commodity plastic is driven by its low production cost and thermal formability. One major disadvantage of polystyrene is that it is quite brittle at room temperature, typically fracturing before 2% strain for compression molded specimens, hindering its use as an engineering plastic.[57] The origin of this brittleness resides in the tendency for tensile stresses to localize into crack-like defects known as crazes when the material is below its ductile-to-brittle transition temperature (~90°C). The fundamental difference between a crack and a craze is that the opening of a craze is bridged by fibrils composed of uncoiled molecular chains. Within the crazed region the fibrils show very high ductility with elongations reaching 300%.[58,59] Stress is highly localized within the craze, which leads to chain scission and chain pull-out, where the latter is the dominant mechanism for craze breakdown in polystyrene.[2] Upon craze breakdown, the unbridged crack rapidly grows and propagates through the polymer glass. Fundamentally, while there is immense ductility at the nanoscale, the potential toughness of polystyrene is typically never realized because of the proclivity for craze formation and breakdown.[59,60]

In this chapter we report extreme ductility in microtomed polystyrene thin films under planar tension. These results have not been observed by any other polymer thin film mechanical test method. We use a quantitative push-to-pull (PTP)-based mechanical testing technique for freestanding polymer thin films (Figure 3.1). This technique provides a versatile platform that enables a large range of testing parameters and *in situ* capabilities.

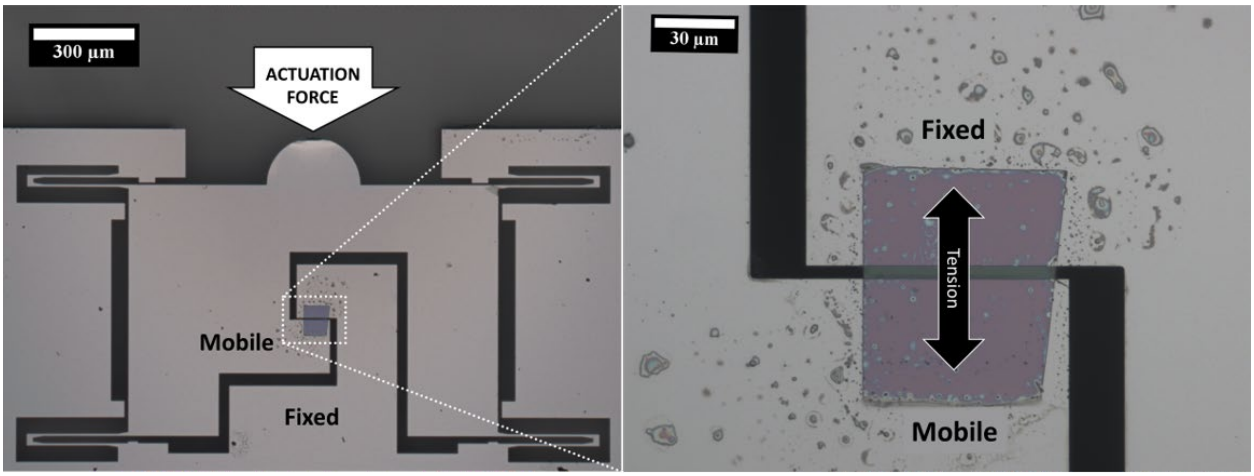

Figure 3.1. Optical images of an oversized Push-to-Pull (PTP) device with a microtomed polystyrene thin film specimen. The mobile region is stabilized by four springs that provide a linear restoring force. When the round 'head' of the mobile region is actuated by a 'pushing' force (LEFT), the 4.5µm wide horizontal gap between the mobile and fixed regions is expanded. This translates the actuation force into a tensile force applied to the specimen spanning the gap (RIGHT). The thickness of the film shown is 240 nm.

3.3 Experimental details

The anionically polymerized polystyrene (M_w = 288,800 g/mol; M_n = 274,600 g/mol; M_w/M_n = 1.05) used for this study was purchased from Pressure Chemical (Pittsburgh, PA) and provided by The Dow Chemical Company. Compression molding was used to produce the bulk polystyrene sample to avoid any molecular alignment artifacts. Thin sections were produced using an RMC PowerTome XL Ultramicrotome equipped with a Diatome diamond knife at a cutting rate of 15 mm/s. A bulk piece of polystyrene was trimmed such that sections were taken far from the compression molded edges. Wet sectioning was performed using deionized water to minimize compression and prevent the thin sections from rolling up. The floating sections were collected and deposited onto a roughened silicon wafer using a loop tool. The thickness of the polystyrene sections ranged from 200 – 500 nm and were 50 – 90 µm wide, as determined by SPM (Figure A.7). This method was validated with a KLA Tencor P17 stylus profilometer (Figure A.5).

In order to deposit and orient an individual thin film section onto a PTP device, a cryo-solvent manipulation technique was developed. The technique makes use of the enhanced viscosity and adhesive properties of ethanol and isopropyl alcohol at cryogenic temperatures. Both of which have a very low solubility in polystyrene and have been shown to have no effect on crazing behavior.[110] Small amounts of either solvent were used in conjunction with a single-hair tool to gently pick up and deposit an individual section across the tensile gap of the PTP device (Figure 3.1). The PTP devices used were obtained from Bruker-Hysitron but were much larger than the typical PTP devices commercially available. The larger dimensions were necessary for controlled

deposition of single sections across the tensile gap using the cyro-solvent manipulation technique. Specifically, the tensile gap of a typical PTP device is 2.5 μm across and 18 μm wide, whereas the oversized PTP devices obtained have a tensile gap of 4.5 μm across and 100 μm wide. When actuated the tensile gap of oversized PTP devices can reach just over 16.6 μm. Due to the limited quantity of oversized PTP devices supplied, we fabricated our own devices. The homemade devices were designed with various gap sizes (2.5 - 30 μm) to better control the amount of strain applied during full actuation and were used to prepare specimens for the postmortem TEM imaging. A detailed description of the sample preparation technique can be found in Chapter 2.

The thin films adhered to the silicon surface of the PTP device very well. Specimen slippage did occur during a couple of tests due to poor specimen placement, which resulted in visible wrinkles and air pockets between the film and the device near the tensile gap as viewed under an optical microscope. Slippage was easily identified by exceptionally large and sharp load drops in the force-displacement curves. The results from these tests were omitted from the analysis. Small particles deposited on and around the thin film during sample preparation acted as fiducial markers to confirm the absence of film slippage by comparing optical images taken before and after testing. These particulates originate from the roughened silicon wafer used to transfer the microtomed films into the cryo-chamber. These particulates are not expected to affect the mechanical response of the film as they are only resting on the surfaces of the film. Excessive particulates underneath the film could potentially hinder the section from fully adhering to the PTP device and lead to slippage, but this is easily identifiable from the force-displacement curve as well as from optical imaging.

The original design intent of the PTP devices was for use with a specialized *in situ* TEM holder (PI 95), but quantitative testing was performed *ex situ* with a Bruker-Hysitron TI 950 TriboIndenter. This is because the higher load capacity of the nanoindenter (~13mN) was necessary to actuate the PTP device with such a large specimen mounted (relative to nanowires). Furthermore, electron beam damage from *in situ* TEM imaging would be detrimental to the mechanical properties of polystyrene and testing *ex situ* also avoided pressure effects from the high vacuum environment of the TEM column. To test the PTP devices in the nanoindenter, they had to be mounted vertically using a custom fabricated mount. A flat punch probe was used to actuate the PTP device to prevent indention of the silicon. Unfortunately, the total travel of the probe was limited to 5 μm, which corresponds to 110% engineering strain. A broad range of strain rates can be reached with the nanoindenter, limited by drift at the slower end. The strain rates used in this work ranged from 0.0033 s^{-1} to 22 s^{-1}. The nanoindenter also has the capability for environmentally controlled testing (temperature and humidity), although all tests were done under ambient conditions. Each PTP device was tested empty, without any specimen, to predetermine the specific spring constant for each device. This allowed the spring force of the device to be subtracted from the experimental data during analysis. It is worth noting here that some of the PTP devices experienced hysteresis or were damaged, leading to inaccuracies when subtracting the spring force from the mechanical response of the film. For these experiments, the derivative of the plastic flow

regime was assumed to be zero in order to remove the device spring force. For the majority of quantitative experiments, the spring force constant for the PTP was accurate when measured before and after testing. Nonetheless, errors introduced by this assumption primarily affect the 2% secant modulus measurement but had an insignificant effect on the SSA.

A 300kV JEOL 3010 was used to acquire all *postmortem* TEM images of the thin films on PTP devices held open at pre-defined amounts of strain. The PTP devices were attached onto a copper stub and mounted onto a Hysitron PI 95 holder. Heavy metal staining was not used, rather significant defocus was applied to properly visualize the deformation features in the strained thin films of polystyrene.

The SPM mode of the nanoindenter was utilized to provide topography maps that were used to determine the film thicknesses. Open-source SPM data visualization and analysis software (Gwyddion 2.52) was used to analyze the topological datasets. This was done by scanning the thin film at an edge near the flat silicon region of the PTP device. The dataset was leveled using the flat silicon as a reference. A histogram of the topography map was generated, and the thicknesses were found by fitting a Gaussian curve to the peaks (Figure A.7).

Topography maps were also generated with a KLA Tencor P17 stylus profilometer using a 2 um radius diamond stylus with 60 degree opening angle. Images were obtained at a scanning rate of 100 μm/s with measurements taken at a 50 Hz rate and a 5 μN stylus force. The scan area was 414 x 250 μm with a pixel size of 2 x 2 μm. The dataset was leveled using the flat silicon wafer as a reference and the RMS surface roughness was determined from these datasets using SPIP software (v6.7.8, Image Metrology, Denmark).

Additionally, an apparatus was constructed to allow PTP testing to be performed *in situ* under an optical microscope (Leica DM2500 M), where actuation of the device was performed using a piezo controlled micromanipulator (Burleigh PCS-5000). *In situ* optical testing was done by mounting self-closing tweezers to the microscope stage, which held the PTP device in place while a micromanipulator fashioned with a needle could be positioned to actuate the device under piezo control. Force measurements were not available during the *in situ* experiments, but strain could be estimated from the images collected using a free image analysis tool (ImageJ 1.52a). The micromanipulator was able to fully extend the PTP gap, which corresponds to ~370% strain. While force measurements were unavailable during these tests, the images provided displacement measurements and insight into the deformation mechanism (Figure 3.2).

Annealing was done after the films were deposited onto the PTP device for >15 hours at a temperature near the bulk T_g of polystyrene (~100°C) and was performed under constant vacuum (~635 Torr). After which, the chamber was cooled to room temperature at a rate of about 0.3 °C/min. Annealing was performed for two reasons: to remove residual solvent from the transfer of the films to the PTP device and to remove residual stresses inflicted via microtomy, which would accelerate physical aging. The effect of residual solvent was expected to be negligible since both ethanol and isopropyl alcohol are poor solvents for polystyrene but may have caused slippage if

excess solvent between the film and PTP device was present. Specific annealing temperatures and times are provided in the figure captions.

3.4 Results

3.4.1 *In situ* optical microscopy

In situ optical microscopy experiments were performed to capture the progression of the deformation. A micromanipulator was used to actuate the PTP device over its full range of motion. The thin films in these tests reached unprecedented strains exceeding 300% (Figure 3.2), which was calculated by measuring the percent change in the PTP gap. The deformation typically initiated at the edges of the PTP gap and grew towards the center of the specimen (Figure 3.2a-c). This is probably due to a stress concentration present at the corner of the silicon where the thin film becomes freestanding.[61] Annealing the films after placing them on the device exaggerated this artifact since the material would creep into the gap to form a kink where the film becomes unsupported, resulting in an even stronger stress singularity. As such, the deformation tended to nucleate at the two edges of the tensile gap but would also nucleate at the centerline of the specimen as larger strains were reached. In any case, the deformation was initially highly localized, where the majority of the material seemed plastically undeformed as there was not any noticeable change in the refractive color of the film. As the tensile experiment proceeded, the regions of nominally undeformed polystyrene were consumed by the growing area of plastic deformation, creating islands of plastically undeformed material. Typically, crazes are oriented perpendicular to the axis of tension and maintain a roughly uniform width.[59] The nonuniform geometry of the deformation features was an indication that these were not the typical crazes seen in bulk polystyrene. Although most films remained largely intact at the maximum attainable strains, some films experience failure through void nucleation and ductile tearing, rather than the expected brittle fracture (Figure 3.2c). Close-up views of the macroscopic deformation features at the highest strains (separate experiments) are shown in Figure 3.2d, e. The microstructure in the deformed state could not be determined from these images due to the limited resolution of optical microscopy.

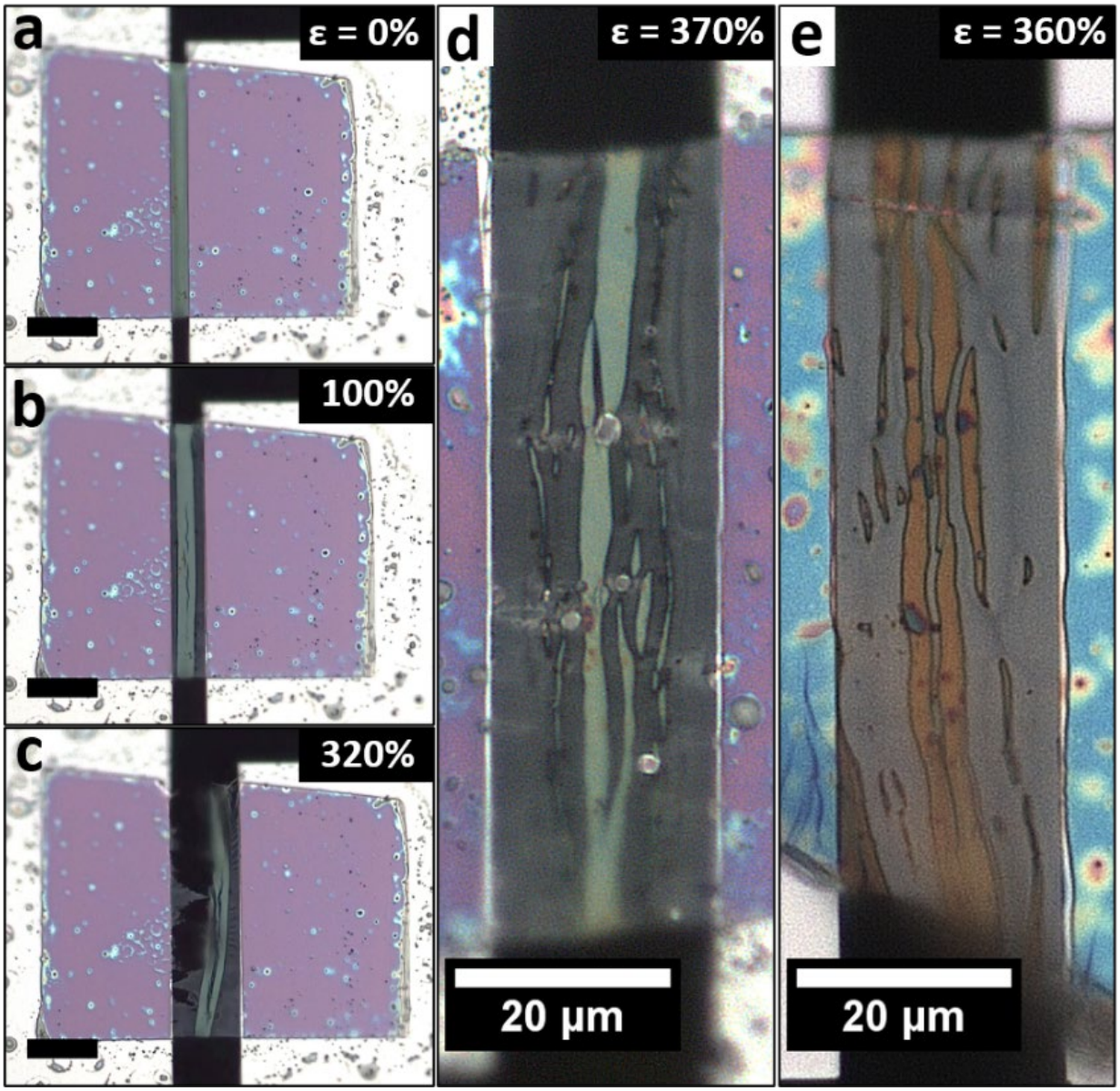

Figure 3.2. Snapshots taken from videos obtained during in situ optical microscopy experiments revealing the macroscopic deformation features of microtomed polystyrene thin films. a-c) Sequence of images taken at 0%, 100%, and 320% engineering strain (scale bars = 20 μm). b) Deformation tended to initiate at the edges of the tensile gap, but also nucleated at the centerline as the test proceeded. c) Some thin films experienced ductile tearing, but even at large strains the fracture does not propagate across the film to cause catastrophic failure. d-e) Zoomed in images of the deformation features taken at the largest strains reached for each experiment. The loss of color in the deformed regions indicates the thickness has been reduced below the half-wavelengths of visible light, where only the islands of nominally undeformed material retain their original interference color (polystyrene is otherwise colorless). e) The film shown was mounted 90° to the cutting direction so that the straining direction was perpendicular to the cutting direction. This

omits any potential anisotropic effects induced during microtomy as the source of the extreme ductility observed. (Prior to testing these films were annealed at 95°C for 15 hours. Thicknesses = 240 (a-c), 280 (d), and 250 nm (e).

3.4.3 *Postmortem* TEM

By holding the PTP device open at selected strain levels, TEM was used to characterize the deformation microstructure of polystyrene thin films (Figure 3.3). The effect of thermal annealing was also investigated by comparing the microstructure of films that were strained within 12 hours of microtoming to films of the same batch that were annealed (100°C for 20 hours). Even though all of the films tested experienced great ductility without catastrophic failure, there was a stark difference between the annealed and unannealed thin films: the annealed films deformed by crazing while the freshly microtomed films exhibited shear yielding. For the annealed films, crazing was ubiquitous even at lower strains (Figure 3.3a, b). The crazes did not propagate in the typical fashion observed in bulk but instead propagated with crack-like geometries that intersected each other and isolated islands of nominally undeformed material. The craze fibrils also possessed a mixed character between bulk "3D crazes" and thin film "2D crazes" as described elsewhere.[5,20,22,62] Fine fibrils with diameters ranging from 5-10 nm consistent with 3D crazes were accompanied by coarse 2D craze fibrils with diameters ranging from 40-60 nm. In some instances, the annealed films contained sparse regions where the deformation did not have any fibrillation or resembled overlapping perforated sheets with layers of unconnected holes (Figure A.1). Even though the annealed films experienced crazing similar to their bulk counterparts, they did not experience brittle fracture. Rather, a film brought to ~50% engineering strain had no voids or tears and another film brought to ~150% engineering strain had only one large void near the edge (Figure A.2a, b).

Polystyrene films that were microtomed, strained, and imaged within the same day without any thermal annealing were found to plastically deform through shear yielding and out-of-plane necking, but not crazing (Figure 3.3c, d). An unannealed film strained to an engineering strain of ~50% was completely devoid of any fibrillation, even upon cycling the load three times. For this film, through-thickness necking was very uniform and featureless, consisting of a single uninterrupted band that spanned the entire width of the film (Figure A.2c). No voiding or fracture occurred. For another unannealed film brought to exceptionally large strains (~275%), several regions of shear deformation nucleated and propagated in a crack-like geometry, intersecting to produce islands of undeformed material similar to the geometry of annealed films. In some of the highly deformed regions, streaks of uneven thinning were oriented parallel to the axis of tension (Figure 3.3d). Some coarse fibrillation occurred, but only in small volumes between two isolated islands of undeformed material (see top left corner of Figure 3.3d). The films were also extremely tolerant to any notches or damage present at the edge of the film. A small notch was accidentally introduced on the edge of an unannealed film, but it did not propagate to cause catastrophic failure

even at exceptionally large strains. This indicates that besides extreme ductility, the films are also extraordinarily tough (Figure A.2d).

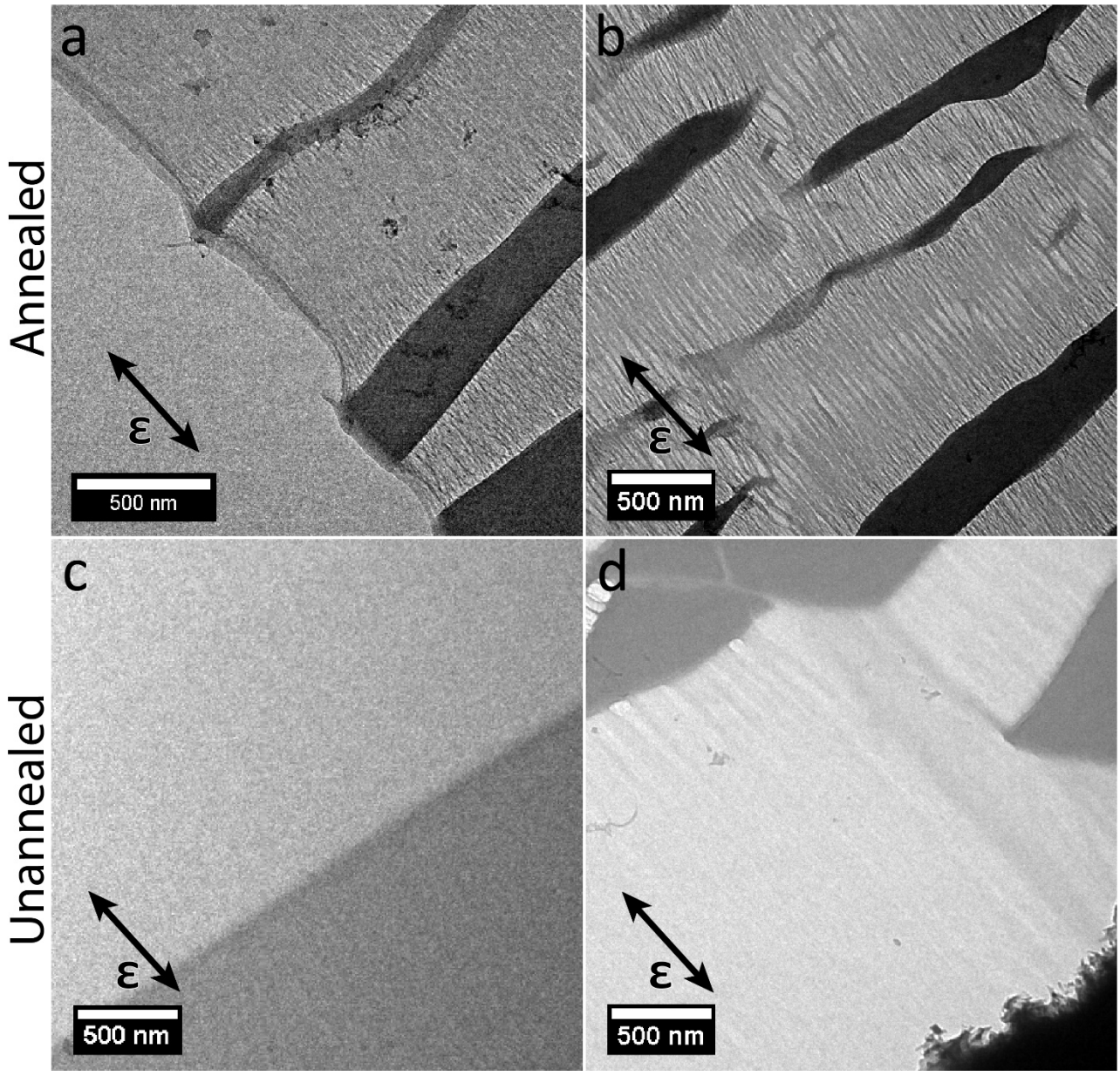

Figure 3.3. Postmortem brightfield TEM images of four polystyrene thin films deformed in planar tension using a PTP device and held at ~50% (a, c), ~150% (b) or ~275% (d) engineering strain to compare the effect of annealing on the deformation microstructure. The arrows indicate the tensile axis. a) Annealed for 20 hours at 100°C before straining to ~50% engineering strain, resulting in fine crazes present at all the crack-like deformation features across the film. b) Annealed for 20 hours at 100°C before straining to ~150% engineering strain, resulting in crazing with thicker, more spaced fibrils in-between islands of nominally undeformed material. c) Unannealed and

strained to ~50% engineering strain, resulting in no crazing even after cycling the load three times. A continuous region of through-thickness thinning spanned the entire width of the film. d) Unannealed and strained to ~275% engineering strain, resulting in deformation dominated by shear yielding. Streaks of thickness variation oriented parallel to the axis of strain appeared in some of the deformed regions. The thicknesses of the films in a, b, c, and d were 270, 240, 250, and 260 nm, respectively. Optical images of these same films are shown in Figure A.2**.**

3.4.4 Quantitative mechanical testing

Quantitative mechanical testing of freestanding polystyrene thin films was performed using the PTP-based technique[63,64] described in the experimental section. All of the specimens exhibited extreme ductility, even though bulk polystyrene is quite brittle at the testing temperatures, viz. room temperature. The nanoindenter used to actuate the PTP devices for quantitative measurement (as opposed to the more coarse method of using a micromanipulator for the tests under the optical microscope) was limited to a displacement of five microns and thus strains using the nanoindenter were limited to a maximum of 110%. Notwithstanding, none of these tests resulted in fracture even though the strains attained in these experiments were two orders of magnitude larger than what is possible in bulk tensile testing of polystyrene. Two example stress-strain curves generated from this technique are shown in Figure 3.4a. The nanoindenter was capable of high data acquisition rates (up to 30kHz) and mechanical stability that allowed a wide range of strain rates to be used ($\dot{\varepsilon} = 10^{-4} - 10^{2}$ s^{-1}). Surprisingly, the observed extreme elongation in polystyrene was present even when deforming at the highest strain rate of 22 s^{-1} (Figure A.3).

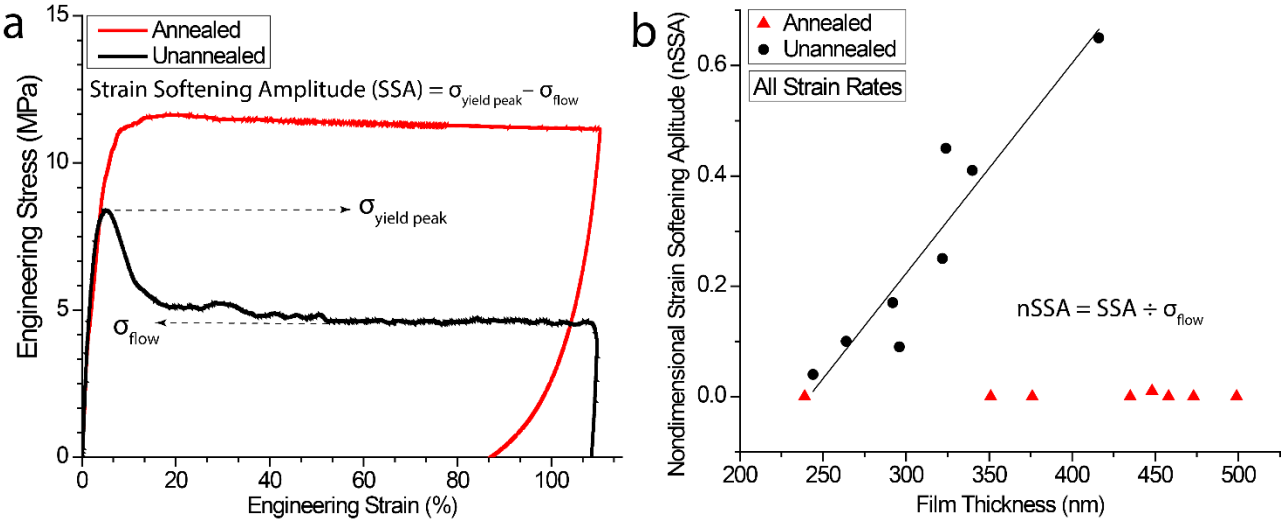

Figure 3.4. a) Example stress-strain curves for polystyrene thin films obtained through the PTP-based polymer thin film technique. Strain softening can be clearly observed in the mechanical response of the unannealed thin film (lower black curve, thickness = 320 nm, $\dot{\varepsilon} = 3$ s^{-1}) but is

practically nonexistent in the annealed thin film (upper red curve, thickness = 450 nm, annealed for 15 hours at 95°C, $\dot{\varepsilon} = 0.03\ s^{-1}$). b) Graph displaying the linear trend of the nSSA (defined by the equations shown in a, b with respect to film thickness. The solid line is a linear best fit to the nSSA datapoints for unannealed films.

From these experiments, mechanical quantities such as the elastic modulus, yield stress, and flow stress could be extracted from the engineering stress-strain curves. Besides the severely abnormal ductility, other mechanical features diverged significantly from the typical response observed in bulk polystyrene as well as spin-cast thin films. The most obvious was the post-yield plastic flow. This type of cold drawing behavior is typical for many ductile glassy polymers, but has not been observed for polystyrene films at room temperature to date.[65] Annealing seemed to have no impact on the ability of the films to enter plastic flow, nor did it seem to have an effect on the flow stress (Figure A.4b). This was peculiar since TEM imaging revealed that annealing altered the deformation mode from shear yielding to crazing (Figure 3.3). Strain softening was always present in unannealed films, but even mild annealing prior to straining caused a gradual yielding without any sign of strain softening. Following the analysis method used by Chen and Schweizer,[66] the strain softening amplitude (SSA) was quantified by taking the difference between the peak yield stress and the plastic flow stress (Figure 3.4a). The yield and plastic flow stresses were found to strongly depend upon the strain rate, although more data at the upper strain rates are needed to confidently characterize any strain rate dependencies. This was expected since this kind of strain rate dependence is known to occur in polystyrene under compression[67] and in tension at elevated temperatures.[68] Because of this, the SSA was normalized by dividing by the flow stress, referred to as the nondimensional strain softening amplitude (nSSA), in order to compare different strain rates (Figure 3.4b).[66] Interestingly, the nSSA of unannealed films seemed to linearly depend upon their thicknesses. No other thickness dependent trends were found (Figure A.4).

The values of the 2% secant modulus varied significantly, yet even the largest value was an order of magnitude lower than the elastic modulus for bulk polystyrene. This was the case regardless of annealing conditions or strain rate (Figure A.4). Potential origins of the reduced elastic modulus are addressed in the discussion section below.

3.5 Discussion

While there have been major contributions to understanding the mechanical properties of polymer glasses, a definitive model that can successfully describe all of the phenomena exhibited by glassy polymers is nonexistent. Thus, it is difficult to assign a particular mechanism as being responsible for the observations presented here with a high level of certainty. In light of this, we make best efforts to compare our observations with current theoretical models and similar phenomena in the following discussion.

3.5.1 Specimen geometry and constraint

One of the most interesting aspects of the extreme ductility we have observed is that the films tested were quite thick, between 200 and 500 nm, compared to previous studies on spin-cast ultrathin films. In the literature dealing with freestanding polymer thin films, no deviation from bulk mechanical properties, such as the elastic modulus, is reported for films thicker than ~150 nm.[5,6,11–17,20–22] Furthermore, none of these studies report any significant thickness effects on the strain-to-fracture. The microtomed films in this study are thick enough such that the mechanical properties would be expected to belong in the bulk regime. Instead, the microtomed films deviate from this trend in several ways: compared to either bulk or spin-cast experiments, the strain-to-fracture is two orders of magnitude larger and the elastic modulus (as measured by the 2% secant) and flow stress are a magnitude lower. Within the thickness range tested, however, neither the 2% secant modulus or flow stress showed any thickness dependent behavior (Figure A.4), implying that the phenomena observed in the microtomed films is not a mere extension of the thin-film effect observed in spin-cast films.

Thickness variation was present in our microtomed films, but since only a small fraction of the film bridged the PTP gap for straining, any gradual thickness gradient in the film would be negligible. Periodic features parallel to the cutting direction were observed in microtomed films thicker than 300 nm. These features were consistent with microtome-induced through-thickness shear bands in poly(methyl methacrylate) (PMMA) characterized by Sun and coworkers.[48,50,69] Similar to their work, once below a critical thickness of roughly 300 nm for the cutting speed used (15 mm/s), the polystyrene films became smooth and absent of periodic shear bands. All films reached extreme elongations regardless of the appearance of microtome-induced shear bands as well as when the film was strained perpendicular to the cutting direction (Figure 3.2e, Figure 3.3b). The through-thickness shear banding also did not affect the strain softening behavior, since this did not occur in films microtomed thinner than 300 nm and the linear nSAA trend does not deviate on either side of this thickness. Additionally, the root-mean-square (RMS) surface roughness was found to be less than 4 nm across the entire film (Figure A.5).

It is important to observe that the planar tension test differs from an ordinary tension test. The specimens adhere to the PTP surface and do not slip. This allows for the application of tensile forces to open the tensile gap, but it also inhibits the transverse contraction of the material in the width. Given the large width, the normal strain component in the width direction is effectively zero. This constraint generates a tensile normal stress in the width direction which induces through thickness thinning, on top of the thinning induced by the gap opening normal stresses. This deformation state, in the context of rubber elasticity where the material is typically incompressible, is termed 'pure shear.' The terminology stems from the fact that the material elements angled at 45-degrees through the thickness of the specimen are deformed in pure shear. In the context of polystyrene, the deformation state is not exactly pure shear at 45-degrees but is still approximately so.

Linear elastic simulations were performed to investigate the stress and strain distributions of a thin film when tested with a PTP device (Appendix B). The simulations considered the fact that the film is asymmetrically gripped by one surface in the planar tension specimen geometry. The simulations predict a contraction at the sides, which is observed experimentally (Figure B.8). As expected, there is a stress concentration at the edge of the tensile gap where the thin film becomes freestanding and a shear stress concentration where the film adheres to the PTP device (Figure B.9 – B.12). Apart from near the edges of the tensile gap and sides of the film, the stress field is very uniform throughout the freestanding volume of the film. The deformation features, albeit shear or crazing, were observed both at the edge of the PTP gap as well as throughout the freestanding region. Taken together, the experimental evidence and the simulations confirm that the enhanced ductility is not due to non-uniform stress distributions or any abnormalities imparted by the specimen geometry or single-sided gripping configuration of the PTP device. Further analysis and discussion can be found in the Appendix B.

Furthermore, nanoindentation was also performed on thick spin-cast films (~1μm), thick microtomed films (~1μm), and the microtomed surface of a bulk block-face. The indentation moduli measured for each type of sample were consistent with each other and reasonably close to reported values for bulk polystyrene (Figure A.6). These results imply that the mechanism(s) responsible for low stress plastic deformation is activated primarily in planar tension.

3.5.2 Microtomy *versus* spin-casting

As mentioned in the introduction, spin-cast films initially contain residual solvent and chain conformations are far from equilibrium. Depending on the molecular weight used, vacuum annealing may not be sufficient to remove these artifacts.[32–34] Furthermore, several studies have concluded that the packing density for spin-cast films is lower than in the bulk.[70–72] A microtomed film, however, is a 'slice from bulk' maintaining the bulk packing density and is devoid of any residual solvent. Regardless, we are unaware of any studies that suggest that these factors alone are enough to explain the dramatic difference in mechanical properties between the two sample preparation methods. Other, more relevant factors, are discussed below.

Another difference to consider is the method used to shape the tensile specimen. Hasegawa *et al*. use oxygen reactive ion etching with a mask to produce their specimens for pseudo-freestanding tensile tests.[15] Reactive ion etching is known to induce crosslinking in many polymers, including polystyrene.[73] Therefore the dogbones fabricated by Hasegawa *et al*. may have had a significant amount of crosslinking at the edges. At high levels of crosslinking densities, both crazing and shear yielding are suppressed, leading to cracks propagating in a brittle manner at relatively low strains.[74] The rectangular pseudo-freestanding specimens prepared by Liu *et al*. were cut with a razor blade, which may have introduced flaws at the edges leading to premature fracture.[14] This is apparent in the stress-strain curves of their films, which exhibited abrupt fracture without any sign of yielding. Improvements to the technique were subsequently made by Bay *et al*. using a laser to cut a dogbone geometry from spin-cast films of polystyrene.[11,13] While these

tensile tests resulted in yielding, the strain-to-fracture did not exceed 12% for any of the films tested. It has also been shown that laser ablation of polystyrene leads to degradation and a reduction in T_g but it is not clear how this might affect the mechanical properties, specifically strain-to-fracture.[75] These examples not only highlight the difficulty in fabricating thin film tensile specimens but may offer an explanation as to why spin-cast polystyrene films do not achieve anywhere near the ductility observed in this work. Note that the 12% strain-to-fracture observed by Bay *et al*. is larger than typical bulk polystyrene fracture strain, possibly indicating that spin cast thin films may actually be more ductile than currently realized. In contrast, here a microtome was used to trim the bulk material into the appropriate geometry with a high quality diamond knife, which should provide thin film specimens with far fewer defects at the edges. It is further noted that our films are resistant to crack propagation from damage incidentally inflicted to the film edge during handling (Figure A.2d).

Concerning the role of chain entanglement effects in enhanced ductility, research by Si *et al*. predicts an increase in strain-to-fracture due to loosely entangled chains and less *inter*chain entanglement in ultrathin polystyrene films.[16] Modeling of "thin layer yielding" in polystyrene by Michler and coworkers also predicts highly ductile behavior, with strain-to-fracture reaching 300% for films with a thickness less than 30 nm.[58] Mechanical testing of multilayered tapes of co-extruded polystyrene and polyethylene showed enhanced ductility in the polystyrene phase when the thickness of the layers was reduced below 800 nm, giving rise to a strain-to-fracture of 30%.[76] It is also worth noting that the stress-strain curves they obtained showed strain softening followed by a plastic flow regime similar to our results. It is surprising then that enhanced ductility not yet been reported for freestanding polystyrene thin films until now.

A possible explanation for the lack of ductility reported in literature is the fact that spin-cast preparations are more vulnerable to contamination. Spin-cast films have an area on the order of several square centimeters or more, so unless the solvent is well filtered and spin-casting is performed in a dust-free environment, the probability of a dust particle contaminating the thin film is significant. Such contamination is reported in several TEM investigations involving solvent cast thin films of polystyrene, where fracture initiates from an embedded dust particle.[59,74,77,78] In studies by Yang and coworkers, "ultraclean" thin films of polystyrene prepared by filtering the solution prior to spin-casting resulted in significant increase in craze stability and strain-to-failure; where the median strain for fibril breakdown doubled to reach 20%.[77,79] Furthermore, TEM images of fibril breakdown at the site of a dust particle leave a void with a sharp edge, whereas voids in the filtered films show gradual thinning and a fan-like tapered edge.[77] The latter type of fibril breakdown was observed by TEM in the microtomed films in this work. Particulate contamination is also thought to be the source of internal crazing in bulk polystyrene, with dust particles clinging, by electrostatic attraction, to the pellets used in thermal molding processes.[80] The thin films used in this study were prepared via microtomy, where sections were cut from a compression-molded bulk sample. If we assume the concentration of particulates in the bulk sample used for microtomy is equal to that found in spin-casting methods, the probability of any particulates being found

within a volume (~0.0002 mm^3) that is orders of magnitude lower is proportionally lower. Without explicit knowledge of the sample preparation methods used in other studies, it is unknown to what degree contamination hinders larger strains from being reached in spin-cast films. For the microtomed films tested here, however, the volume is so small that it should be devoid of embedded particulates and any premature fracture due to contamination would be easily identified by TEM, which did not occur.

Particulate contamination and edge effects aside, the primary difference between spin-cast and microtomed thin films is the surfaces. During microtomy, the diamond knife inflicts brittle fracture by means of chain scission and chain pullout. Experiments in which the reduction in molecular weight was measured found that chain scission is the predominant fracture mechanism during room temperature microtomy of polystyrene.[81,82] These researchers also calculated the areal density of fractured chains to be 6.5 x 10^{13} scissions/cm^2, which was shown to be independent of molecular weight. Using the equations from their analysis of polymer entanglements, the number of chain segments to pass through an arbitrary plane was calculated to be 9.2 x 10^{13} segments/cm^2 for polystyrene (calculation in SI).[81] Thus, compared to the surfaces of spin-cast films, the surfaces of microtomed thin films contain a much higher concentration of chain ends and a broader molecular weight distribution. The chains at the native surface of bulk polystyrene are known to have enhanced mobility, residing in a rubbery state.[83,84] Due to the dominance of chain scission at the fractured surfaces, the microtomed films are expected to have a large concentration of chain ends relative to bulk. Based on the provided areal densities, the microtomed surface consist of roughly 70% chain ends by area. Chain ends are known to reduce the local density and friction as well as enhance local segmental mobility.[2,85–87] For example, depression of T_g with decreasing molecular weight is thought to be due to the increasing chain end concentration.[87] Therefore, the chains at the fractured surfaces of microtomed thin films can be expected to have a segmental mobility that is much higher than the native surface chains of bulk polystyrene. To better understand how this might lead to enhanced ductility, we must discuss a related phenomenon known as mechanical rejuvenation.

3.5.3 Mechanical rejuvenation

Room temperature ductility in bulk polystyrene has been observed in the special case of mechanical rejuvenation.[88–90] When bulk polymer glasses are mechanically pre-conditioned, by cold rolling for example, the material is toughened and exhibits enhanced ductility, even in tension. This phenomenon is transient, however, and is especially short lived in polystyrene. Tensile experiments on bulk polystyrene specimens immediately after cold rolling resulted in ductile behavior with elongations reaching 20% before fracture, but when allowed to age for as little as 30 minutes at room temperature the low-strain brittle fracture behavior returned.[89] The ductility of mechanically rejuvenated polystyrene has been reported to persist after a week of aging, but even mild annealing at 20°C below T_g for three days accelerates the aging to restore brittle behavior.[88,90] In the case of the thin films studied here, mechanical rejuvenation may have been inflicted through

microtomy, but there are a few major differences between our observations and the trends reported for bulk polystyrene.

Firstly, thin films that were annealed for 15 hours at 115°C exhibited extreme elongation when strained three weeks after microtomy. Furthermore, aging has been shown to be accelerated in thin films of glassy polymers ranging from tens of nanometers to several microns thick.[91–97] Therefore, it is difficult to imagine that mechanical rejuvenation effects would remain in thin films when these conditions are enough to erase the phenomenon in bulk specimens. Secondly, both compression and tension, mechanical rejuvenation of bulk polystyrene removes strain softening. If mechanically rejuvenated bulk polystyrene is allowed to age, the strain softening and yield stress increases logarithmically with time until brittle behavior inevitably returns.[88] As shown in Figure 3.4a, the trend appears to be opposite in microtomed films: unannealed specimens exhibit strain softening yet annealed specimens do not. Interestingly, semi-freestanding spin-cast thin films performed by Bay *et al*. and Hasegawa *et al*. exhibit strain softening, but the phenomenon is not observed in the stress-strain curves of Bay *et al*.'s experiments on freestanding films.[11,13,15] Lastly, strain softening is thought to be important in the initiation of strain localization, in which its absence leads to homogeneous deformation if the intrinsic strain hardening behavior is sufficiently large.[89] This too is contrary to our observations, in which crazing appears in annealed films and shear yielding is the preferred deformation mode in unannealed films (Figure 3.3).

Mechanical rejuvenation alone cannot explain the extreme ductility observed, but there are aspects of the microtomed films which are analogous to the phenomenon, particularly with respect to changes in the segmental mobility of the molecular chains. Therefore, much insight can be gained by considering the current molecular theories describing mechanical rejuvenation in regard to the situation of microtomed thin films.

3.5.4 Enhanced segmental mobility

Creep experiments performed on mechanically rejuvenated polystyrene by van Melick *et al.* show that segmental mobility is increased after cold rolling even though the density increased. The researchers also pointed out that the recovery of the yield stress is independent of molecular weight, ascribing the relaxation of the polymer chains to be on a segmental scale.[88] The predominant understanding of ductility in polymer glasses is that it is highly dependent upon main-chain segmental dynamics. Only when the time constant for segmental relaxation is near or below the experimental time scale, as determined by the strain rate, can brittle fracture be avoided through segmental rearrangement.[2,98,99] Similarly, the ductile-to-brittle transition temperature for glassy polymers is highly dependent upon segmental dynamics.[98,100]

The role of segmental dynamics in mechanical rejuvenation effects is described well by the molecular theory put forward by Chen and Schweizer (Chen-Schweizer theory). In their work, a nonlinear Langevin equation-based microscopic theory for polymer glasses under deformation identifies the amplitude of density fluctuations, S_0, as a primary variable that can be affected by external deformation.[66,101–103] S_0 can be thought of as the amount of segmental disorder, or a

segmental packing parameter, which is directly related to segmental mobility and describes how far the system is from equilibrium. The authors point out that in several studies of aging in polymer glasses, the equilibration times for the volume, enthalpy and mechanical properties are essentially identical, pointing towards a single generic molecular process that dictates all observables: the mean structural or alpha relaxation time, τ_α.[101] In their theory, the segmental dynamics are described in terms of a dynamic free energy in which intersegmental interactions impose a potential energy barrier, i.e. segmental caging. Thus, the alpha relaxation time depends on S_0 through the potential barrier. Moreover, yielding occurs when the alpha relaxation time becomes sufficiently short such that plastic deformation can take place via segmental rearrangement as a result of a reduced potential barrier height, else crazing occurs. This model successfully accounts for several phenomena found in polymer glasses, including mechanical rejuvenation, which drives S_0 higher, and physical aging, which reduces S_0.

Building upon the Chen-Schweizer theory, Wang and coworkers proposed a phenomenological model in which the polymer glass can be divided into a hybrid structure, consisting of a network of load-bearing strands (LBSs) and the primary structure composed of non-load-bearing strands (nLBSs).[2,104] Often, the entanglement density is used as a predictor of ductility in polymer glasses, but this line of reasoning does not account for processes that increase ductility without increasing the entanglement density, such as increased temperature, melt stretching, and mechanical rejuvenation. Wang *et al*. realize that some fraction of entanglements become load-bearing (LBSs) when the material is strained. Under an applied stress the LBSs undergo increased tension between thier molecular entanglements, whereas the nLBSs only interact through van der Waals forces. In their model, only when segmental mobility is high enough can LBSs adjust to relieve chain tension; similarly, only in this condition can nLBSs convert to LBSs. These processes prevent chain tension from building up beyond the threshold of chain failure, typically in the form of chain pullout. It is worth noting here that tensile experiments performed in a high pressure environment lead to suppressed crazing and ductile behavior in polystyrene. Therefore, one can conclude that chain pullout is the dominant mode of molecular scale failure in polystyrene and not chain scission; this follows, since chain scission is related to bond strength, which should not change with ambient pressure.[2] As sufficiently high segmental mobility (relative to the strain rate) delays chain failure, the network of LBSs becomes denser and distributes the stress across more LBSs to suppress strain localization (i.e. the polymer glass exhibits ductility). Conversely, if segmental mobility is too low during deformation, the chain tension of LBSs will exceed the threshold for chain failure, which will lead to highly localized deformation (crazing) and subsequent brittle fracture.[2] In short, segmental mobility is crucial for ductility in a polymer glass.

A key finding in the work by Chen and Schweizer relevant to our data is that the density fluctuation amplitude, S_0, is linearly proportional to the strain softening amplitude (SSA).[66,103] This was shown explicitly by computing the constitutive equation of their model using material parameters of PMMA, where strain hardening was ignored as a simplification.[66] Their

simplification was the actual case in our study, since none of the microtomed films exhibited strain hardening for at least 110% strain regardless of thermal annealing, strain rate, or the presence of microtomed-induced shear bands. Following their analysis, the SSA was defined as the difference between the peak yield and plastic flow stresses. They found that the SSA increases with strain rate, implicating that even though the yield and flow stresses are both roughly logarithmically dependent on the deformation rate, the yield stress is more sensitive. In order to normalize for the different strain rates, the nondimensional strain softening amplitude (nSSA) was employed; defined as the SSA divided by the flow stress. In their model, they attribute the relationship between the nSSA and time of aging after mechanical rejuvenation to directly depend on S_0, which in turn enhances segmental mobility.

3.5.5 Thickness dependence of strain softening in unannealed films

As outlined in the proceeding sections, the aging kinetics in bulk polystyrene are fast relative to other polymers, leading to short-lived ductility following mechanical rejuvenation, and aging has been shown to be accelerated in thin films.[91–97] This leads us to believe that any microtomed-induced mechanical rejuvenation of the polystyrene thin films can be expected to be promptly diminish before straining experiments could be performed. In comparison to other thin film studies, these films are thick enough such that they should exhibit bulk properties, such as strain softening. However, the situation at the microtome fractured surfaces is quite different. The high chain end concentration effectively creates a layer of persistent segmental disorder and reduced alpha relaxation time.[2,85–87]

We propose that the enhanced dynamics at the microtomed surfaces of the film dominate the mechanical behavior below some critical thickness, which is greater than 500 nm based upon our data, leading to extreme ductility. As the film becomes thicker, the disordered surfaces contribute less and the well-aged volume in the middle of the film increasingly dominates the mechanical response. Thus, the strain softening amplitude is approximately linear with respect to increasing film thickness since the disordered layer of high chain end concentration remains constant in total volume (Figure 3.4b). As the disordered volume becomes negligible with respect to the total volume, the nSSA would be expected to become constant until the inevitable return of bulk brittleness dominates again. However, the details of this transition are unknown since we were unable to prepare and test films thicker than 500 nm. A linear fit of the nSSA data for unannealed films predicts zero strain softening at a thickness near 240 nm. This indicates that any surface effect induced by the microtome propagates about 120 nm into the film from each surface. This distance is several factors larger than that of an individual polymer coil (R_g = 15 nm for 288.8 kg/mol polystyrene), implying that the effect cannot simply originate from the fractured chains at the surfaces alone. It is possible that the fractured chains are strained during microtomy and may transfer stress to entangled chains farther from the surface such that S_0 is increased deeper within the film. This idea is supported by finite element analysis by Sun *et al*. that modeled plastic strains imposed during the microtomy of 200 nm PMMA thin films using a cutting speed low enough to avoid shear band formation.[50] These researchers showed that plastic strains of 0.005 – 0.01 were

reached throughout the entire film thickness and strains as high of 0.5 were inflicted over 80 nm away from the cut surface. Thus, it is not unreasonable to assume that inelastic effects can penetrate 120 nm into a microtomed film, as indicated by our data. So, even though the inner core of the film is well aged and exhibits the expected strain softening, the situation at the microtomed surfaces is analogous to the phenomenon of mechanical rejuvenation in that S_0 has been significantly increased. The difference is that the increase in S_0 originates from chain scission and plastic deformation inflicted by microtomy, which is able to persist at room temperature for up to several weeks based upon our experiments. Therefore, a plausible explanation for why our microtomed thin films exhibit enhanced ductility is that they are analogous to mechanically rejuvenated bulk polystyrene in this manner.

3.5.6 Effect of annealing

The question remains of why crazing is suppressed in unannealed thin films, but even mild annealing results in crazes. Further puzzling is how the crazes can be so stable such that the film remains highly ductile. Crazes are thought to initiate at heterogeneities in the molecular network, such as well as at surface defects or particulate contaminants, but theories describing the molecular mechanism are not completely satisfactory at this point.[105,106] It is thus more useful to consider the well-established theory regarding craze advance and growth. It is generally accepted that craze propagation is best described by the Taylor meniscus instability mechanism, first proposed Argon and Salama.[107] In short, the meniscus of the strain-softened polymer melt ahead of the craze is too viscous to uniformly retract as the surface area grows under strain. This instability causes a finger-like structure to form and fibrils are formed as the craze propagates. Furthermore, the growth of the craze is sustained by the surface drawing of unfibrillated material into the craze, analogous to macroscopic fibril drawing of polymers. The meniscus instability mechanism has been very successful in predicting craze growth velocities, fibril thickness, and has been directly observed via TEM imaging.[78,107–109] Furthermore, a crazing model termed a "two stage entanglement network model" or "domain model" proposed by Kausch and further developed by Michler argues that chain ends, nonentangled shorter macromolecules, defects, and local concentrations of free volume constitute a mechanically weaker material between entangled segments. The authors claim their model better describes the details of the craze structure than the meniscus instability model. What is interesting about their model is that it recognizes the role of chain ends and short chains, both of which are in higher concentration at the surfaces of microtomed thin films. Additionally, the craze morphology of polymer thin films has been shown to change due to the lack of out-of-plane stress. These "2D crazes" contain coarser fibrils than bulk crazes and can even avoid fibrillation altogether; forming a perforated sheet.[5,20,22,78] TEM images of our annealed microtomed films revealed coarse 2D fibrils as perforated sheets consistent with this literature (Figure A.1). The reasoning for the change in microstructure is as follows: the lack of out-of-plane constraint results in a reduction in the fibril stress required for surface drawing.[20] This leads to an increase in the perturbation wavelength of the unstable meniscus, resulting in coarser craze fibrils.[22]

As previously discussed, we assert that the high chain end concentration enhances segmental mobility at the microtomed surfaces. The Taylor meniscus instability mechanism is consistent with the observations in the unannealed films. If the viscosity of the strain-induced meniscus is lower, such that it is sufficiently stable under strain, then surface drawing can occur without fibrillation, and crazing would be avoided. When annealed, whole chain mobility provides a means to relieve residual strain and allow chains to conform to a configuration closer to their equilibrium coil size. This will serve to reduce S_0 further than attainable during room temperature aging. When a tensile stress is applied to the annealed films, the viscosity of the strain-induced meniscus is increased such that it becomes unstable at lower strain rates and crazing occurs. As previously mentioned, a reduction in S_0 is associated with crazing[101] and chain ends are one source believed to initiate crazes along with surface roughness.[58,106] So the fractured surfaces may provide a means to initiate multiple crazing events and the lack of out-of-plane stress may allow surface drawing to occur at a lower stress. In support of this interpretation, we found evidence of extreme fibril stability in the *postmortem* TEM imaging of highly strained annealed films. The fibrils at the midrib of the craze coarsened significantly with large voids between them, as can be seen in Figure 3.3b. Also revealed in TEM imaging was evidence that crazes seemed to initiate and grow from the surfaces. Fibrillation was observed to be superimposed on top of the islands of undeformed material, which also had reduced contrast due to thinning from surface drawing, also shown in Figure 3.3b. This supports the idea of a highly mobile surface layer easily drawing into the craze, enabling stable craze growth. Finally, the lack of particulate contamination provides the crazes the opportunity to grow with extreme stability.

3.6 Summary & conclusions: A unique phenomenon

The experimental findings presented surprising results for the hitherto unexplored mechanical properties of free-standing polystyrene thin films cut from bulk via microtomy. These results stand in contrast to similar studies performed on solvent cast films, which is the prevalent fabrication method for polymer thin film studies. The most unexpected aspect of these results is the extreme elongation measured in what are typically brittle polystyrene thin films. *In situ* optical microscopy experiments allowed the progression of the deformation to be visualized in real time, revealing the growth of crack-like features unlike typical crazes. *Postmortem* TEM imaging provided microstructure characterization of the thin film deformation, elucidating a transition from shear yielding to crazing as a result of thermal annealing prior to deformation.

While the origins of the enhanced ductility leave much to be explored, several insights into the importance of specimen preparation methods and their consequences have been discussed. Several factors may be contributing to the enhanced ductility, namely the lack of embedded particulates and an absence of out-of-plane stress, but the linear thickness dependence of the nSSA indicates that the fractured surfaces are a primary source of ductility. A molecular mechanism describing how this actually occurs is unclear, but we provide an explanation analogous to the ductility inducing phenomenon known as mechanical rejuvenation. We propose that the effect of microtomy is to increase S_0 at the surfaces and influence the structure up to 120 nm into the film.

Unlike bulk mechanical rejuvenation, the effect persisted even when the films were allowed to age at room temperature for several weeks.

The PTP-based testing method presented in this work is a general method that could be used to mechanically test any polymer that can be microtomed and fixed across the device gap. Our results also suggest that spin-cast films could potentially exhibit greater ductility if sample preparation artifacts were addressed. In future work it will be interesting to explore the generality of this phenomenon and whether other properties of more complex polymer thin film systems might be drastically modified due to the presence of a high surface concentration of chain ends.

Chapter 4 – Fractured Surfaces Lead to Extreme Ductility in PMMA Thin Films

4.1 Overview

Extreme ductility and a reduction in the glass transition temperature has been quantitatively measured in microtomed thin films (100 – 300 nm) of poly(methyl methacrylate). The yielding behavior was found to depend on thermal history, where annealed films did not exhibit strain softening. These findings are consistent with recent observations on microtomed thin films of polystyrene, suggesting that the phenomenon of extreme ductility for microtomed thin films is general to glassy polymers as a whole. The microtome-induced fracture is hypothesized to enhance segmental chain mobility in a manner analogous to, but distinct from, the phenomenon of mechanical rejuvenation. This explanation is supported by the suppression of crazing and a reduction in the glass transition temperature.

4.2 Motivation

Glassy polymers have found a multitude of uses in both commodity products and engineering applications, often chosen because of their high transparency and formability. However, a significant drawback of glassy polymers is that they are typically quite brittle at room temperature. The most notable exception to this is polycarbonate (PC), the ductility and toughness of which has led to high performance applications such as in canopies for military aircrafts.[111] Poly(methyl methacrylate) (PMMA) is another glassy polymer widely used in engineering applications, and while it is brittle at room temperature it has several advantages over PC, primarily cost. PMMA is not only significantly less expensive, but has better clarity, is much more resistant to scratches, and unlike PC, PMMA can be polished.[112] Thus, enhancing the ductility of glassy polymers, such as PMMA, is highly desirable.

The growing use of glassy polymers in thin film applications, such as micro- and nano-electronics, coatings, gas permeable membranes, and biosensors, has generated interest in how reduced geometries might affect material properties.[113–115] A large portion of literature on the topic has focused on the depression of the glass transition temperature (T_g) in ultrathin polymer films, specifically polystyrene (PS),[28] but there has also been increased attention to the mechanical properties of thin films.[6,11,14,15,116]

In the previous chapter, it was revealed that the ductility of PS can be greatly enhanced by preparing thin films *via* microtomy.[47] Microtomy is typically used to prepare microscopy specimens, and is a fundamentally different processing route as compared to the solvent casting methods that are typically used to prepare polymer thin films a the larger scale. In microtomy, thin slices are sectioned from the bulk material using a sharp knife, producing films with small lateral dimensions (on the order of a mm^2). The small size of the films introduces practical challenges in their characterization outside of microscopy. While microtomy is not an efficient method to produce polymer thin films, it does produce a well-controlled geometry to investigate how the fractured surfaces might alter the material properties when these surfaces account for a significant

portion of the total volume. Using our recently developed technique, a push-to-pull (PTP) device was employed to enable small-scale nanomechanical testing of microtomed thin films (Figure 4.1). Our recent discovery of extreme ductility in a classically brittle polymer, PS, motivated further investigations into the mechanism and generality of this phenomenon. The work presented here suggests the phenomenon is general to polymer glasses as a whole, as microtomed thin films of PMMA also exhibit greatly enhanced ductility. In addition, the capabilities of the PTP technique have been expanded to enable temperature-controlled dynamic mechanical analysis (DMA) for the purpose of measuring T_g. These measurements revealed a reduction in T_g in microtomed films of PMMA, supporting the hypothesis of enhanced chain mobility at the fractured surfaces that was introduced in chapter 3.

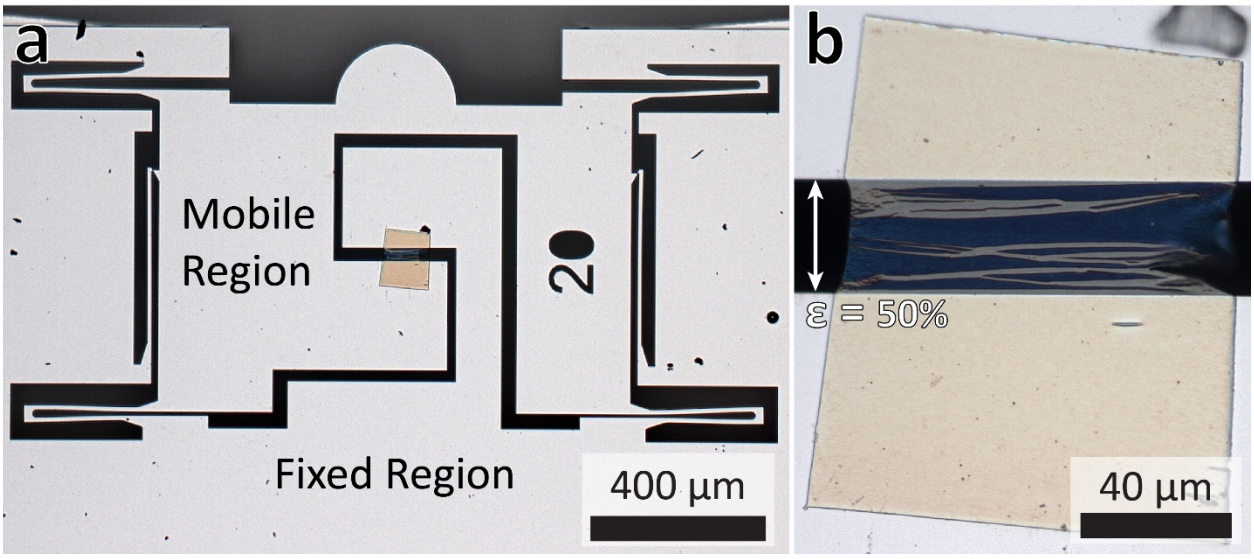

Figure 4.1. a) Optical image of an annealed microtomed thin film (220 nm thickness) of PMMA deposited across the tensile gap of a PTP device equipped with a strain-locking mechanism (shown here in the locked position. The mobile region, suspended by four springs, is actuated by an in-plane force at the apex of the round 'head' of the device (push). The pushing force is translated to a tensile force (pull) applied to the specimen as the gap widens between the mobile and fixed regions. b) Higher magnification image of the ductile deformation after straining by roughly 50% using the PTP device.

4.3 Experimental details

The polymethylmethacrylate was purchased from Sigma-Aldrich and was manufactured by Goodfellow as a cast sheet. A 0.5 mm thick sheet was used as the bulk substrate and for preparing microtomed thin films. A 3.0 mm thick sheet was used for bulk DMA testing.

An RMC PowerTome XL Ultramicrotome equipped with a Diatome diamond knife was used to prepare the thin films of PMMA with thicknesses ranging from 100 to 300 nm. Through thickness shear banding was present in the microtomed films of PMMA. The presence of shear

bands is a function of the cutting speed and sectioning thickness during microtomy.[50,69] The shear banding was unavoidable since the lowest cutting speed of the microtome was still too fast give for film thicknesses above 100 nm. The orientation of the shear bands with respect to the tensile direction did not seem to affect the mechanical response. While we cannot completely rule out the contribution that the presence of shear banding may have had on the mechanical properties of microtomed films of PMMA, shear banding was able to be avoided in previous work on PS and was found not to affect the final result.[47]

A Bruker-Hysitron TI 950 TriboIndenter equipped with an xSol 800 temperature stage was used to perform DMA and quasistatic quantitative mechanical testing using a diamond flat punch probe to actuate the PTP device. A conospherical probe with a radius of roughly 10 μm was used to directly test films deposited onto a PMMA substrate. A conospherical probe with a radius of roughly 300 nm was used in the scanning probe microscopy (SPM) mode to determine the thicknesses of the films.

PTP nanoDMA testing was performed by actuating the PTP device with flat punch probe with an oscillating force at a frequency of 3 Hz while ramping the temperature upwards at a rate of 2 °C/min. An empirical study revealed less than a 2 °C change in the measured T_g between heating rates of 6 °C/min and 2 °C/min, indicating that the heating rate used was sufficiently slow enough to avoid significantly thermal lag. Due to the 5 μm displacement limit of the transducer and thermal expansion of the system, temperature sweeps were limited to a 20 °C range in a single test. Before each test, the probe was placed in contact with the PTP device to determine when thermal expansion had ceased, indicating the system was equilibrated. The load amplitude was set to 5 μN, correlating with a displacement amplitude of 1 – 5 nm (depending on the temperature). At the lowest temperature for the range to be tested, the peak load was increased incrementally until a non-zero value of tan-delta was achieved, indicating the film was being strained and accounting for any slack in the film. This minimized strain to be within the linear viscoelastic region and avoided yielding. This is because in films strained beyond a yielding event, T_g was measured to be near bulk values. Thermal cycling was also found to increase the measured value of T_g after every excursion above T_g, eventually settling at a value roughly 10 °C higher than the first measurement. The temperature stage was calibrated using multiple thermocouples and found to be accurate to within 1 °C.

Bulk DMA data were acquired using an ARES-G2 strain-controlled rheometer (TA Instruments) in oscillatory bar torsion mode. 3.0 mm thick PMMA sheets were cut into rectangular bars (roughly 40 x 12.5 mm) and tested at a strain of 0.02% and an oscillation frequency of 3 Hz while ramping the temperature at 2 °C/min.

TEM imaging was performed with a 300kV JEOL JEM-3010 using a Hysitron PI 95 holder only to mount the PTP devices (not used for mechanical testing). All imaging was done in brightfield mode using an objective aperture and significant defocus to enhance contrast.

4.4 Results

4.4.1 Quantitative mechanical testing and *postmortem* TEM

Microtomed films of PMMA, with thicknesses between 100 to 300 nm, were deposited onto custom designed strain-locking PTP devices using the cryo-solvent manipulation technique described in Chapter 2. Quantitative mechanical testing of the microtomed films revealed extreme ductility with strains reaching over 300%, where the microtomed films reached strains far exceeding the bulk strain-to-failure value (< 4%) at comparable strain rates (Figure 4.1, 4.2). In fact, the stress-strain response of unannealed films closely resembled that observed for bulk tensile tests performed at elevated temperatures near T_g.[117] Stress-strain analysis of PTP testing of microtomed films of PMMA gave an elastic modulus that ranged between 0.45 and 1.3 GPa, significantly lower than the expected range quoted by the manufacturer of the bulk PMMA sheet (2.4 – 3.3 GPa).[118] P*ostmortem* TEM imaging revealed the deformation mode to be entirely due to shear yielding (Figure 4.2b) without any sign of crazing, which is atypical in room temperature tensile testing of bulk specimens.[119] Annealed films also exhibited extreme ductility but lacked strain softening, similar to previously reported results on microtomed films of PS (Figure 4.2c).[47] The primary difference between microtomed films of PMMA and PS was that crazing did not return as the dominant deformation mode in annealed PMMA films as it did in annealed PS films. Rather, when annealed at 115 °C for 115 hours the PMMA films deformed primarily by through thickness thinning (shear yielding), with only small regions of crazing observed (Figure 4.2d). This was also true for films annealed at 130 °C for 24 hours. At large strains (>100%), ductile tearing of the film was observed to initiate at one of the sides on occasion. Even in the presence of a tear, none of the films could be strained to complete failure before reaching the highest strain attainable by the PTP device (>300% engineering strain, depending on the initial gap distance).

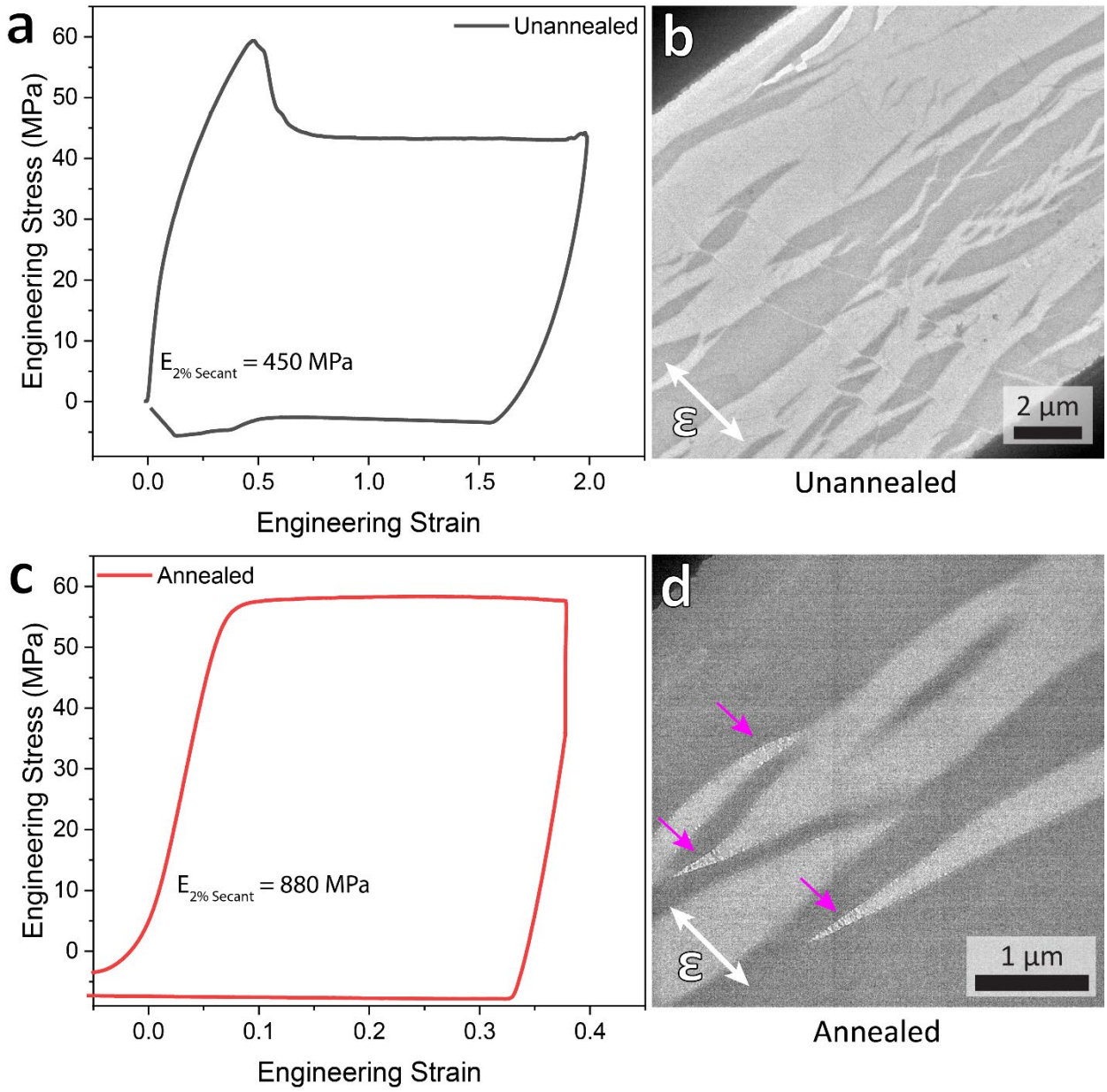

Figure 4.2. a) Stress-strain curve of an unannealed microtomed thin film (270 nm) of PMMA tested using a PTP device at a strain rate of 0.1 s^{-1}. The initial deformation of the film was elastic, with a 2% secant modulus of 450 MPa, followed by yielding, strain softening and plastic flow. Note the upward slope at the highest strain is not due to strain hardening, but rather contact with the strain-locking mechanism at the end of its range. The initial tensile gap was 2.5 µm. b) Brightfield TEM image of a highly strained (roughly 300%) unannealed microtomed thin film (260 nm) of PMMA. The darkest regions at the upper-left and lower-right corners are the edges of the PTP device gap (initially 2.5 µm across). No crazing was present, only through-thickness thinning (light grey). c) Stress-strain curve of an annealed microtomed thin film (250 nm) of PMMA tested using a PTP device at a strain rate of 0.05 s^{-1}. The initial deformation of the film was elastic, with a 2% secant modulus of 880 MPa, followed by yielding, and plastic flow without strain softening. Note the

vertical load drop was due to stress relaxation during a 20 second hold at maximum displacement. Slack in the film led to a "toe" at the beginning of the test, which was removed in accordance with ATSM D638.[56] The initial tensile gap of the PTP device was 10 µm across. d)) Brightfield TEM image of a highly strained (roughly 200%) annealed microtomed thin film (220 nm) of PMMA. The darkest region at the upper-left corner was the edge of the PTP device gap (initially 5 µm across). Deformation was dominated by shear yielding (light grey) with a few small regions of crazing (indicated by arrows).

4.4.2 T_g measurements of microtomed PMMA thin films *via* PTP nanoDMA

Temperature-controlled DMA tests of microtomed PMMA films were performed using an instrumented nanoindenter (nanoDMA) equipped with a heating stage. These experiments were carried out by actuating a PTP device that had a film spanning the tensile gap in the same geometry as the tensile deformation experiments. An oscillating force at 3 Hz was applied while slowly increasing the temperature. By continuously measuring the storage and loss modulus, tan-delta could be calculated as a function of temperature to determine T_g (Figure 4.3).[55] Since tan-delta is defined as the ratio of the loss modulus to the storage modulus, the purely elastic response of the PTP device dominated much of the mechanical response and so the magnitude of tan-delta was less than measured in the bulk measurement.

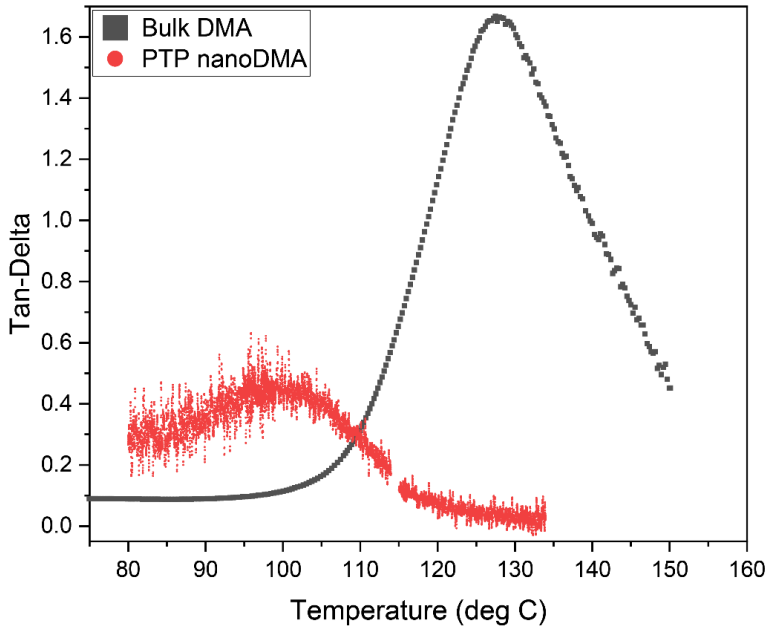

Figure 4.3. Results from bulk DMA and PTP nanoDMA experiments, where the peak in tan-delta as a function of temperature was used to determine T_g in a bulk sheet and a microtomed thin film of PMMA. A significant T_g depression of roughly 30 °C was measured in the microtomed thin

film. Both DMA tests were performed at a frequency of 3 Hz and a heating rate of 2 °C/min (see Experimental for details). The thickness of the film was 200 nm.

The reduction in T_g reported here is distinct from T_g depression due to the confinement effects reported in the literature for spin-cast ultrathin films. In the large body of research regarding this topic, T_g only begins to deviate from bulk values in freestanding spin-cast films when the thickness is less than about 100 nm. Furthermore, the reduction in T_g is subtle until the film thickness approaches the characteristic coil size of the polymer.[28,120,121] Using differential scanning calorimetry, Nam *et al.* reported a significant T_g depression (>20 °C) in freestanding spin-cast thin films of PMMA with a molecular weight of 996 kg/mol (comparable to the PMMA used in this study) only when the thickness of the films was less than 100 nm.[122] Since the films in this work were thicker than 100 nm, confinement effects alone cannot explain the T_g depression observed here. Both the extreme ductility and T_g depression are instead believed to be a consequence of microtome-induced fracture at the surfaces of the films. These results are consistent with the findings in Chapter 2, where a reduction in T_g was measured in a microtomed film (140 nm thick) of PS using a PTP device (Figure 2.5).

4.5 Discussion: PMMA compared to PS

As discussed in further detail in our previous work on PS, we attributed the phenomenon to the enhanced segmental mobility at the surfaces due to the fractured chains and deformation inflicted through microtomy. The effect of microtomy is analogous to that of mechanical rejuvenation, where the surfaces can be thought of as heavily rejuvenated with a bulk-like core of the microtomed film. As the bulk-like core is reduced with decreasing film thickness, so is the strain softening amplitude until a critical thickness at which the effect of the fractured surfaces dominates. This explanation is supported by the thickness dependence of the strain softening amplitude in microtomed films of PS[47] and now by a reduction in T_g in microtomed films of PMMA. Ductility in polymer glasses is governed by segmental dynamics, which is directly related to T_g.[104,123] Therefore, the reduction in T_g supports the hypothesis that the extreme ductility is a consequence of enhanced molecular mobility due to the microtome-induced fracture at the surfaces of the films.[47]

Interestingly, the analogy of mechanically rejuvenated surfaces with enhanced segmental mobility fails to account for the lack of strain softening in annealed microtomed films. In mechanically rejuvenated bulk specimens, annealing or physical aging leads to the return of strain softening and brittle behavior.[89,104] Instead, we found that microtomed films that were annealed maintained enhanced ductility but no longer exhibited strain softening. As previously mentioned, annealing changes the deformation mode from shear yielding to crazing in PS, but annealed films of PMMA show very little crazing or none at all. This is likely due to differences in chain stiffness, where PMMA is less stiff than PS, as given by their characteristic ratios (C_∞) of about 8 and 10, respectively.

Other than the strain softening amplitude, no other thickness dependencies were observed in our previous work on microtomed films of PS or this current work on PMMA, and an upper thickness limit at which for when the bulk brittleness is restored was not reached for PTP experiments using films with thicknesses up to 500 nm. The existence of an upper thickness limit is expected as the volume fraction of material affected by the fractured surfaces inevitably becomes insufficient to drive the mechanical response. High-voltage TEM work conducted by G. Michler to study crazing in several polymer glasses used microtomy to prepare semithin (0.5 – 5.0 μm) films.[124] In the cited work, small-scale tensile testing revealed typical crazing in all of the polymer glasses, except for a "peculiarity" observed in PMMA. The crazes in PMMA were described as having very weak fibrillization and became "homogeneous" as the craze thickness grew. The TEM images of the "homogeneous crazes" appear to be very similar to the deformation imaged in this work. The thickness of the semithin PMMA films were not explicitly stated, but the similarity in the deformation suggests the microtome-induced extreme ductility may apply to films that are several microns thick.

4.6 Summary: Induced ductility as a general phenomenon in glassy polymers

Microtomed films of PMMA were shown to exhibit extreme ductility and deformation *via* shear yielding a phenomenon shared with PS. This implies that the phenomenon is not specific to either material, but rather is general to all glassy polymers. The reduction in T_g supports the hypothesis that enhanced segmental mobility originating at the fractured surfaces dramatically alters the mechanical behavior of the films. Further research is required to fully understand the underlying mechanisms, especially in the case of annealed films. In future work, alternative processing methods to induce extreme ductility through fractured surfaces can be explored by probing the upper limit of film thickness for which brittle behavior returns could not be reached using the present methods.

Chapter 5 – Trends in PTP nanoDMA Testing

5.1 Overview

The novelty of using an instrumented nanoindenter to perform nanoDMA testing with a PTP device to measure T_g in a microtome thin film presented several unique experimental challenges. One of these challenges was determining the proper testing parameters to provide the best results while avoiding artifacts and minimizing error. To do this, several empirical studies were performed on PMMA and PS to evaluated trends with respect to parameters such as heating rate, thermal cycling, and applied peak load. These studies revealed that a heating rate of 2 °C/min was sufficiently slow enough to provide an accurate measurement of T_g, but also revealed several factors which affected the measured value of T_g. Loading the film past the yield point and thermal excursions beyond T_g were both found to significantly shift the measured value for T_g upwards. Lastly, when the feedback mode was changed from open-loop to load-controlled, the T_g peak was found to split into two peaks with relative magnitudes changing with increasing load. Recognizing these trends were pivotal in the proper interpretation of PTP nanoDMA data and elucidated potential future studies to provide more information on the mechanisms behind T_g reduction and extreme ductility observed in microtomed thin films of glassy polymers.

5.2 Increased T_g post-yield

In general, obtaining an accurate measurement of T_g using DMA requires that the strain must be small enough such that the deformation is within the linear viscoelastic region of the polymer being tested.[cite] Accomplishing this when performing nanoDMA on a PTP device can be challenging for several reasons. First, it is difficult to pre-determine the proper peak load to apply since the stiffness of the PTP device varies slightly between devices and can be much large than the stiffness of the film, depending on its thickness and width. If there is no slack in the film spanning the PTP gap, then a very low load is required to avoid yielding (on the order of 10s of μN). Conversely, if slack is present in the film then a considerably larger load must be applied until the film becomes taut, indicated by a deflection in the force-displacement curve. A large amount of slack can be seen under an optical microscope beforehand, but a small amount of slack is more problematic. The value of tan-delta can be used as a guide to determine if the film is being strained, but they can be near zero (on the order of 10^{-2}) below T_g, which are lower than typical bulk DMA testing since the elastic response of the PTP device dominates much of the signal. Second, the films are prone to yielding at the PTP gap edge where the film becomes freestanding due to the stress concentration (Figure B.6), especially at elevated temperatures as the polymer becomes softer. Finally, thermal expansion of the system causes the load/strain to increase throughout the DMA test. Yielding events can only be identified in the force-displacement curve after testing has already been performed. For these reasons, the minimum possible strain be applied so that the film does not yield during the experiment.

The effect of yielding on the measured value of T_g is shown in Figure 5.1. If yielding has occurred prior to DMA testing, T_g was found to increase significantly, exceeding the bulk value.

The value of tan-delta was also observed to drop in films that had yielded, especially in PS. This effect may be due to the extension and alignment of molecular chains in plastically deformed regions of the polymer glass, reducing the mobility of these chains where strain has become localized. Thus, avoiding yielding is key in obtaining an accurate measurement of T_g for PTP DMA testing.

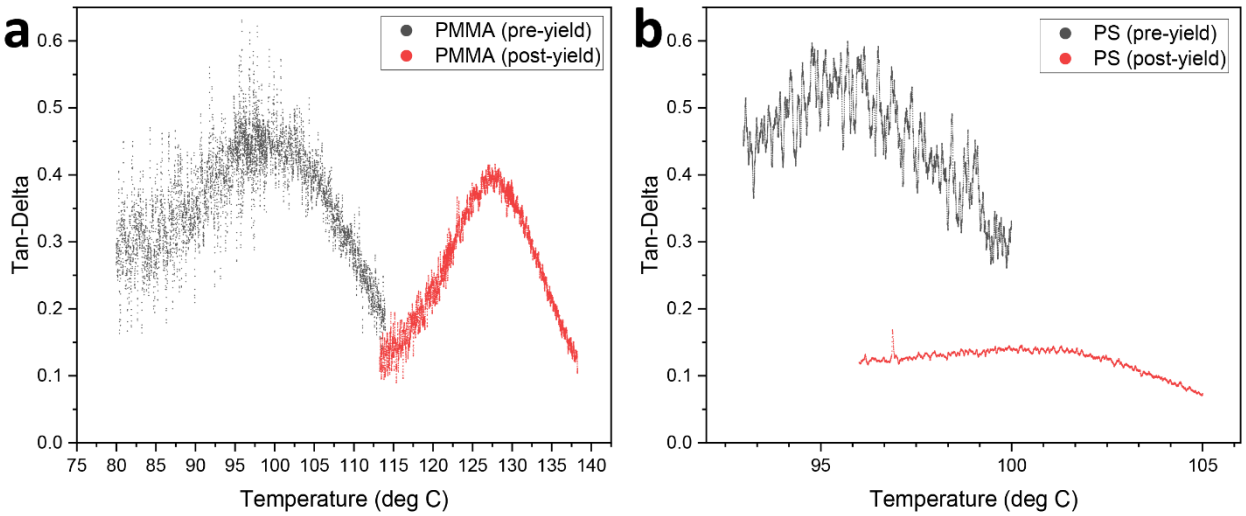

Figure 5.1. Tan-Delta as a function of temperature for PMMA (a) and PS (b) showing an increase in the measured value of T_g before and after the film has yielded. An oscillating force with an amplitude of 5 μN at a frequency of 3 Hz was used, except for PS (pre-yield), which was done at 1 μN and 4 Hz. A heating rate of 2 °C/min was used, except for PS (pre-yield), which was 4 °C/min.

5.3 Effect of temperature cycling on T_g

Cyclic excursions beyond T_g were found to incrementally increase the measured value of T_g (Figure 5.2a). This effect seemed to be stronger prior to yielding, where once yielding occurred the new value of T_g was found to be quite stable (Figure 5.2b). This effect indicates an evolution of chain mobility upon annealing above T_g and may be related to the change from shear yielding to crazing after annealing microtomed films of polystyrene (Figure 3.3). It may be that some of the fractured chains at the surface are small enough to diffuse into the film, but further investigations are needed to explore this possibility.

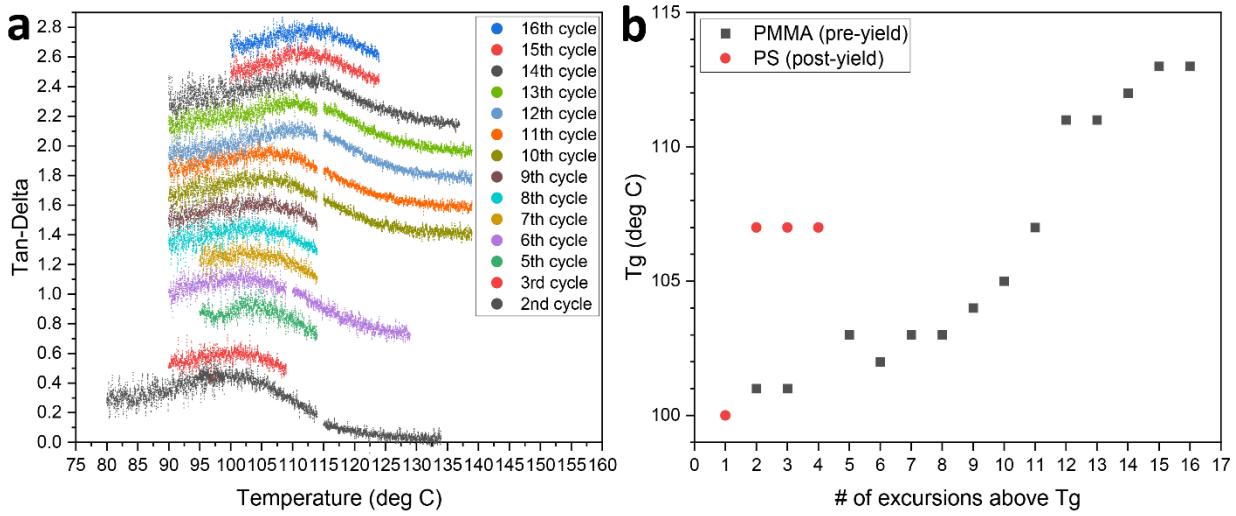

Figure 5.2. a) Evolution of tan-delta peaks as the temperature is cycled above T_g (y-axis offset of 0.17 in between curves for clarity). b) Plot of T_g as a function of thermal cycles above T_g for PMMA (pre-yield) and PS (post-yield). An oscillating force with an amplitude of 5 μN at a frequency of 3 Hz was and the heating rate was 2 °C/min for all tests shown.

5.4 Heating rate and thermal lag

Concerns with proper heat conduction to the sample were empirically studied to determine the magnitude of thermal lag during a continuous temperature sweep (Figure 5.3). It was found that T_g shifted less than 3 °C between heating rates of 1 °C/min and 6 °C/min due to thermal lag.

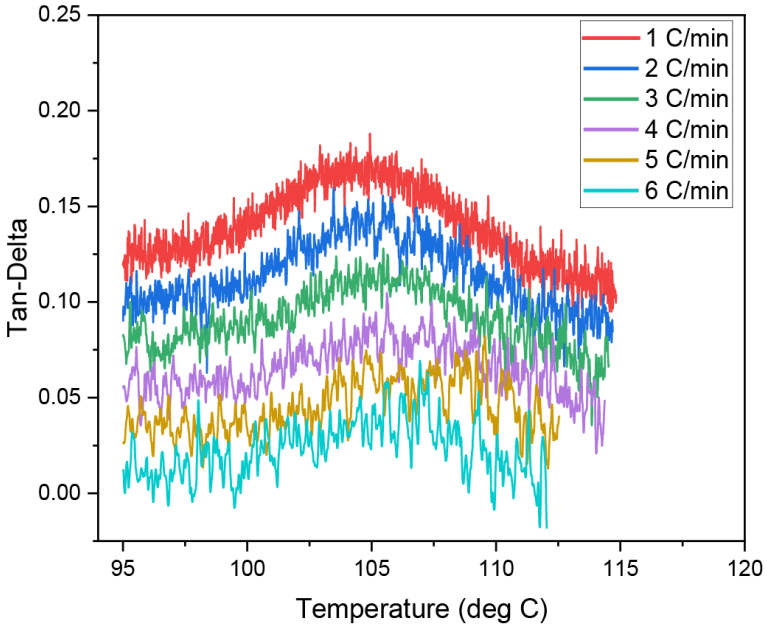

Figure 5.3. Plot of tan-delta as a function of temperature for different heating rates for a microtomed film of PS (post-yield). An oscillating force with an amplitude of 5 μN at a frequency of 3 Hz was used for all tests shown. (0.02 y-axis offset between curves.)

5.5 Effect of feedback control mode

In an attempt to keep the thermal expansion from increasing the load/strain on the film during DMA testing, experiments with the feedback controller set to load-controlled mode were done. Previous tests were all done using the open-loop feedback mode. In this mode low frequency testing was not available and had to be done at 200 Hz. This led to a significant increase in the measured T_g in post-yield films of PS (Figure 5.4a). Additionally, a load series revealed a splitting of the T_g peak. The relative magnitudes of peaks changed with increasing load, where the higher temperature peak was reduced and the lower temperature peak increased (Figure 5.4b). At low loads, the load-controlled mode seemed to have erroneous spikes at the beginning of the tests (Figure 5.4a), but also seemed to reveal a peak in tan-delta around 75 °C. Both the T_g peak splitting and the lower temperature tan-delta peak are interesting but require further investigation and better tuning of the load-controlled parameters to determine their origins.

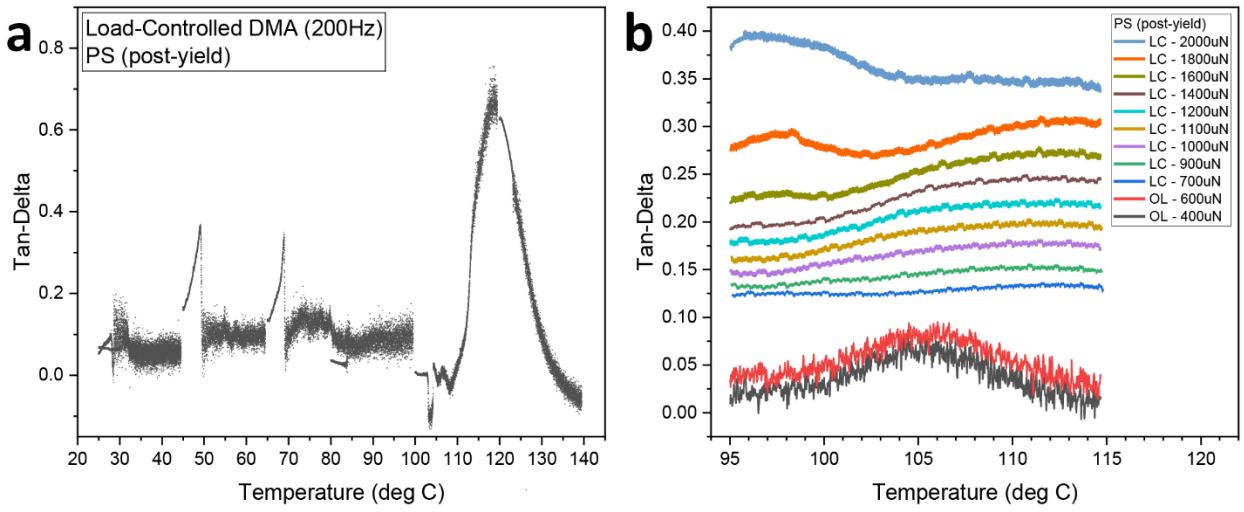

Figure 5.4. a) Load-controlled DMA testing results for PS, where multiple sweeps were taken to cover the temperature range shown. The large peak in tan-delta indicates T_g, which is roughly 15 °C larger than that measured in tests with the feedback controller in open-loop mode. b) Load series beginning with two curves taken with the feedback controller in open-loop mode (3 Hz) and all subsequent tests in load-controlled mode (200 Hz). (0.02 y-axis offset between curves.)

5.6 Summary & outlook in DMA testing with a PTP device

The primary purpose of the tests shown in this chapter were to empirically determine the direction and magnitude experimental parameters affected the measurement of T_g in PTP DMA testing of microtomed films of PS and PMMA. The primary outcome of this experiments was realizing the importance of ensuring T_g measurements were made prior to yielding. The heating rate series measured the extent of thermal lag, which was negligible at 2 °C/min. T_g was found to evolve with thermal cycling any may be an interesting avenue to study in future work. Finally, the double T_g measured with the feedback controller in load-controlled mode was puzzling and requires more work to determine if this effect was an artifact or a real material phenomenon.

Chapter 6 – Concluding Remarks

6.1 Summary & conclusions

In Chapter 2 of this dissertation a new method for small-scale mechanical testing of freestanding microtomed polymer thin films using a push-to-pull device is presented. This required a redesign of the commercially available device to allow films to be deposited and tested without the need for focused ion beam milling. This was necessary due to the ion beam irradiation damage, which was shown to drastically alter the mechanical response of polymer films. The new design also included a strain-locking mechanism to hold a predetermine for *postmortem* imaging in both the TEM and optical microscope. Additional modifications to the technique allowed the push-to-pull devices to be compatible with an instrumented nanoindenter. This enabled experiments previously unavailable when testing with push-to-pull device, including temperature-controlled dynamic mechanical testing to measure the glass transition temperature.

In Chapters 3 and 4, the newly developed method was applied to two polymer glasses: polystyrene and poly(methyl methacrylate). The microtomed thin films were found to be extremely ductile, despite the fact that both these polymers are brittle at room temperature and thin films of the same materials produced *via* spin-casting have been shown to maintain their brittle behavior in the literature. Quantitative mechanical testing revealed that the strain softening amplitude linearly depended upon the film thickness, indicative that the mechanism for extreme ductility is a surface phenomenon. We proposed a hypothesis in which the fractured surfaces inflicted through microtomy leads to enhanced segmental mobility of the surface chains. The chain scission from microtomy produces a high chain-end concentration and reduction in molecular weight at the surfaces of the film, both of which have been shown to enhance segmental mobility in the literature. Insufficient segmental mobility, relative to the deformation rate, is known to strongly correlate with brittle behavior and crazing. *Postmortem* TEM imaging revealed a suppression of crazing in unannealed microtomed films displaying extreme ductility. A reduction in the glass transition temperature was measured in the microtomed films, further supporting this hypothesis.

6.2 Outlook

The methodology developed in this work may be used to test a wide variety of materials, not limited to microtomed polymer films. The cryo-solvent manipulation technique may be useful for preparing delicate specimens, such as biological specimens, fibers, or other thin films (polymer or otherwise), for use with a push-to-device or other delicate substrates (e.g.: SiN_x windows). The strain-locking mechanism is an upgrade to the commercially available push-to-pull device that provides a mechanically stable way to hold a specimen at a fixed strain for microscopy investigations. The adaptation for instrumented nanoindenters expands the utility of push-to-pull devices to include characterization modes previously unavailable.

The fact that extreme ductility is observed in microtomed films of both polystyrene and poly(methyl methacrylate) is indicative that this phenomenon is general to all glassy polymers. Of

course, fully understanding the molecular-level understanding of this phenomenon requires further exploration. Questions still remain regarding observations such as the fact that bulk T_g values return to microtomed films after annealing (or excursions) above T_g, yet the films remain ductile. How exactly the microtomy process changes the structure of the thin film before and after annealing is not clear, as is whether microtomy is even required to achieve ductility in freestanding thin films of glassy polymers. For example, if spin-cast films could be produced in the required size and manipulated onto the PTP device for mechanical testing, would they produce similar extreme ductility? The variation in the elastic modulus for the free-standing thin films is also an interesting observation that merits further study. In addition, the size scales probed here in terms of thin film thickness were constrained by the experimental approach (microtomy, PTP testing), but it would be interesting to study how elastic modulus and tensile ductility change as a function of film thickness. Semicrystalline polymers may also experience some version of this phenomenon since they contain some degree of amorphous phase. We recognize microtomy is not a scalable process, but perhaps other methods to induce fractured surfaces in polymer films with a larger area or a composite bulk material may be developed to exploit this phenomenon. Lastly, the presence of fractured surface chains may alter more than the mechanical properties of more complex polymer systems. Future work to study the effect of fractured surfaces in conducting or semiconducting polymer thin films, for example, may lead to other unexpected material properties.

References

(1) Roth, C. B.; Baglay, R. R. Fundamentals of Polymers and Glasses. In *Polymer Glasses*; CRC Press, 2016; pp 3–19. https://doi.org/10.1201/b21864.

(2) Wang, S.-Q.; Cheng, S. Experiments-Inspired Molecular Modeling of Yielding and Failure of Polymer Glasses under Large Deformation. In *Polymer Glasses*; Roth, C. B., Ed.; CRC Press, Taylor & Francis Group: Boca Raton, FL, 2016; pp 396–419.

(3) Hartwig, G. Fracture Behavior of Polymers. In *Polymer Properties at Room and Cryogenic Temperatures*; Springer US: Boston, MA, 1994; pp 187–218. https://doi.org/10.1007/978-1-4757-6213-6.

(4) Beahan, P.; Bevis, M.; Hull, D. The Morphology of Crazes in Polystyrene. *Philos. Mag.* **1971**, *24* (192), 1267–1279. https://doi.org/10.1080/14786437108217412.

(5) Donald, A. M.; Chan, T.; Kramer, E. J. The Effect of Film Thicknesses on Craze Microstructure. *J. Mater. Sci.* **1981**, *16* (3), 669–675. https://doi.org/10.1007/BF02402784.

(6) Stafford, C. M.; Harrison, C.; Beers, K. L.; Karim, A.; Amis, E. J.; Vanlandingham, M. R.; Kim, H. C.; Volksen, W.; Miller, R. D.; Simonyi, E. E. A Buckling-Based Metrology for Measuring the Elastic Moduli of Polymeric Thin Films. *Nat. Mater.* **2004**, *3* (8), 545–550. https://doi.org/10.1038/nmat1175.

(7) VanLandingham, M. R.; Villarrubia, J. S.; Guthrie, W. F.; Meyers, G. F. Nanoindentation of Polymers: An Overview. *Macromol. Symp.* **2001**, *167* (1), 15–44. https://doi.org/10.1002/1521-3900(200103)167:1<15::AID-MASY15>3.0.CO;2-T.

(8) Alisafaei, F.; Han, C. S. Indentation Depth Dependent Mechanical Behavior in Polymers. *Adv. Condens. Matter Phys.* **2015**, *2015*. https://doi.org/10.1155/2015/391579.

(9) Dokukin, M. E.; Sokolov, I. On the Measurements of Rigidity Modulus of Soft Materials in Nanoindentation Experiments at Small Depth. *Macromolecules* **2012**, *45* (10), 4277–4288. https://doi.org/10.1021/ma202600b.

(10) Tweedie, C. A.; Constantinides, G.; Lehman, K. E.; Brill, D. J.; Blackman, G. S.; Van Vliet, K. J. Enhanced Stiffness of Amorphous Polymer Surfaces under Confinement of Localized Contact Loads. *Adv. Mater.* **2007**, *19* (18), 2540–2546. https://doi.org/10.1002/adma.200602846.

(11) Bay, R. K.; Crosby, A. J. Uniaxial Extension of Ultrathin Freestanding Polymer Films. *ACS Macro Lett.* **2019**, 1080–1085. https://doi.org/10.1021/acsmacrolett.9b00408.

(12) O'Connell, P. A.; McKenna, G. B. Dramatic Stiffening of Ultrathin Polymer Films in the Rubbery Regime. *Eur. Phys. J. E* **2006**, *20* (2), 143–150. https://doi.org/10.1140/epje/i2005-10125-4.

(13) Bay, R. K.; Shimomura, S.; Liu, Y.; Ilton, M.; Crosby, A. J. Confinement Effect on Strain Localizations in Glassy Polymer Films. *Macromolecules* **2018**, *51* (10), 3647–3653. https://doi.org/10.1021/acs.macromol.8b00385.

(14) Liu, Y.; Chen, Y.-C.; Hutchens, S.; Lawrence, J.; Emrick, T.; Crosby, A. J. Directly Measuring the Complete Stress–Strain Response of Ultrathin Polymer Films. *Macromolecules* **2015**, *48* (18), 6534–6540. https://doi.org/10.1021/acs.macromol.5b01473.

(15) Hasegawa, H.; Ohta, T.; Ito, K.; Yokoyama, H. Stress-Strain Measurement of Ultra-Thin Polystyrene Films: Film Thickness and Molecular Weight Dependence of Crazing Stress. *Polymer* **2017**, *123*, 179–183. https://doi.org/10.1016/j.polymer.2017.07.018.

(16) Si, L.; Massa, M. V.; Dalnoki-Veress, K.; Brown, H. R.; Jones, R. A. L. Chain Entanglement in Thin Freestanding Polymer Films. *Phys. Rev. Lett.* **2005**, *94* (12), 1–4. https://doi.org/10.1103/PhysRevLett.94.127801.

(17) Chung, J. Y.; Lee, J. H.; Beers, K. L.; Stafford, C. M. Stiffness, Strength, and Ductility of Nanoscale Thin Films and Membranes: A Combined Wrinkling-Cracking Methodology. *Nano Lett.* **2011**, *11* (8), 3361–3365. https://doi.org/10.1021/nl201764b.

(18) Kremer, F.; Tress, M.; Mapesa, E. U. Glassy Dynamics and Glass Transition in Nanometric Layers and Films: A Silver Lining on the Horizon. *J. Non. Cryst. Solids* **2015**, *407*, 277–283. https://doi.org/10.1016/j.jnoncrysol.2014.08.016.

(19) Pye, J. E.; Roth, C. B. Two Simultaneous Mechanisms Causing Glass Transition Temperature Reductions in High Molecular Weight Freestanding Polymer Films as Measured by Transmission Ellipsometry. *Phys. Rev. Lett.* **2011**, *107* (23), 1–5. https://doi.org/10.1103/PhysRevLett.107.235701.

(20) Chan, T.; Donald, A. M.; Kramer, E. J. Film Thickness Effects on Craze Micromechanics. *J. Mater. Sci.* **1981**, *16* (3), 676–686. https://doi.org/10.1007/BF02402785.

(21) Stafford, C. M.; Vogt, B. D.; Harrison, C.; Julthongpiput, D.; Huang, R. Elastic Moduli of Ultrathin Amorphous Polymer Films. *Macromolecules* **2006**, *39* (15), 5095–5099. https://doi.org/10.1021/ma060790i.

(22) Krupenkin, T. N.; Fredrickson, G. H. Crazing in Two and Three Dimensions. 1. Two-Dimensional Crazing. *Macromolecules* **1999**, *32* (15), 5029–5035. https://doi.org/10.1021/ma981014g.

(23) Li, L.; Encarnacao, L. M.; Brown, K. A. Polymer Nanomechanics: Separating the Size Effect from the Substrate Effect in Nanoindentation. *Appl. Phys. Lett.* **2017**, *110* (4). https://doi.org/10.1063/1.4975057.

(24) Askar, S.; Torkelson, J. M. Stiffness of Thin, Supported Polystyrene Films: Free-Surface, Substrate, and Confinement Effects Characterized via Self-Referencing Fluorescence. *Polymer* **2016**, *99*, 417–426. https://doi.org/10.1016/j.polymer.2016.07.042.

(25) Rowland, H. D.; King, W. P.; Pethica, J. B.; Cross, G. L. W. Molecular Confinement Accelerates Deformation of Entangled Polymers During Squeeze Flow. *Science* **2008**, *322* (5902), 720–724. https://doi.org/10.1126/science.1157945.

(26) Liu, Y.; Chen, Y. C.; Hutchens, S.; Lawrence, J.; Emrick, T.; Crosby, A. J. Directly Measuring the Complete Stress-Strain Response of Ultrathin Polymer Films. *Macromolecules* **2015**, *48* (18), 6534–6540.

https://doi.org/10.1021/acs.macromol.5b01473.

(27) Chang, J.; Toga, K. B.; Paulsen, J. D.; Menon, N.; Russell, T. P. Thickness Dependence of the Young's Modulus of Polymer Thin Films. *Macromolecules* **2018**, *51* (17), 6764–6770. https://doi.org/10.1021/acs.macromol.8b00602.

(28) Forrest, J. a; Dalnoki-Veress, K. The Glass Transition in Thin Polymer Films. *Adv. Colloid Interface Sci.* **2001**, *94* (1–3), 167–195. https://doi.org/10.1016/S0001-8686(01)00060-4.

(29) Rowland, H. D.; King, W. P.; Cross, G. L. W.; Pethica, J. B. Measuring Glassy and Viscoelastic Polymer Flow in Molecular-Scale Gaps Using a Flat Punch Mechanical Probe. *ACS Nano* **2008**, *2* (3), 419–428. https://doi.org/10.1021/nn700211g.

(30) Nguyen, H. K.; Inutsuka, M.; Kawaguchi, D.; Tanaka, K. Direct Observation of Conformational Relaxation of Polymer Chains at Surfaces. *ACS Macro Lett.* **2018**, *7* (10), 1198–1202. https://doi.org/10.1021/acsmacrolett.8b00411.

(31) García-Turiel, J.; Jérôme, B. Solvent Retention in Thin Polymer Films Studied by Gas Chromatography. *Colloid Polym. Sci.* **2007**, *285* (14), 1617–1623. https://doi.org/10.1007/s00396-007-1733-6.

(32) Reiter, G.; Hamieh, M.; Damman, P.; Sclavons, S.; Gabriele, S.; Vilmin, T.; Raphaël, E. Residual Stresses in Thin Polymer Films Cause Rupture and Dominate Early Stages of Dewetting. *Nat. Mater.* **2005**, *4* (10), 754–758. https://doi.org/10.1038/nmat1484.

(33) Reiter, G.; Napolitano, S. Possible Origin of Thickness-Dependent Deviations from Bulk Properties of Thin Polymer Films. *J. Polym. Sci. Part B Polym. Phys.* **2010**, *48* (24), 2544–2547. https://doi.org/10.1002/polb.22134.

(34) Bäumchen, O.; McGraw, J. D.; Forrest, J. A.; Dalnoki-Veress, K. Reduced Glass Transition Temperatures in Thin Polymer Films: Surface Effect or Artifact? *Phys. Rev. Lett.* **2012**, *109* (5), 1–5. https://doi.org/10.1103/PhysRevLett.109.055701.

(35) Russell, T. P.; Chai, Y. 50th Anniversary Perspective: Putting the Squeeze on Polymers: A Perspective on Polymer Thin Films and Interfaces. *Macromolecules* **2017**, *50* (12), 4597–4609. https://doi.org/10.1021/acs.macromol.7b00418.

(36) Brûlet, A.; Boué, F.; Menelle, A.; Cotton, J. P. Conformation of Polystyrene Chain in Ultrathin Films Obtained by Spin Coating. *Macromolecules* **2000**, *33* (3), 997–1001. https://doi.org/10.1021/ma9906783.

(37) Uchic, M. D.; Dimiduk, D. M.; Florando, J. N.; Nix, W. D. Sample Dimensions Influence Strength and Crystal Plasticity. *Science* **2004**, *305* (5686), 986 LP – 989. https://doi.org/10.1126/science.1098993.

(38) Bei, H.; Shim, S.; Pharr, G. M.; George, E. P. Effects of Pre-Strain on the Compressive Stress–Strain Response of Mo-Alloy Single-Crystal Micropillars. *Acta Mater.* **2008**, *56* (17), 4762–4770. https://doi.org/https://doi.org/10.1016/j.actamat.2008.05.030.

(39) Ye, J.; Mishra, R. K.; Minor, A. M. Relating Nanoscale Plasticity to Bulk Ductility in Aluminum Alloys. *Scr. Mater.* **2008**, *59* (9), 951–954.

https://doi.org/https://doi.org/10.1016/j.scriptamat.2008.06.052.

(40) Lançon, F.; Ye, J.; Caliste, D.; Radetic, T.; Minor, A. M.; Dahmen, U. Superglide at an Internal Incommensurate Boundary. *Nano Lett.* **2010**, *10* (2), 695–700. https://doi.org/10.1021/nl903885p.

(41) Kiener, D.; Motz, C.; Dehm, G.; Pippan, R. Overview on Established and Novel FIB Based Miniaturized Mechanical Testing Using In-Situ SEM. *Int. J. Mater. Res.* **2009**, *100* (8), 1074–1087. https://doi.org/10.3139/146.110149.

(42) Wu, B.; Heidelberg, A.; Boland, J. J. Mechanical Properties of Ultrahigh-Strength Gold Nanowires. *Nat. Mater.* **2005**, *4* (7), 525–529. https://doi.org/10.1038/nmat1403.

(43) Nix, W. D. Yielding and Strain Hardening in Metallic Thin Films on Substrates: An Edge Dislocation Climb Model. *Math. Mech. Solids* **2009**, *14* (1–2), 207–219. https://doi.org/10.1177/1081286508092612.

(44) Orso, S.; Wegst, U. G. K.; Eberl, C.; Arzt, E. Micrometer-Scale Tensile Testing of Biological Attachment Devices. *Adv. Mater.* **2006**, *18* (7), 874–877. https://doi.org/10.1002/adma.200501807.

(45) Chisholm, C.; Bei, H.; Lowry, M. B.; Oh, J.; Syed Asif, S. A.; Warren, O. L.; Shan, Z. W.; George, E. P.; Minor, A. M. Dislocation Starvation and Exhaustion Hardening in Mo Alloy Nanofibers. *Acta Mater.* **2012**, *60* (5), 2258–2264. https://doi.org/https://doi.org/10.1016/j.actamat.2011.12.027.

(46) Guo, H.; Chen, K.; Oh, Y.; Wang, K.; Dejoie, C.; Syed Asif, S. A.; Warren, O. L.; Shan, Z. W.; Wu, J.; Minor, A. M. Mechanics and Dynamics of the Strain-Induced M1–M2 Structural Phase Transition in Individual VO2 Nanowires. *Nano Lett.* **2011**, *11* (8), 3207–3213. https://doi.org/10.1021/nl201460v.

(47) Velez, N. R.; Allen, F. I.; Jones, M. A.; Govindjee, S.; Meyers, G. F.; Minor, A. M. Extreme Ductility in Freestanding Polystyrene Thin Films. *Macromolecules* **2020**, *53* (19), 8650–8662. https://doi.org/10.1021/acs.macromol.0c01387.

(48) Sun, F.; Li, H.; Lindberg, H.; Leifer, K.; Gamstedt, E. K. Polymer Fracture and Deformation during Nanosectioning in an Ultramicrotome. *Eng. Fract. Mech.* **2017**, *182*, 595–606. https://doi.org/10.1016/j.engfracmech.2017.05.044.

(49) Wyeth, D. J.; Atkins, A. G. Mixed Mode Fracture Toughness as a Separation Parameter When Cutting Polymers. *Eng. Fract. Mech.* **2009**, *76* (18), 2690–2697. https://doi.org/10.1016/j.engfracmech.2009.07.023.

(50) Sun, F.; Gamstedt, E. K. Homogeneous and Localized Deformation in Poly(Methyl Methacrylate) Nanocutting. *Nanomanufacturing Metrol.* **2019**, *2* (1), 45–55. https://doi.org/10.1007/s41871-018-0034-7.

(51) Sezen, M.; Plank, H.; Fisslthaler, E.; Chernev, B.; Zankel, A.; Tchernychova, E.; Blümel, A.; List, E. J. W.; Grogger, W.; Pölt, P. An Investigation on Focused Electron/Ion Beam Induced Degradation Mechanisms of Conjugated Polymers. *Phys. Chem. Chem. Phys.* **2011**, *13* (45), 20235–20240. https://doi.org/10.1039/C1CP22406A.

(52) Kim, S.; Jeong Park, M.; Balsara, N. P.; Liu, G.; Minor, A. M. Minimization of Focused Ion Beam Damage in Nanostructured Polymer Thin Films. *Ultramicroscopy* **2011**, *111* (3), 191–199. https://doi.org/https://doi.org/10.1016/j.ultramic.2010.11.027.

(53) Allen, F. I.; Velez, N. R.; Thayer, R. C.; Patel, N. H.; Jones, M. A.; Meyers, G. F.; Minor, A. M. Gallium, Neon and Helium Focused Ion Beam Milling of Thin Films Demonstrated for Polymeric Materials: Study of Implantation Artifacts. *Nanoscale* **2019**, *11* (3), 1403–1409. https://doi.org/10.1039/C8NR08224C.

(54) Egerton, R. F.; Li, P.; Malac, M. Radiation Damage in the TEM and SEM. *Micron* **2004**, *35* (6), 399–409. https://doi.org/https://doi.org/10.1016/j.micron.2004.02.003.

(55) Rieger, J. The Glass Transition Temperature of Polystyrene. *J. Therm. Anal.* **1996**, *46* (3–4), 965–972. https://doi.org/10.1007/BF01983614.

(56) ASTM D638-14, Standard Test Method for Tensile Properties of Plastics, ASTM International, West Conshohocken, PA, 2014, Www.Astm.Org. https://doi.org/10.1520/D0638-14.

(57) Mark, H. F.; Kroschwitz, J. I. Encyclopedia of Polymer Science and Engineering. In *Styrene Polymers to Toys, Volume 16*; Mark, H. F., Bikales, N. M., Overberger, C. G., Menges, G., Kroschwitz, J. I., Eds.; Wiley-Interscience: New York, NY, 1989; pp 234–235.

(58) Michler, G. H.; Kausch, H. H.; Adhikari, R. Modeling of Thin Layer Yielding in Polymers. *J. Macromol. Sci. Part B Phys.* **2006**, *45 B* (5), 727–739. https://doi.org/10.1080/00222340600890505.

(59) Donald, A. M.; Kramer, E. J. The Competition between Shear Deformation and Crazing in Glassy Polymers. *J. Mater. Sci.* **1982**, *17* (7), 1871–1879. https://doi.org/10.1007/BF00540402.

(60) Van Melick, H. G. H.; Govaert, L. E.; Meijer, H. E. H. Prediction of Brittle-to-Ductile Transitions in Polystyrene. *Polymer* **2002**, *44* (2), 457–465. https://doi.org/10.1016/S0032-3861(02)00770-X.

(61) Vable, M. Integrating Fracture Mechanics into Undergraduate Design. *ASEE Annu. Conf. Expo. Conf. Proc.* **2005**, 8377–8384.

(62) Kramer, E. J. Microscopic and Molecular Fundamentals of Crazing. In *Crazing in Polymers*; Springer-Verlag: Berlin/Heidelberg, 1983; pp 1–56. https://doi.org/10.1007/BFb0024055.

(63) Chisholm, C.; Bei, H.; Lowry, M. B.; Oh, J.; Syed Asif, S. A.; Warren, O. L.; Shan, Z. W.; George, E. P.; Minor, A. M. Dislocation Starvation and Exhaustion Hardening in Mo Alloy Nanofibers. *Acta Mater.* **2012**, *60* (5), 2258–2264. https://doi.org/10.1016/j.actamat.2011.12.027.

(64) Guo, H.; Chen, K.; Oh, Y.; Wang, K.; Dejoie, C.; Syed Asif, S. A.; Warren, O. L.; Shan, Z. W.; Wu, J.; Minor, A. M. Mechanics and Dynamics of the Strain-Induced M1-M2 Structural Phase Transition in Individual VO2 Nanowires. *Nano Lett.* **2011**, *11* (8), 3207–3213. https://doi.org/10.1021/nl201460v.

(65) Cheng, S.; Wang, S.-Q. Elastic Yielding after Cold Drawing of Ductile Polymer Glasses. *Macromolecules* **2014**, *47* (11), 3661–3671. https://doi.org/10.1021/ma500570w.

(66) Chen, K.; Schweizer, K. S. Theory of Yielding, Strain Softening, and Steady Plastic Flow in Polymer Glasses under Constant Strain Rate Deformation. *Macromolecules* **2011**, *44* (10), 3988–4000. https://doi.org/10.1021/ma200436w.

(67) Bowden, P. B.; Raha, S. A Molecular Model for Yield and Flow in Amorphous Glassy Polymers Making Use of a Dislocation Analogue. *Philos. Mag.* **1974**, *29* (1), 149–166. https://doi.org/10.1080/14786437408213560.

(68) Bowden, P. B.; Raha, S. The Formation of Micro Shear Bands in Polystyrene and Polymethylmethacrylate. *Philos. Mag.* **1970**, *22* (177), 463–482. https://doi.org/10.1080/14786437008225837.

(69) Sun, F.; Li, H.; Leifer, K.; Gamstedt, E. K. Rate Effects on Localized Shear Deformation during Nanosectioning of an Amorphous Thermoplastic Polymer. *Int. J. Solids Struct.* **2017**, *129*, 40–48. https://doi.org/10.1016/j.ijsolstr.2017.09.016.

(70) Reiter, G. Dewetting as a Probe of Polymer Mobility in Thin Films. *Macromolecules* **2002**, *27* (11), 3046–3052. https://doi.org/10.1021/ma00089a023.

(71) DeMaggio, G. B.; Frieze, W. E.; Gidley, D. W.; Zhu, M.; Hristov, H. A.; Yee, A. F. Interface and Surface Effects on the Glass Transition in Thin Polystyrene Films. *Phys. Rev. Lett.* **1997**, *78* (8), 1524–1527. https://doi.org/10.1103/PhysRevLett.78.1524.

(72) Jean, Y. C.; Zhang, R.; Cao, H.; Yuan, J.-P.; Huang, C.-M.; Nielsen, B.; Asoka-Kumar, P. Glass Transition of Polystyrene near the Surface Studied by Slow-Positron-Annihilation Spectroscopy. *Phys. Rev. B* **1997**, *56* (14), R8459–R8462. https://doi.org/10.1103/PhysRevB.56.R8459.

(73) Hall, J. R.; Westerdahl, C. A. L.; Devine, A. T.; Bodnar, M. J. Activated Gas Plasma Surface Treatment of Polymers for Adhesive Bonding. *J. Appl. Polym. Sci.* **1969**, *13* (10), 2085–2096. https://doi.org/10.1002/app.1969.070131006.

(74) Henkee, C. S.; Kramer, E. J. Crazing and Shear Deformation in Crosslinked Polystyrene. *J. Polym. Sci. Polym. Phys. Ed.* **1984**, *22* (4), 721–737. https://doi.org/10.1002/pol.1984.180220414.

(75) Sancaktar, E.; Lu, H. The Effects of Excimer Laser Irradiation at 248 Nm on the Surface Mass Loss and Thermal Properties of PS, ABS, PA6, and PC Polymers. *J. Appl. Polym. Sci.* **2006**, *99* (3), 1024–1037. https://doi.org/10.1002/app.22598.

(76) van der Sanden, M. C. M.; Meijer, H. E. H.; Lemstra, P. J. Deformation and Toughness of Polymeric Systems: 1. The Concept of a Critical Thickness. *Polymer* **1993**, *34* (10), 2148–2154. https://doi.org/10.1016/0032-3861(93)90743-T.

(77) Yang, A. C. M.; Kramer, E. J.; Kuo, C. C.; Phoenix, S. L. Craze Fibril Stability and Breakdown in Polystyrene. *Macromolecules* **1986**, *19* (7), 2010–2019. https://doi.org/10.1021/ma00161a039.

(78) Kramer, E. J.; Berger, L. L. Fundamental Processes of Craze Growth and Fracture. *Adv.*

Polym. Sci. **1990**, *91--92*, 1–68. https://doi.org/10.1007/bfb0018018.

(79) Yang, A. C. M.; Kramer, E. J.; Kuo, C. C.; Phoenix, S. L. Crazes in Diluted Entanglement Networks of Polystyrene. *Macromolecules* **1986**, *19* (7), 2020–2027. https://doi.org/10.1021/ma00161a040.

(80) Bucknall, C. B. New Criterion for Craze Initiation. *Polymer* **2007**, *48* (4), 1030–1041. https://doi.org/10.1016/j.polymer.2006.12.033.

(81) Wool, R. P. Polymer Entanglements. *Macromolecules* **1993**, *26* (7), 1564–1569. https://doi.org/10.1021/ma00059a012.

(82) Willett, J. L.; O'Connor, K. M.; Wool, R. P. The Role of Chain Scission in Fracture of Amorphous Polymers. *J. Polym. Sci. Part B Polym. Phys.* **1986**, *24* (11), 2583–2589. https://doi.org/10.1002/polb.1986.090241114.

(83) Meyers, G. F.; DeKoven, B. M.; Seitz, J. T. Is the Molecular Surface of Polystyrene Really Glassy? *Langmuir* **1992**, *8* (9), 2330–2335. https://doi.org/10.1021/la00045a042.

(84) Kawaguchi, D.; Tanaka, K.; Kajiyama, T.; Takahara, A.; Tasaki, S. Mobility Gradient in Surface Region of Monodisperse Polystyrene Films. *Macromolecules* **2003**, *36* (4), 1235–1240. https://doi.org/10.1021/ma025667f.

(85) Miwa, Y.; Yamamoto, K.; Sakaguchi, M.; Sakai, M.; Makita, S.; Shimada, S. Direct Detection of High Mobility around Chain Ends of Poly(Methyl Methacrylate) by the Spin-Labeling. *Macromolecules* **2005**, *38* (3), 832–838. https://doi.org/10.1021/ma048287y.

(86) Welp, K. A.; Wool, R. P.; Agrawal, G.; Satija, S. K.; Pispas, S.; Mays, J. Direct Observation of Polymer Dynamics: Mobility Comparison between Central and End Section Chain Segments. *Macromolecules* **1999**, *32* (15), 5127–5138. https://doi.org/10.1021/ma990196r.

(87) Miwa, Y.; Shimada, S.; Urakawa, O.; Nobukawa, S. Origin of High Segmental Mobility at Chain Ends of Polystyrene. *Macromolecules* **2010**, *43* (17), 7192–7199. https://doi.org/10.1021/ma1013644.

(88) van Melick, H. G. H. G. H.; Govaert, L. E. E.; Raas, B.; Nauta, W. J. J.; Meijer, H. E. H. E. H. Kinetics of Ageing and Re-Embrittlement of Mechanically Rejuvenated Polystyrene. *Polymer* **2003**, *44* (4), 1171–1179. https://doi.org/10.1016/S0032-3861(02)00863-7.

(89) Govaert, L. E.; Van Melick, H. G. H.; Meijer, H. E. H. Temporary Toughening of Polystyrene through Mechanical Pre-Conditioning. *Polymer* **2001**, *42* (3), 1271–1274. https://doi.org/10.1016/S0032-3861(00)00477-8.

(90) Van Melick, H. G. H.; Govaert, L. E.; Meijer, H. E. H. Localisation Phenomena in Glassy Polymers: Influence of Thermal and Mechanical History. *Polymer* **2003**, *44* (12), 3579–3591. https://doi.org/10.1016/S0032-3861(03)00089-2.

(91) Pfromm, P. H.; Koros, W. J. Accelerated Physical Ageing of Thin Glassy Polymer Films: Evidence from Gas Transport Measurements. *Polymer* **1995**, *36* (12), 2379–2387. https://doi.org/10.1016/0032-3861(95)97336-E.

(92) Dorkenoo, K. D.; Pfromm, P. H. Accelerated Physical Aging of Thin Poly[1-(Trimethylsilyl)-1-Propyne] Films. *Macromolecules* **2000**, *33* (10), 3747–3751. https://doi.org/10.1021/ma9921145.

(93) McCaig, M. S.; Paul, D. R. Effect of Film Thickness on the Changes in Gas Permeability of a Glassy Polyarylate Due to Physical Aging: Part I. Experimental Observations. *Polymer* **2000**, *41* (2), 629–637. https://doi.org/10.1016/S0032-3861(99)00172-X.

(94) Huang, Y.; Paul, D. R. Physical Aging of Thin Glassy Polymer Films Monitored by Gas Permeability. *Polymer* **2004**, *45* (25), 8377–8393. https://doi.org/10.1016/j.polymer.2004.10.019.

(95) Huang, Y.; Paul, D. R. Experimental Methods for Tracking Physical Aging of Thin Glassy Polymer Films by Gas Permeation. *J. Memb. Sci.* **2004**, *244* (1–2), 167–178. https://doi.org/10.1016/j.memsci.2004.06.058.

(96) Huang, Y.; Paul, D. R. Physical Aging of Thin Glassy Polymer Films Monitored by Optical Properties. *Macromolecules* **2006**, *39* (4), 1554–1559. https://doi.org/10.1021/ma050533y.

(97) Boucher, V. M.; Cangialosi, D.; Alegría, A.; Colmenero, J. Enthalpy Recovery in Nanometer to Micrometer Thick Polystyrene Films. *Macromolecules* **2012**, *45* (12), 5296–5306. https://doi.org/10.1021/ma300622k.

(98) Aharoni, S. M. Ductile and Brittle Behavior of Amorphous Polymers. Relationship with Activation Energy for Glass Transition and Mechanical Fracture. *J. Appl. Polym. Sci.* **1972**, *16* (12), 3275–3284. https://doi.org/10.1002/app.1972.070161219.

(99) Van Melick, H. G. H.; Govaert, L. E.; Meijer, H. E. H. On the Origin of Strain Hardening in Glassy Polymers. *Polymer* **2003**, *44* (8), 2493–2502. https://doi.org/10.1016/S0032-3861(03)00112-5.

(100) Aharoni, S. M. Correlations between Chain Parameters and Failure Characteristics of Polymers below Their Glass Transition Temperature. *Macromolecules* **1985**, *18* (12), 2624–2630. https://doi.org/10.1021/ma00154a045.

(101) Chen, K.; Schweizer, K. S. Theory of Physical Aging in Polymer Glasses. *Phys. Rev. E - Stat. Nonlinear, Soft Matter Phys.* **2008**, *78* (3), 1–15. https://doi.org/10.1103/PhysRevE.78.031802.

(102) Chen, K.; Schweizer, K. S. Molecular Theory of Physical Aging in Polymer Glasses. *Phys. Rev. Lett.* **2007**, *98* (16), 1–4. https://doi.org/10.1103/PhysRevLett.98.167802.

(103) Chen, K.; Saltzman, E. J.; Schweizer, K. S. Molecular Theories of Segmental Dynamics and Mechanical Response in Deeply Supercooled Polymer Melts and Glasses. *Annu. Rev. Condens. Matter Phys.* **2010**, *1* (1), 277–300. https://doi.org/10.1146/annurev-conmatphys-070909-104110.

(104) Wang, S. Q.; Cheng, S.; Lin, P.; Li, X. A Phenomenological Molecular Model for Yielding and Brittle-Ductile Transition of Polymer Glasses. *J. Chem. Phys.* **2014**, *141* (9). https://doi.org/10.1063/1.4893765.

(105) Deblieck, R. A. C.; Van Beek, D. J. M.; Remerie, K.; Ward, I. M. Failure Mechanisms in Polyolefines: The Role of Crazing, Shear Yielding and the Entanglement Network. *Polymer* **2011**, *52* (14), 2979–2990. https://doi.org/10.1016/j.polymer.2011.03.055.

(106) Bucknall, C. B. Role of Surface Chain Mobility in Crazing. *Polymer* **2012**, *53* (21), 4778–4786. https://doi.org/10.1016/j.polymer.2012.08.034.

(107) Argon, A. S.; Salama, M. M. Growth of Crazes in Glassy Polymers. *Philos. Mag.* **1977**, *36* (5), 1217–1234. https://doi.org/10.1080/14786437708239790.

(108) Donald, A. M.; Kramer, E. J. The Mechanism for Craze-Tip Advance in Glassy Polymers. *Philos. Mag. A Phys. Condens. Matter, Struct. Defects Mech. Prop.* **1981**, *43* (4), 857–870. https://doi.org/10.1080/01418618108239496.

(109) Kramer, E. J. Craze Fibril Formation and Breakdown. *Polym. Eng. Sci.* **1984**, *24* (10), 761–769. https://doi.org/10.1002/pen.760241006.

(110) Kambour, R. P.; Gruner, C. L.; Romagosa, E. E. Solvent Crazing of "Dry" Polystyrene and "Dry" Crazing of Plasticized Polystyrene. *J. Polym. Sci. Polym. Phys. Ed.* **1973**, *11* (10), 1879–1890. https://doi.org/10.1002/pol.1973.180111003.

(111) DeRudder, J. L. Commercial Applications of Polycarbonates. In *Handbook of Polycarbonate Science and Technology*; LeGrand, D. G., Bendler, J. T., Eds.; Plastics Engineering; Taylor & Francis, 1999; pp 303–317.

(112) Ali, U.; Karim, K. J. B. A.; Buang, N. A. A Review of the Properties and Applications of Poly (Methyl Methacrylate) (PMMA). *Polym. Rev.* **2015**, *55* (4), 678–705. https://doi.org/10.1080/15583724.2015.1031377.

(113) Bates, C. M.; Seshimo, T.; Maher, M. J.; Durand, W. J.; Cushen, J. D.; Dean, L. M.; Blachut, G.; Ellison, C. J.; Willson, C. G. Polarity-Switching Top Coats Enable Copolymer Domains. *Science* **2012**, *338* (November), 775–779.

(114) Rowe, B. W.; Freeman, B. D.; Paul, D. R. Physical Aging of Ultrathin Glassy Polymer Films Tracked by Gas Permeability. *Polymer* **2009**, *50* (23), 5565–5575. https://doi.org/10.1016/j.polymer.2009.09.037.

(115) Xia, W.; Keten, S. Size-Dependent Mechanical Behavior of Free-Standing Glassy Polymer Thin Films. *J. Mater. Res.* **2014**, *30* (1), 36–45. https://doi.org/10.1557/jmr.2014.289.

(116) O'Connell, P. A.; McKenna, G. B. Novel Nanobubble Inflation Method for Determining the Viscoelastic Properties of Ultrathin Polymer Films. *Rev. Sci. Instrum.* **2007**, *78* (1). https://doi.org/10.1063/1.2409777.

(117) Van Loock, F.; Fleck, N. A. Deformation and Failure Maps for PMMA in Uniaxial Tension. *Polymer* **2018**, *148*, 259–268. https://doi.org/10.1016/j.polymer.2018.06.027.

(118) Polymethylmethacrylate - Sheet PMMA, Acrylic ME303006 http://www.goodfellow.com/catalogue/GFCat4J.php?ewd_token=kx25jGdytx10voV4kR0eaoWFEcr07l&n=L6wFXhEy0a4fhiPiglZL1jpvRdnDH5 (accessed Feb 26, 2021).

(119) Matsushige, K.; Radcliffe, S. V.; Baer, E. The Pressure and Temperature Effects on Brittle-to-ductile Transition in PS and PMMA. *J. Appl. Polym. Sci.* **1976**, *20* (7), 1853–1866. https://doi.org/10.1002/app.1976.070200714.

(120) Keddie, J. L.; Jones, R. A. L.; Cory, R. A. Interface and Surface Effects on the Glass-Transition Temperature in Thin Polymer Films. *Faraday Discuss.* **1994**, *98*, 219. https://doi.org/10.1039/fd9949800219.

(121) Hsu, D. D.; Xia, W.; Song, J.; Keten, S. Glass-Transition and Side-Chain Dynamics in Thin Films: Explaining Dissimilar Free Surface Effects for Polystyrene vs Poly(Methyl Methacrylate). *ACS Macro Lett.* **2016**, *5* (4), 481–486. https://doi.org/10.1021/acsmacrolett.6b00037.

(122) Nam, J. E.; Lee, J. K.; Mauldin, T. C. Isothermal Physical Aging of Thin PMMA Films near the Glass Transition Temperature. *Polym. Bull.* **2010**, *65* (8), 825–835. https://doi.org/10.1007/s00289-010-0333-7.

(123) Chen, K.; Saltzman, E. J.; Schweizer, K. S. Segmental Dynamics in Polymers: From Cold Melts to Ageing and Stressed Glasses. *J. Phys. Condens. Matter* **2009**, *21* (50). https://doi.org/10.1088/0953-8984/21/50/503101.

(124) Michler, G. H. Crazes in Amorphous Polymers I. Variety of the Structure of Crazes and Classification of Different Types of Crazes. *Colloid Polym. Sci.* **1989**, *267* (5), 377–388. https://doi.org/10.1007/BF01410182.

(125) Williams, M. Stress Singularities Resulting From Various Boundary Conditions in Angular Corners of Plates in Extension. *J. Appl. Mech.* **1952**.

(126) Taylor, R. L.; Govindjee, S. FEAP - A Finite Element Analysis Program: Version 8.6 User Manual. 2020.

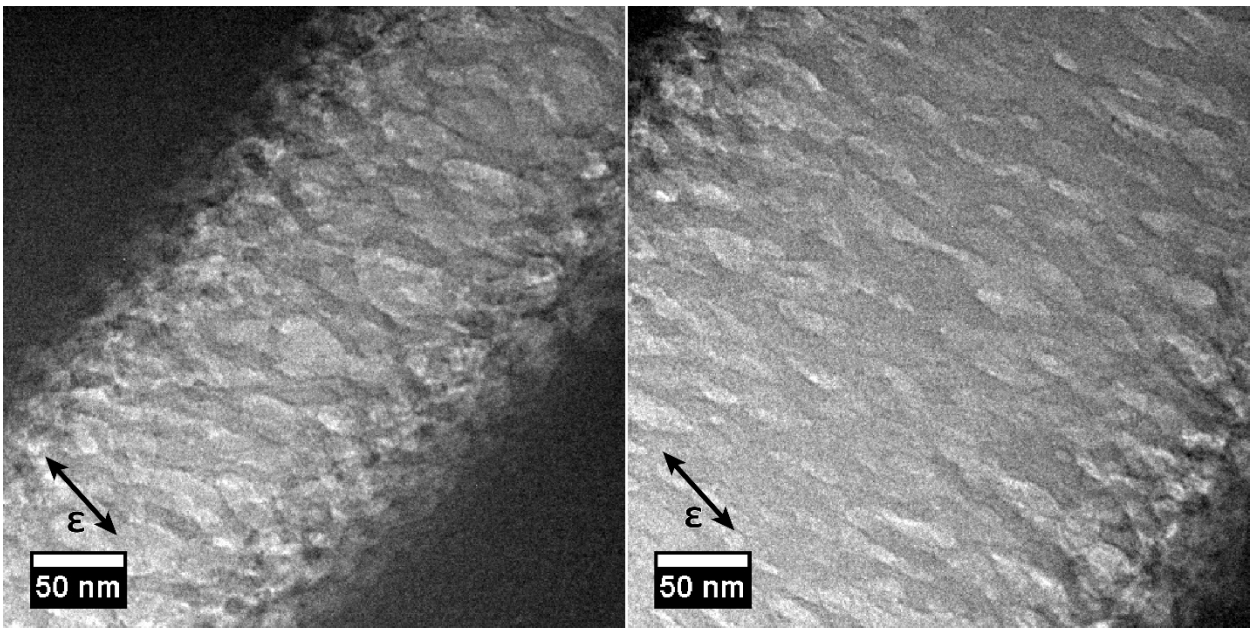

Figure A.1. Two TEM images of an annealed thin film of polystyrene displaying the 2D crazing morphology known as "perforated sheets," which results from the absence of out-of-plane stress. (Thickness = ~250 nm; arrows indicate the direction of strain.)

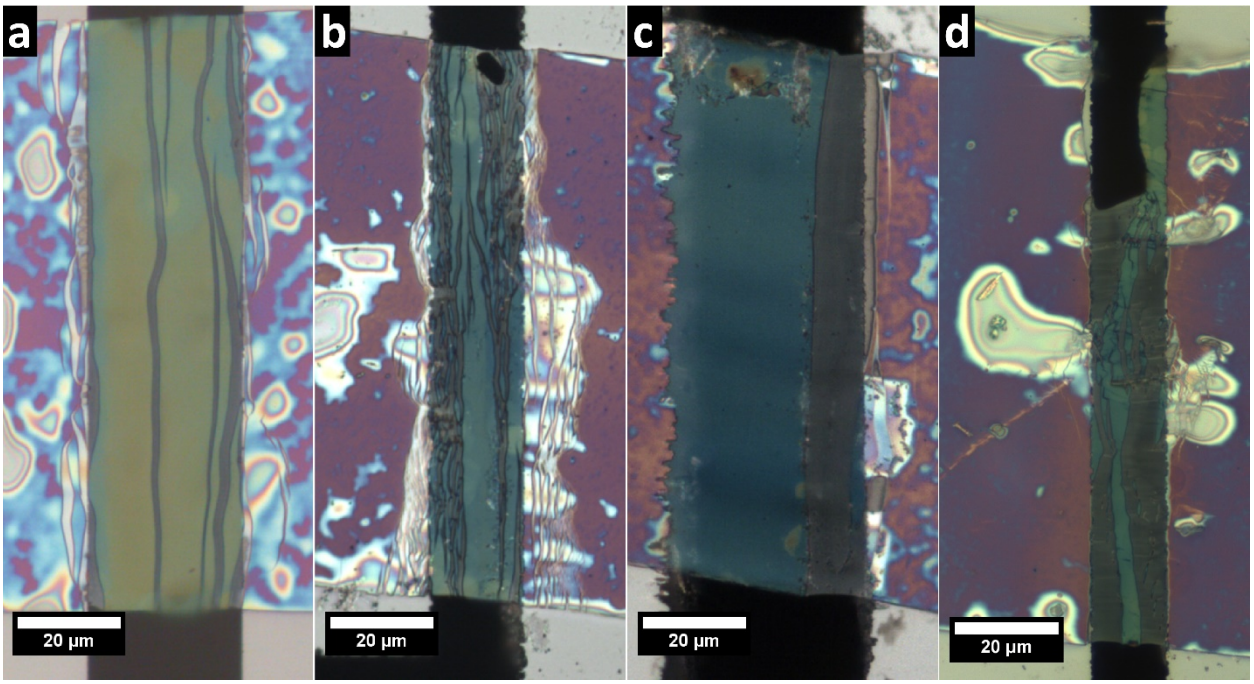

Figure A.2. Correlating optical images of polystyrene thin films shown in Figure 3.3. a) Annealed, 270 nm thick film strained to ~50%. b) Annealed, 240 nm thick film strained to ~150%, oriented such that the tensile direction was perpendicular to the cutting direction. c) Unannealed, 250 nm thick film strained to ~50%. d) Unannealed, 260 nm thick film strained to ~275%. Notch was

introduced at top edge during deposition, but only propagated partially across the film upon straining. Initial tensile gaps in (a-d) were 20, 7, 25, and 4 μm, respectively.

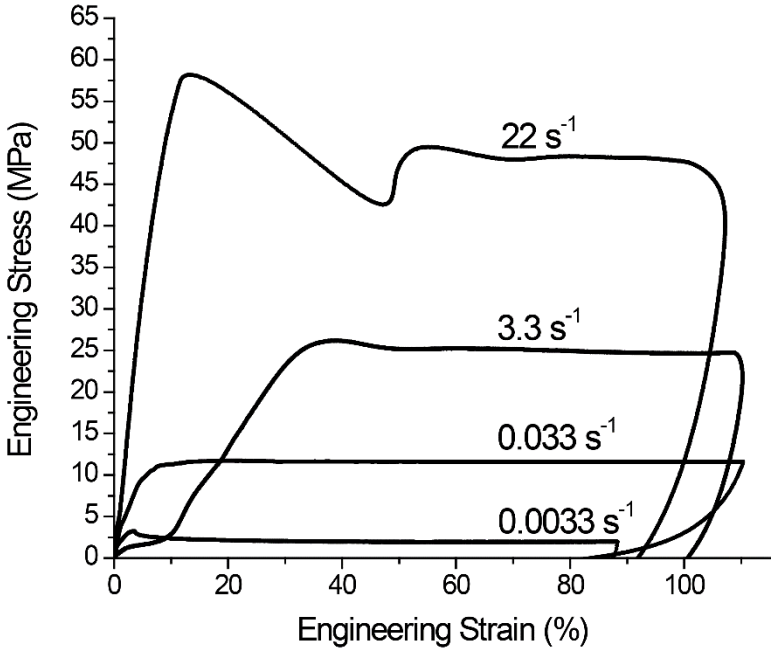

Figure A.3. Stress-strain curves obtained at different strain rates (indicated above each curve). From top to bottom, the film thicknesses are: 290, 240, 450, and 340 nm. The negative unloading segments are omitted for clarity.

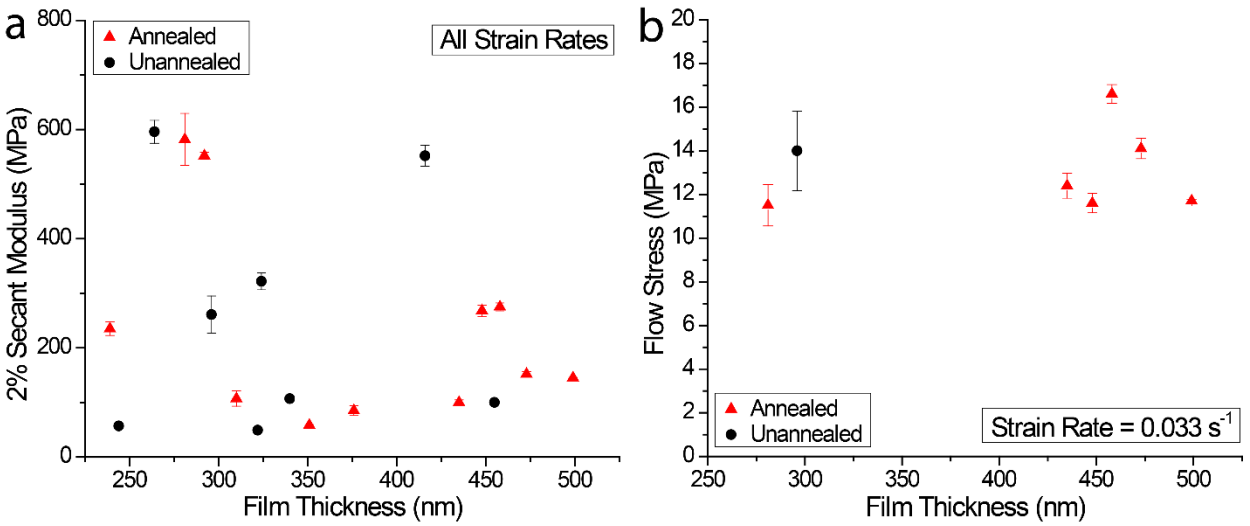

Figure A.4. a) Plot of the 2% secant modulus with respect to film thickness for all strain rates. While the values are an order of magnitude lower than for bulk polystyrene ~3 GPa), there does not appear to be any dependence on annealing or on film thickness in the range tested. b) Plot of the flow stress (strongly strain-rate dependent) with respect to film thickness for experiments performed at a strain rate of 0.033 s^{-1}. Similar to the 2% secant modulus, the flow stress does not

appear to exhibit any thickness dependence. (Error bars derived from the standard deviation between thickness measurements acquired from several SPM images taken at different regions of the film.)

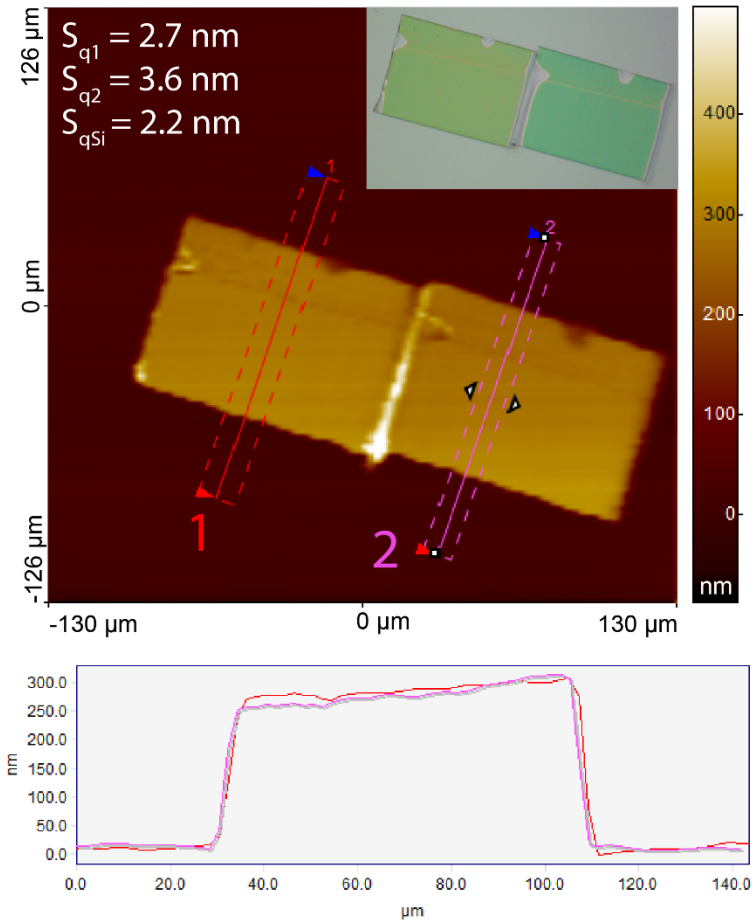

Figure A.5. TOP) Topography map of two microtomed thin films of polystyrene deposited onto a silicon wafer obtained with a KLA Tencor P17 stylus profilometer. The RMS surface roughness, S_q, was calculated for each film, using the region of interest indicated (S_{q1} = 2.7 nm and S_{q2} = 3.6 nm), as well as the silicon substrate (S_{qSi} = 2.2 nm). An optical image of the films is shown in the inset. BOTTOM) Line profiles of the films indicated by the solid line for each region of interest.

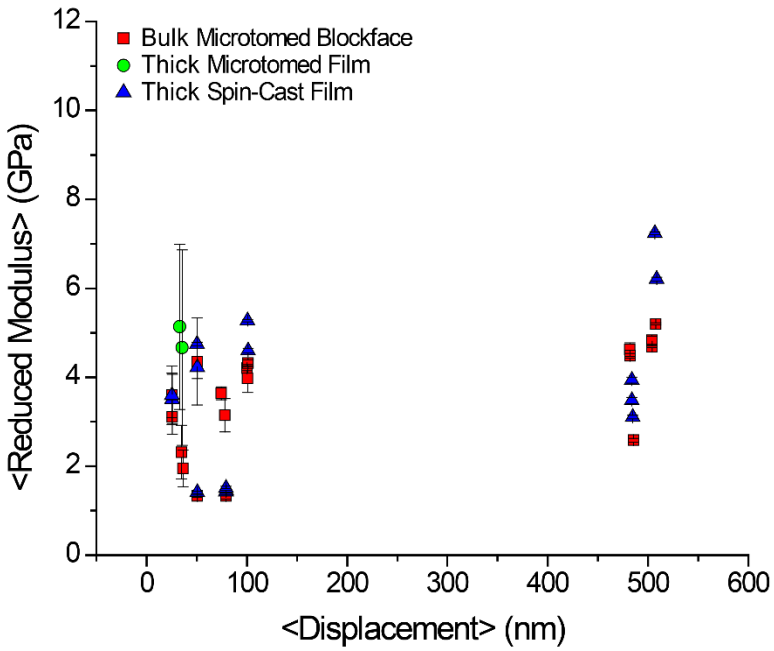

Figure A.6. Nanoindentation data for the bulk microtomed blockface, thick (~1 µm) microtomed films, and thick (~1 µm) spin-cast films. No significant difference between the sample preparation types is observed and the values are near the expected value of 3 GPa. Each datapoint represents 25 indents.

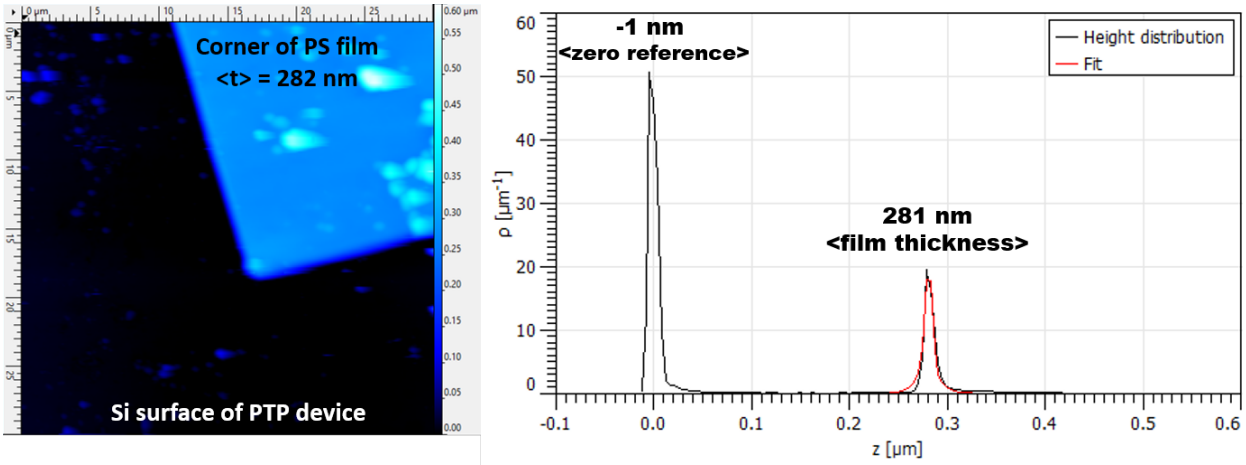

Figure A.7. LEFT) 30x30 µm topography image showing the corner of a polystyrene thin film (blue) deposited on a PTP device (black). Color scale indicates z-height, ranging from 0 to 600 nm. RIGHT) Histogram of z-height values where the positions of the film and substrate peaks (indicated) were determined by fitting a Gaussian curve (red line shows the Gaussian fit for the film height). Gwyddion (v2.52) software was used for all SPM analysis.

Appendix B – Linear Elastic Simulation of a Thin Film in Planar Tension

The basic deformation state of the specimen in the Push-to-Pull (PTP) device is one of plane-strain tension. Assuming that the x-coordinate direction aligns with the opening direction of the PTP device, the y-direction aligns with the through-thickness sample direction, and the z-direction aligns with the width direction of the sample, then the specimen experiences (predominantly) a tensile stress in the x-direction, and an induced tension (due to a Poisson effect) in the z-direction. The specimen is largely stress free in the y-direction. Shear stresses are largely absent.

There are, however, grip effects which induce local stress concentrations and artifacts associated with the asymmetric (bottom only) gripping. As noted by Williams (1952) when a free surface is sharply clamped a stress singularity is induced at the location where the displacements are first restrained; in the case of linear elasticity this singularity has the same order as that at the tip of a sharp crack $O(1/\sqrt{r})$.[125] Surprisingly, the exceedingly high ductilities that we observe are robust even in the presence of these "crack-like" stress concentrations.

To better elucidate the deformation state of the specimen, we have performed three-dimensional linear elastic finite element computations to highlight the deformation state in the PTP. This gives a fuller picture of the tests performed. The computation were run using the general purpose finite element code FEAP.[126] The material was modeled using linear elastic 27-noded tri-quadratic brick elements in quarter-symmetry. In the quarter-symmetric model there were 8 nodes in the y-direction, 72 nodes in the x-direction for the freestanding part of the film, 32 nodes in the x-direction over the grip, and 80 nodes in the z-direction. The resulting quarter-symmetry model consisted of 687,834 nodes and 74,880 elements, giving a total of 1,965,255 equations after accounting for boundary conditions. To simulate the grips, the nodes on the underside of the specimen were fixed and displaced in the x-direction.

Linear elasticity was used to model the material since to-date there are no well accepted constitutive models for the behavior we have seen in the experiments. Notwithstanding, linear elasticity still allows one to gain a sound understanding of the deformation state during the test. For examples run the Young's modulus was E = 3.5 GPa and the Poisson ratio was $\nu = 0.35$. The film thickness t = 250 nm, the full-width $\omega = 70$ μm, full-span s = 4.5 μm, and the grip overhang g = 1 μm – a distance sufficient to eliminate any free-edge effects. In all results shown, the grips were displaced so as to induce a strain in the x-direction of approximately 1.42 mstrain.

B.1 Plane-strain nature of deformation

Figure B.1 demonstrates the plane strain nature of the deformation of the specimen. The view shown is a top-down look and the contours correspond to the z-displacement of the specimen. Note that the z-displacement is largely zero, with a small amount of pull-in at the free edges, top and bottom.

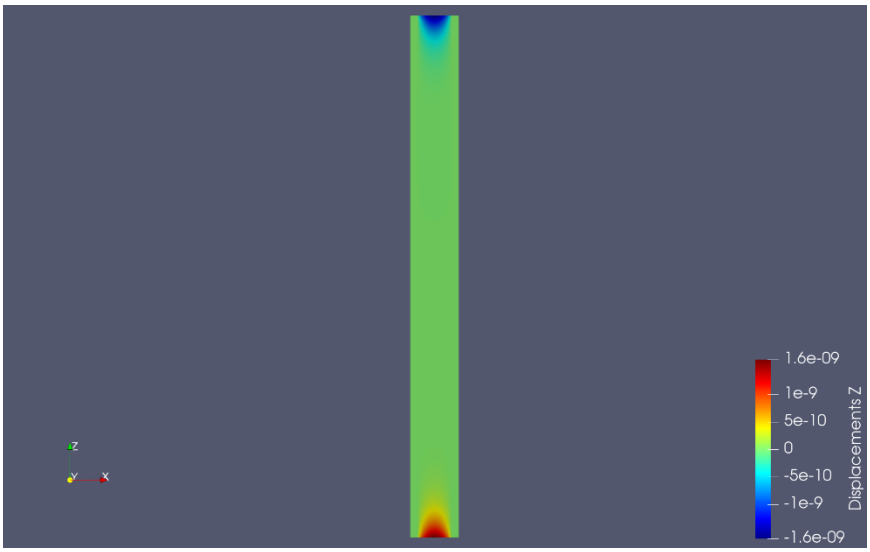

Figure B.1. z-displacement in the test film (linear elastic simulation) at an opening strain of approximately 1.42 mstrain. Displacement in meters.

B.2 Opening stress

Figures B.2 and B.3 show the uniformity of the x-direction stress in the specimen, giving a top and bottom view, respectively. It is seen that the stress field in the freestanding portion is very uniform. The dark blue stripes are the portions of the film resting on the grip. When viewed from below (Figure B3) the grip edge is sharply delineated. From the top there is a slight diffusion indicating a slight through-thickness effect from the grip geometry. This effect can be seen more clearly in Figure B.4 which shows a cross-sectional view of the x-direction stress at the mid-plane of the full specimen. Also note the stress concentration on the bottom edge due to the grip, which can also be see in the cross-sectional plot of the Mises stress in Figure B.5 – observe the red "hot-spots."

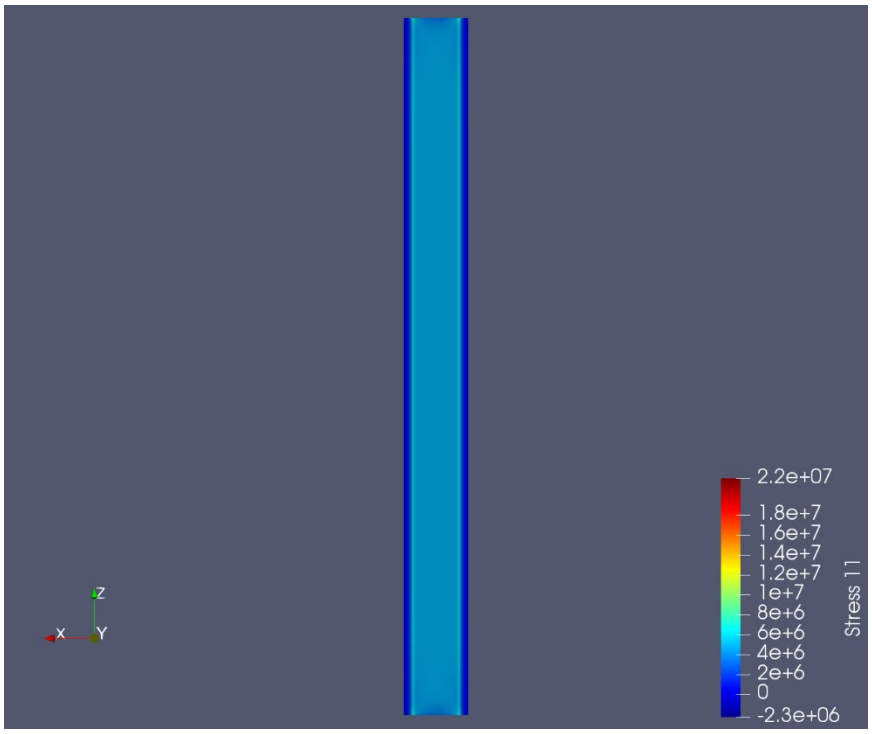

Figure B.2. X-direction stress in the test film (linear elastic simulation) at an opening strain of approximately 1.42 mstrain; top view. Stress in Pascals.

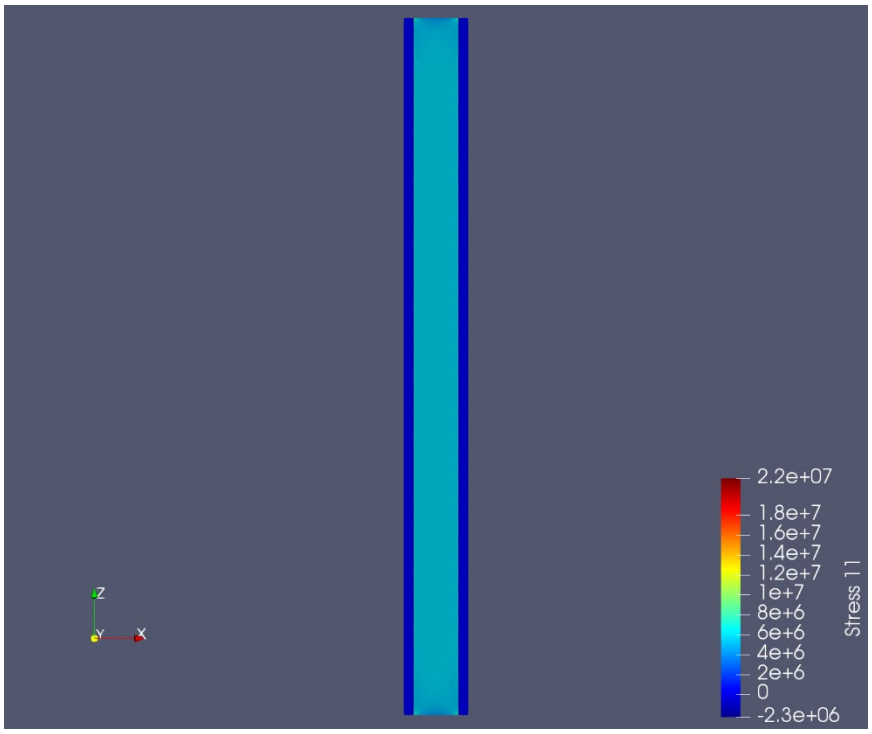

Figure B.3. X-direction stress in the test film (linear elastic simulation) at an opening strain of approximately 1.42 mstrain; bottom view. Stress in Pascals.

Figure B.4. X-direction stress in the test film at mid-span (linear elastic simulation) at an opening strain of approximately 1.42 mstrain; cross-sectional view. Stress in Pascals.

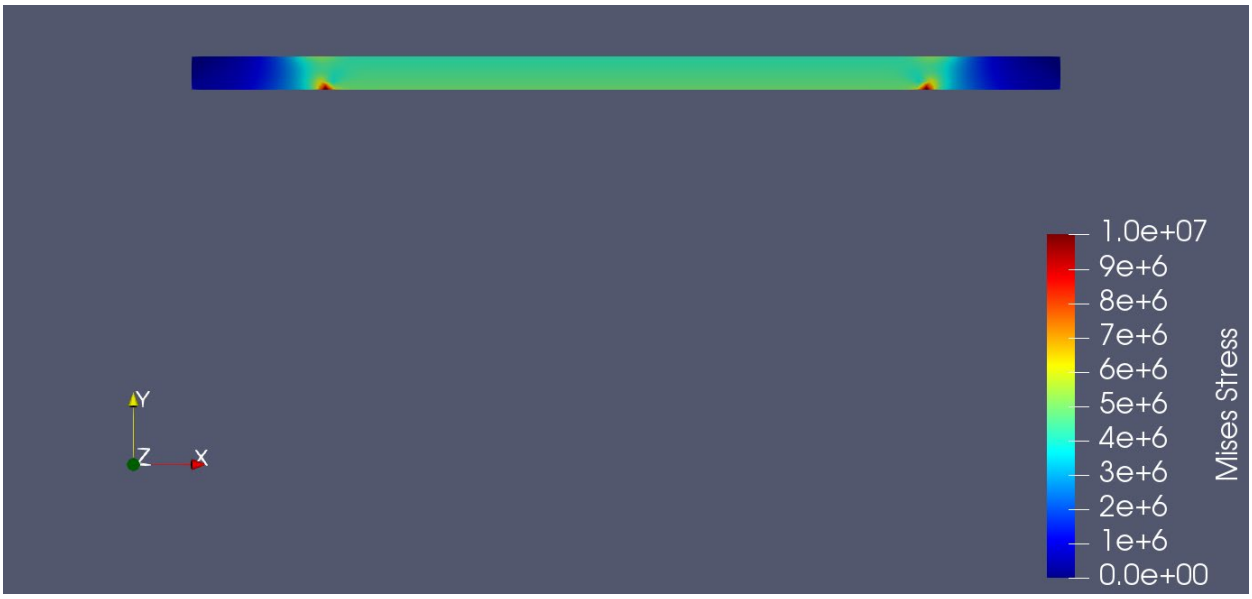

Figure B.5. Mises stress in the test film at mid-span (linear elastic simulation) at an opening strain of approximately 1.42 mstrain; cross-sectional view. Stress in Pascals.

B.3 Shear stress

The xy-shear stress magnitude is shown in Figure B.6. This shows how the grips induce a shear stress in the film above the grips which is converted by the geometry into the tensile stress in the freestanding portion of the specimen. Note that the xy-shear stresses rapidly decrease in the freestanding portion of the film. Observe also the stress concentration at the edge of the grips.

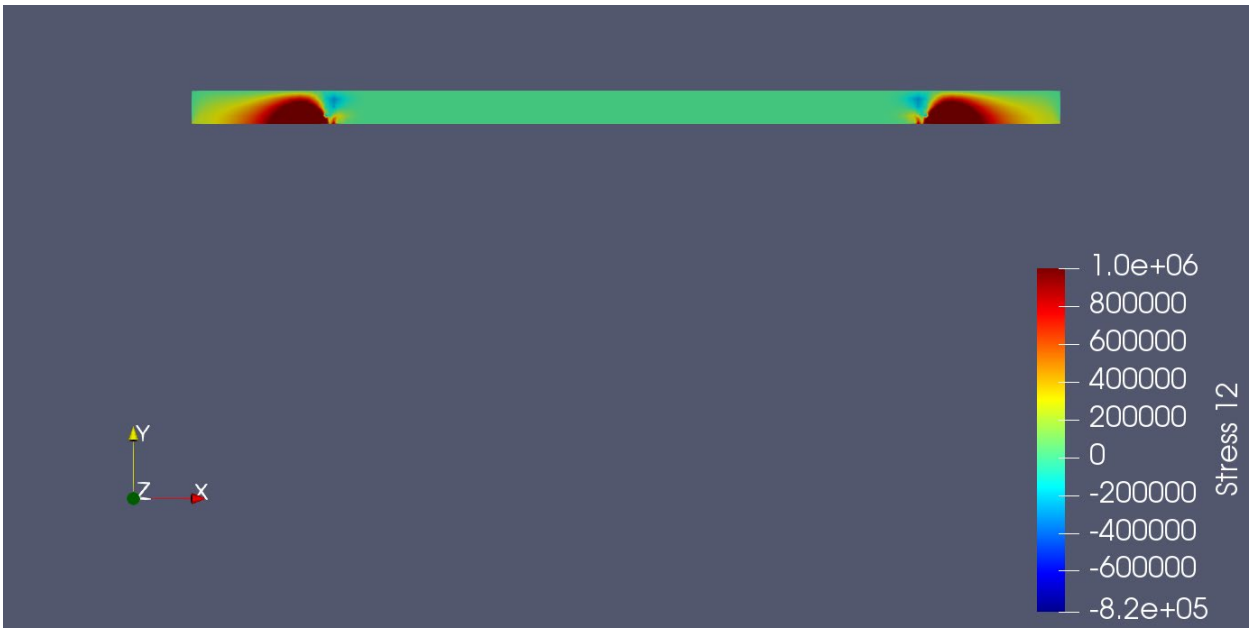

Figure B.6. Shear stress magnitude in the test film at mid-span (linear elastic simulation) at an opening strain of approximately 1.42 mstrain; cross-sectional view. Stress in Pascals.

Appendix C – Areal Chain Segment Density Calculation

Using the analysis provided by Wool (1993) the molecular area, a, can be estimated using the volume-to-length ratio of the unit cell:[81]

$$a = \sqrt{2}\frac{V}{L}$$

where: L = c-axis length (backbone direction)

The prefactor, $\sqrt{2}$, accounts for the random orientation of chains crossing the plane, and:

$$V = \frac{zM_0}{\rho N_A}$$

where: z = number of monomers per c-axis length
M_0 = monomer molecular weight
N_A = Avogadro's number
ρ = density

The values for polystyrene were obtained from Table 1 in [80]:

$L = 6.5$; $z = 3$; $M_0 = 104$ g/mol

For the polystyrene used in this work: $\rho = 1.04$ g/cm^3

Substituting yields: $a = 1.1 \times 10^{-14}$ cm^2

The areal chain segment density is then: $p = \frac{1}{a} = 9.2 \times 10^{13} \ \frac{segments}{cm^2}$

Appendix D – Push-to-Pull Device Fabrication Process

The following protocol was developed by Wei Li, continued by Yunsu Park, and outlines the photolithography parameters for the microfabrication of PTP devices. This protocol was written specifically for the equipment in the Marvell NanoLab, located in the CITRIS headquarters building, Sutardja Dai Hall, UC Berkeley.

Starting SOI Wafer

- Vendor: Ultrasil
- SOI, Diameter: 6" (150 +/- 0.5 mm), Polish: DSP-double sided polish, Type/Dopant: P/B
- Orientation: <1-0-0>
- Device Thickness: 30 +/- 1 um
- Box (SiO2) Thickness: 1 um
- Handle Thickness: 400 +/- 10 um
- Resistivity: 1-30 ohm-cm

Device Side Fabrication

Photolithography

1. Spincoat (Instrument: Picotrack 1)
    - Resist: MiR701
    - Thickness: 2um
    - Flow Recipe: 'TI_MiR201_2.0um'
        - Prime: HMDS, 100C, 30 sec on track
        - Coat: 900rpm, 60 sec
    - Soft bake: 90C for 90 sec
2. Stepper UV Expose (Instrument: gcaws6: GCA8500)
    - Flow Recipe: "weili\check"
        - Used for Fujifilm OiR 906-12
        - Also works for MiR701
    - Flow Recipe:
        - Expose Power: 180 mJ/cm^2
        - Used for MiR701
3. Post Exposure Bake & Develop (picotrack 2)

- Post Exposure Bake: 110 C, 90 sec, contact
- Developer: MF-26A
  - Spray: 5 sec
  - Puddle: 60 sec

4. Hard Bake/UV Bake (axcelis: fusion M200PCU Photostabilizer)

   - UV Bake (recommended)
     - Flow Recipe: “Recipe U”
       1. 110C idle
       2. 110C OFF
       3. 140C 20sec LOW 10sec
       4. 140C HIGH N/A
     - 2J
   - Oven Bake
     - 120C for 30 min

Silicon Etch

5. RIE (STS2: surface tech system advanced silicon etch)

   - Recipe: “DEEP SILICON1” (used for 550 um handle layer thickness, but works for 550 umas well)
     - 70 cycles (used for 40um device thickness)
     - UPDATE: 55 cycles (updated for 30um device thickness)
     - Etch rate: ~750 nm/cycle
     - Selectivity to AZ-P: 70+:1

Parameter	Passivation	Etch
Cycle Time (sec)	**7**	**10**
C4F8 (sccm)	**80**	**0**
SF6 (sccm)	**0**	**130**
O2 (sccm)	**0**	**13**
Coil Power (W)	**600**	**600**
Bias Power (W)	**0**	**20**
Bias Frequency (MHz)	**-**	**13.56**
Platen Chiller (C)	**25**	**25**

** MAY BE USEFUL TO LOOK INTO DIFFERENT ETCH RECIPE SHOWN BELOW*

- Recipe: "Smooth Wall" standard recipe
- Cycles: 120 cycles
  - Etch Rate: ~350 nm/cycle
  - Cycle Time: 13 sec
  - AZP selectivity: 50+:1

Parameter	Passivation	Etch
Cycle Time (sec)	**5**	**7**
C4F8 (sccm)	**100**	**0**
SF6 (sccm)	**0**	**130**
O2 (sccm)	**0**	**13**
Coil Power (W)	**600**	**600**
Bias Power (W)	**0**	**20**
Bias Frequency (MHz)	**-**	**13.56**
Platen Chiller (C)	**25**	**25**

6. Photoresist Removal (recommended: matrix, alternately msink1)
   - Ash Time: 150 sec
   - Recipe: Standard Recipe

Parameter	
Pressure (torr)	**3.75**
MFC1	**40%**
MFC2	**0%**
MFC3	**0%**
RF Power (W)	**400**
Pin	**Down**
End Point	**Timed**
Chuck (C)	**250**

Deposition

7. PECVD (Oxford 2)

   - SiO2 thickness: 1um
   - Flow Recipe: "weili2um"
     - Coat 1um 2 times: abort when 1um thickness reached

Handle Side Fabrication

2. Spin Coat (picotrack 1)

    - Resist: AZ P4620
    - Thickness: 15um
        - Recipe: “6inch_AZ4620_15um_noT”
    - Thickness: 12um (both 15 and 12um works)
        - Prime: HMDS, 100C, 30 sec
        - Coat: 1790 rpm 60 sec
        - Soft Bake: 110C, 80sec, proximity
        - Rest: 20-70% humidity, 20C, 30 min

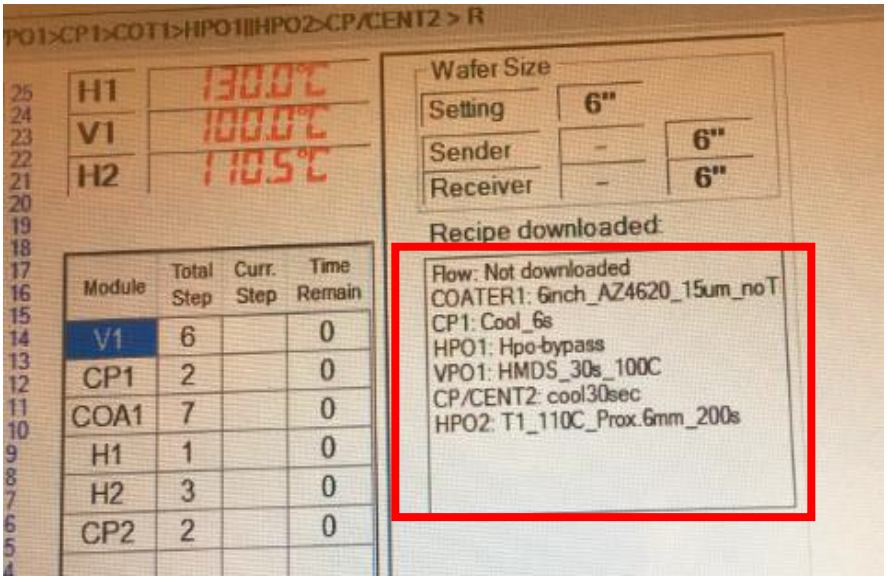

3. UV-Expose (ksaligner)

    - Thickness: 15um
        - Multi-expose/soft-contact/90um/9s/3times
    - Thickness: 12um
        - Power: 980 mJ/cm2

4. Post Exposure Bake
    - **Not Recommended for AZ resist (DO NOT PEB)**

5. Spin Develop (picotrack 2)

- Thickness: 15um
    - Recipe: “MF26A_Puddle4x60s”
- Thickness: 12um
    - Recipe: “T2_NoPEB_MF26A2x60s_2spray”
    - MF-26A Developer
        - 4x (spray 5 sec, puddle 60 sec)

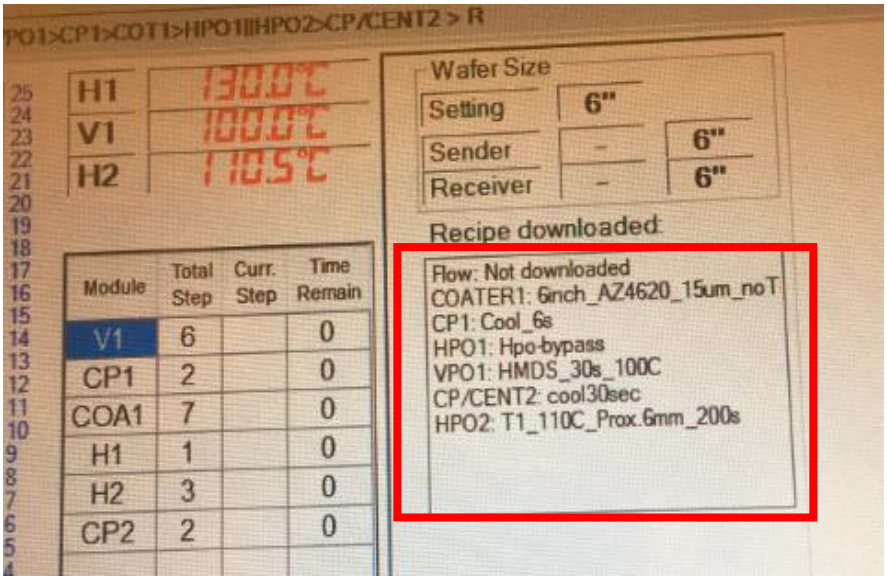

6. Hard Bake

    - (UV bake not recommended for AZ-P)
    - Recommended:
        - Oven: 120C, 1 hr.
    - Time Sensitive:
        - Oven: 90C, 30min
        - Hotplate: 90C, 5min

7. Cool Grease Bond

    - Cool grease bond on device side with handle wafer
    - Heat 70C for 10min

8. RIE (sts2)

    - Recipe: “DEEP SILICON1” (used for 550 um handle layer thickness, but works for 550 umas well)

- 700 cycles
- Etch rate: ~750 nm/cycle
- Selectivity to AZ-P: 70+:1

Parameter	Passivation	Etch
Cycle Time (sec)	**7**	**10**
C4F8 (sccm)	**80**	**0**
SF6 (sccm)	**0**	**130**
O2 (sccm)	**0**	**13**
Coil Power (W)	**600**	**600**
Bias Power (W)	**0**	**20**
Bias Frequency (MHz)	**-**	**13.56**
Platen Chiller (C)	**25**	**25**

Box Side Fabrication

1. Separate handle wafer on SOI wafer
    - Clean cool grease with Acetone

2. HF-vapor etch (primaxx)

    - Recipe: “recipe3”
        - 3 cycles
        - Thermal oxide etch rate = 900 A/min

Parameter	N2 (sccm)	EtOH (sccm)	HF (sccm)
Stabilize	**1000**	**400**	**0**
Etch	**1000**	**400**	**525**
Pump	**0**	**0**	**0**

3. Plasma Etch (technics-c)

    - O2 plasma
    - 300W, 5min, 180-190 mTorr

4. Remove MEMS device
    - Break tether with tweezer
        - Be very careful!